



National Library
of Canada

Acquisitions and
Bibliographic Services Branch

395 Wellington Street
Ottawa, Ontario
K1A 0N4

Bibliothèque nationale
du Canada

Direction des acquisitions et
des services bibliographiques

395, rue Wellington
Ottawa (Ontario)
K1A 0N4

Your file - Votre référence

Our file - Notre référence

NOTICE

The quality of this microform is heavily dependent upon the quality of the original thesis submitted for microfilming. Every effort has been made to ensure the highest quality of reproduction possible.

If pages are missing, contact the university which granted the degree.

Some pages may have indistinct print especially if the original pages were typed with a poor typewriter ribbon or if the university sent us an inferior photocopy.

Reproduction in full or in part of this microform is governed by the Canadian Copyright Act, R.S.C. 1970, c. C-30, and subsequent amendments.

AVIS

La qualité de cette microforme dépend grandement de la qualité de la thèse soumise au microfilmage. Nous avons tout fait pour assurer une qualité supérieure de reproduction.

S'il manque des pages, veuillez communiquer avec l'université qui a conféré le grade.

La qualité d'impression de certaines pages peut laisser à désirer, surtout si les pages originales ont été dactylographiées à l'aide d'un ruban usé ou si l'université nous a fait parvenir une photocopie de qualité inférieure.

La reproduction, même partielle, de cette microforme est soumise à la Loi canadienne sur le droit d'auteur, SRC 1970, c. C-30, et ses amendements subséquents.

UNIVERSITY OF ALBERTA

**PERFORMANCE LIMITATION OF SPECTRALLY SLICED LIGHT
EMITTING DIODES FOR DIGITAL FIBER OPTIC TRANSMISSION
SYSTEMS**

BY

ERIC CAUCHON



A thesis submitted to the Faculty of Graduate Studies and Research in partial fulfillment of the requirements for the degree of **MASTER OF SCIENCE**.

DEPARTMENT OF ELECTRICAL ENGINEERING

EDMONTON, ALBERTA
FALL 1993



National Library
of Canada

Bibliothèque nationale
du Canada

Acquisitions and
Bibliographic Services Branch

Direction des acquisitions et
des services bibliographiques

395 Wellington Street
Ottawa, Ontario
K1A 0N4

395, rue Wellington
Ottawa (Ontario)
K1A 0N4

Your file *Votre référence*

Our file *Notre référence*

The author has granted an irrevocable non-exclusive licence allowing the National Library of Canada to reproduce, loan, distribute or sell copies of his/her thesis by any means and in any form or format, making this thesis available to interested persons.

L'auteur a accordé une licence irrévocable et non exclusive permettant à la Bibliothèque nationale du Canada de reproduire, prêter, distribuer ou vendre des copies de sa thèse de quelque manière et sous quelque forme que ce soit pour mettre des exemplaires de cette thèse à la disposition des personnes intéressées.

The author retains ownership of the copyright in his/her thesis. Neither the thesis nor substantial extracts from it may be printed or otherwise reproduced without his/her permission.

L'auteur conserve la propriété du droit d'auteur qui protège sa thèse. Ni la thèse ni des extraits substantiels de celle-ci ne doivent être imprimés ou autrement reproduits sans son autorisation.

ISBN 0-315-88364-2

UNIVERSITY OF ALBERTA

RELEASE FORM

NAME OF THE AUTHOR: **ERIC CAUCHON**

TITLE OF THESIS: **PERFORMANCE LIMITATION OF SPECTRALLY
SLICED LIGHT EMITTING DIODES FOR DIGITAL
FIBER OPTIC TRANSMISSION SYSTEMS**

DEGREE: **MASTER OF SCIENCE**

YEAR THIS DEGREE GRANTED: **FALL 1993**

Permission is hereby granted to the University of Alberta Library to reproduce single copies of this thesis and to lend or sell such copies for private, scholarly or scientific research purposes only.

The author reserves all other publication and other rights in association with the copyright in the thesis, and except as hereinbefore provided neither the thesis nor any substantial portion thereof may be printed or otherwise reproduced in any material form without the author's prior written permission.



#306-10565-83 Avenue

Edmonton, Alberta

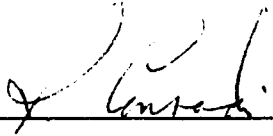
Canada T6E 2E1

DATE: October 7 1993

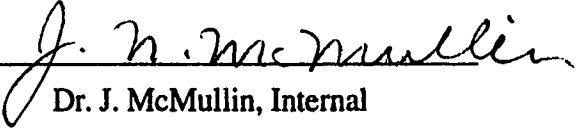
UNIVERSITY OF ALBERTA

FACULTY OF GRADUATE STUDIES AND RESEARCH

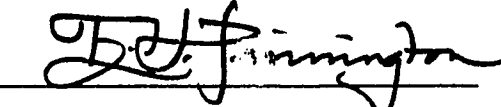
The undersigned certify that they have read, and recommended to the Faculty of Graduate Studies and Research for acceptance a thesis entitled **PERFORMANCE LIMITATION OF SPECTRALLY SLICED LIGHT EMITTING DIODES FOR DIGITAL FIBER OPTIC TRANSMISSION SYSTEMS** in partial fulfillment of the requirements for the degree of **MASTER OF SCIENCE** in Electrical Engineering.



Dr. J. Conradi, Supervisor



Dr. J. McMullin, Internal



Dr. E. H. Pinnington, External

DATE: October 6, 1993

DEDICATED TO

***My parents, Toussaint and Jacqueline Cauchon,
who have always encouraged me and loved me.***

My family and friends, for their continuous support.

Abstract

A study of the performance of spectrally sliced light-emitting diodes (LEDs) for digital fiber optic transmission systems is presented. This study also included the use of erbium doped fiber amplifiers (EDFAs) to increase the LED power. A theoretical model based on the statistics of both the LED emission and the EDFA amplification was developed and used to obtain the bit error rate (BER) for a spectral slicing system composed of an LED, EDFA, optical filter and an optical receiver. It also allowed us to examine the effect of various system parameters such as the LED power and extinction ratio, the EDFA gain and noise factor and the optical filter bandwidth on the BER performance.

This model allowed us to better understand the spectral slicing method as well as the EDFA amplification process. It predicted the appearance of floors in the BER as a function of the power at the optical receiver. These BER floors are caused by an excess noise term present in the variance of the LED photon distribution. The excess noise term is due to the lack of coherence of the LED. We found that this term is always the one that ultimately limits the BER performance and that the use of an EDFA could not improve this performance.

An experimental spectral slicing system operating at 622 Mb/s (OC12) was implemented to verify our model. A series of BER results were obtained from this setup and were compared with the predictions of our model. We found a reasonably good agreement. Finally, we calculated the maximum number of channels achievable and the distance over which these channels could be transmitted in the case when our spectral slicing system was used in a wavelength division multiplexing (WDM) application. We found that 13 channels modulated at 622 Mb/s transmitted through 25 km of optical fiber could be accomplished.

Acknowledgments

I would like to express my sincere gratitude to my supervisor Dr. Jan Conradi, for his guidance and continuous support during this project and for giving me the opportunity to come here in western Canada to study and improve my second language.

I would like also to sincerely thank Dr. R. P. W. Lawson, Graduate Coordinator at the department of Electrical Engineering for his devotion in helping me in various aspects of my registration at the University of Alberta.

In addition, I would like to acknowledge Mr. Dave Clegg for his indispensable help in the laboratory during the experimental phase of my project. I would like to thank Dr. Jim McMullin for his help in some of the theoretical calculations of my project as well as Dave Moore for helping me to take some of the EDFA gain measurements.

During my stay here in Edmonton, I have met many great people through school and other social activities. I would also like to thank them all for making my stay here so wonderful. In particular, I would like to thank Greg May and Kinh Pham for their help and friendship. Also, I would like to thank Amanda Wood for her help in the cutting and pasting work involved in the making of this document and also for simply being there when I needed it.

This work was supported by the Natural Science and Engineering Research Council of Canada (NSERC), Bell Northern Research Ltd. (BNR) and TRILabs through the NSERC/BNR/TRILabs Chair in Fiber Optic Communications at the University of Alberta. Without their support this project would not have been possible.

Finally, I would like to extend my gratitude to the members of the examining committee for reviewing this manuscript in less than the stipulated period.

Table of Contents

1. Introduction	1
1.1 Overview of Optical Communications.....	1
1.1.1 Types of Communication Systems	2
1.1.2 Multiplexed Transmission.....	2
1.1.3 Detection and Performance	3
1.1.4 Optical Amplifiers	4
1.2 Project Description.....	4
1.3 Spectral Slicing.....	5
1.3.1 Optical FDM System.....	6
1.3.2 Carrier Generator	6
LED Source	7
EDFA.....	7
Optical Filter	8
1.3.3 Optical Receiver.....	9
1.3.4 Detection of Light.....	10
Electrical Noise	10
Photon Noise.....	10
Quantum Limit	11
1.4 Conclusion	11
2. Statistics of Filtered Incoherent Light Sources	13
2.1 Statistical Properties of Light.....	13
2.1.1 Coherent and Partially Coherent Sources.....	13
2.1.2 Optical Intensity	14
2.1.3 Temporal Coherence and Spectrum.....	14
2.1.4 Spatial Coherence and Polarization.....	16
2.1.5 Photon Number.....	17
2.2 Statistics of some Light Sources	20
2.2.1 Ideal Laser (Coherent) Light	20
2.2.2 Thermal (Incoherent) Light	21

Narrowband Thermal Light.....	21
Wideband Thermal Light	23
2.2.3 Filtered Thermal Light.....	24
2.3 LED Statistics	30
2.4. Conclusion	30
3. Birth-Death-Immigration Processes Applied to Optical Amplifiers.....	31
3.1 BDI Theory.....	31
3.1.1 Description.....	31
3.1.2 BDI Equations	33
3.1.3 Probability Generating Function	33
3.2 Some Input Distributions.....	36
3.2.1 Deterministic Input.....	36
3.2.2 Poisson Input	37
3.2.3 Negative Binomial Input.....	38
3.3 EDFA Noise Terms.....	44
3.3.1 Discussion.....	47
3.4. Conclusion	48
4. Theoretical Performance of Spectral Slicing with and without the Use of EDFAs.....	49
4.1 System Description.....	49
4.1.1 Signal Power.....	51
4.1.2 Modulation	52
4.1.3 Photodetection	53
4.2 Performance	56
4.2.1 SNR in Absence of Thermal Noise	56
4.2.2 BER in Absence of Thermal Noise	58
4.2.3 Numerical Calculations.....	60
LED Power	61
Optical Filter Bandwidth (Number of Modes)	63
EDFA Gain and Noise Factor	64
LED Extinction Ratio	65
Discussion	66
4.2.4 Comparison with the Gaussian approximation	67
4.3 Thermal Noise	70

4.4 Number of Channels in a WDM applications.....	71
4.5 Conclusion	73
5. Experimental Setup	74
5.1 General Description.....	74
5.2 LED Transmitter	75
5.2.1 Output Power	76
5.2.2 Power Spectrum.....	77
5.2.3 Electrical Response	78
5.2.4 Optical Rise and Fall Times	80
5.3 Optical Link	83
5.3.1 Input Filter	83
5.3.2 Output Filter	85
5.3 EDFAs.....	86
EDFA Gain and Inband ASE	86
5.4 Optical Receiver.....	92
5.4.1 BNR OC12 Receiver.....	93
5.4.2 Electrical Response	93
5.4.3 Sensitivity	93
5.5 Conclusion	96
6. Experimental Results.....	97
6.1 Power Budget	97
6.2 Noise Analysis.....	98
6.3 BER Measurements.....	99
6.3.1 EDFA Input Power	100
6.3.2 EDFA Characteristics.....	104
Noise Factor.....	104
Gain	106
6.3.3 Optical Bandwidth.....	108
6.4 Discussion.....	110
6.4.1 WDM Application.....	111
6.5 Conclusion	113
7. Conclusion	114
7.1 Overview of the Results.....	114
7.2 System Improvements	115

7.3 Future Work.....	116
References	117
Appendix 2A: Bandwidth Definitions	122
Appendix 2B: Expressions for the Number of Modes.....	123
Appendix 4A: Decision Threshold Derivation for the Negative Binomial PDF	124
Appendix 4B: Program Listings	126
Appendix 5A: Veritech Amplifier Information.....	140
Appendix 5B: Mas-Tech LED Information.....	141
LED Specifications:.....	141
LED Hardware.....	142
Drive Circuit.....	142
TEC Control.....	142
Appendix 5C: BT&D, SHF and Mini-Circuit Filter Information.....	145
BT&D Photodetector.....	145
SHF Amplifier.....	146
Mini-Circuit Filter	147
Appendix 5D: Characteristics of Attenuators	148
JDS Fitel VA4 Attenuator	148
JDS Optics 7000 Attenuator.....	148
Appendix 5E: TRILabs EDFAs Information.....	149
Appendix 5F: BNR OC12 Receiver Information	150
Appendix 6A: Program Listings	152

List of Tables

Table 6.1: Power budget results.....	98
Table 6.2: WDM system link power budget	112
Table 2A.1: Bandwidth definitions	122
Table 2B.1: Expressions for the number of modes.....	123

List of Figures

Figure 1.1: Illustration of spectral slicing. Here an optical filter having a periodic transmittance is used to generate a series of slices from the spectrum of a broad LED.	5
Figure 1.2: General block diagram of a FDM system.....	6
Figure 1.3: Block diagram of the carrier generator	7
Figure 1.4: Block diagram of the optical receiver.	9
Figure 2.1: Relation between the autocorrelation function and the power spectral density (Taken from Saleh and Teich [13]). The electric field, the autocorrelation function and the spectrum are shown for the case of a light source having a short coherence.....	16
Figure 2.2: (a) Constant optical power and the corresponding random photon arrival times.(b) Time varying optical power and the corresponding random photon arrival times. (Taken from Saleh and Teich [13])	18
Figure 2.3: Poisson (a) and Bose-Einstein (b) distributions plotted with the mean number of photons as a parameter.	23
Figure 2.4: Negative binomial distribution plotted with μ and N as parameters. (a) N=1, (b) 1.5, (c) 2, (d) 5, (e) 100.	27
Figure 2.5: Plots of the parameter N as a function of the ratio	28
Figure 3.1: Illustration of the birth, death and immigration processes of a BDI medium and their physical correspondence in EDFA amplification.	32
Figure 3.2: Input-output relationship for a BDI medium treated as a system.....	36
Figure 3.3: Plot of Equation (3.40) for N=7.5 and $\mu=8$ with the interaction time t as a parameter.	40
Figure 3.4: Plot of the ratio of the output to the input standard deviations for the case where N=7.5 and $\mu=8$ as a function of the interaction time t.....	41

Figure 3.5: Plot of Equation (3.40) for $t=0.29$ and $N=7.5$ for different values of the input mean	42
Figure 3.6: Plot of the ratio of the output to the input standard deviations as a function of the interaction time t for $N=7.5$ with the input mean as a parameter.	42
Figure 3.7: Plot of Equation (3.40) for $t=0.29$ and $=8$ for different values of the number of modes N	43
Figure 3.8: Plot of the ratio of the output to the input standard deviations as a function of the interaction time t for $=8$ with the number of modes N as a parameter.....	43
Figure 3.9: Plot of the ratio of the output to the input standard deviations as a function of the input mean for $t=0.29$ with the number of modes N as a parameter.....	44
Figure 4.1: Two designs of WDM transmission systems using spectral slicing. In (a) LEDs are directly modulated (DMs) and in (b) external modulators (EMs) are used.....	50
Figure 4.2: Spectral slicing system under study. It is composed of an LED, an EDFA, an optical filter and an optical receiver.....	50
Figure 4.3: Illustration of spectral slicing of a broad LED with a narrow optical filter	51
Figure 4.4: (a) NRZ and (b) RZ signals.....	53
Figure 4.5: Plot of the receiver transfer function for different values of the roll-off factor.	55
Figure 4.6: Illustration of the method for calculating the BER.....	59
Figure 4.7: BER curves as a function of the optical power at the receiver for different LED power . ($r=100$, $G=30$ dB, $=1.5$ and $N=53$)	61
Figure 4.8: BER floor as a function of the LED power . ($r=100$, $G=30$ dB, $=1.5$ and $N=53$).....	62
Figure 4.9: BER floor as a function of the number of modes N . ($=10$ μ W, $r=100$, $G=30$ dB and $=1.5$)	63
Figure 4.10: BER floor as a function of the EDFA gain G . ($=10$ μ W, $r=100$, $=1.5$ and $N=53$).....	64

Figure 4.11: BER floor as a function of the EDFA noise factor . ($=10 \mu\text{W}$, $r=100$, $G=30$ dB and $N=53$).....	65
Figure 4.12: BER floor as a function of the LED extinction ratio r . ($=10 \mu\text{W}$, $G=30$ dB $=1.5$ and $N=53$)	66
Figure 4.13: Comparison of the BER floors for different value of LED power . ($r=100$, $G=30$ dB, $=1.5$ and $N=53$)	67
Figure 4.14: Negative binomial (solid) and Gaussian (dashed) PDFs and their decision thresholds.	68
Figure 4.15: Comparison of the BER curves as a function of LED power with the number of modes as a parameter. Negative binomial (solid), Gaussian approximation (dashed) ($r=100$, $G=30$ dB, $=1.5$).....	69
Figure 4.16: Comparison of BER curves as a function of the number of modes with this time the LED power as a parameter. ($r=100$, $G=30$ dB, $=1.5$)	70
Figure 4.17: Effect of the thermal noise on the noise distribution.....	71
Figure 4.18: Illustration of perfect spectrum slicing of an LED followed by an EDFA in the case where the LED power spectrum is assumed flat over the EDFA bandwidth.....	72
Figure 5.1: Block diagram of spectral slicing setup.....	75
Figure 5.2: LED transmitter block diagram	75
Figure 5.3: Setup for L-I curve measurements.....	76
Figure 5.4: L-I curves of the Mas-Tech LED for different temperatures.	76
Figure 5.5: Setup for the LED power spectrum measurements	77
Figure 5.6: Mas-Tech LED spectra measured in the conditions specified by the manufacturer (100 mA, 25 °C) and in the operating conditions (64 mA, of 5 °C).	78
Figure 5.7: Setup for the frequency response measurement	79
Figure 5.8: Mas-Tech LED frequency response.....	79

Figure 5.9: Setup for the rise and fall time measurements	80
Figure 5.10: Waveforms (a) Pattern generator, (b) Veritech amplifier and (c) LED through the BT&D photodetector.....	81
Figure 5.11: Mas-Tech LED rise (a) and fall (b) times.....	82
Figure 5.12: Block diagram of the optical link.....	83
Figure 5.13: Setup for the measurement of the TB1570 transmittance	84
Figure 5.14: Transmittance of the TB1570 filter at 1537 nm	84
Figure 5.15: Transmittance of the TB1500B filter at 1537 nm.....	85
Figure 5.16: Measurement setup for EDFA gain using the maximum ASE method.....	87
Figure 5.17: Measurement setup for the EDFA gain using the polarization method.	87
Figure 5.18: Visualization of the polarization method.....	88
Figure 5.19: Gain measurement (a) EDFA #R0302, (b): EDFA #R0303.....	89
Figure 5.20: Results for the ASE measurements. (a) EDFA #R0302	90
(b) EDFA #R0303	90
Figure 5.21: Noise factor for (a) EDFA #R0302 and (b) #R0303.	92
Figure 5.22: BNR OC12 receiver sensitivity measurement setup.	93
Figure 5.23: LED optical output waveform (a) and eye diagram (b) as detected by the BNR OC12 receiver.....	94
Figure 5.24: BNR OC12 receiver sensitivity curve. (solid line: actual, dashed line: theoretical)	95
Figure 6.1: Setup for the power budget measurement.....	97
Figure 6.2: Equivalent mean square noise photocurrents plotted as a function of the optical power at the receiver.	99

Figure 6.3: BER measurement setup	100
Figure 6.4: BER curves as a function of the optical power at the OC12 receiver with the input power to the EDFA as a parameter. (EDFA R0303 @ 160 mA, gain G=33 dB, noise factor =2.8, polarization splitter used, number of modes N=280).....	101
Figure 6.5: Calculated and measured BER Floors as a function of input power to the EDFA for linealy polarized and unpolarized light. (EDFA gain G=33 dB, noise factor =2.8)	102
Figure 6.6: BER curves as a function of the optical power at the OC12 receiver with the input power to the EDFA is a parameter. (EDFA R0303 @ 160 mA, gain G=33 dB, noise factor =2.8, polarization splitter removed, number of modes N=560)	103
Figure 6.7: BER curves as a function of the optical power at the OC12 receiver with the input power to the EDFA as a parameter. (EDFA R0302 @ 160 mA, gain G=28 dB, noise factor =2.5, polarization splitter removed, number of modes N=560)	105
Figure 6.8: Comparison of the BER floors as a function of the input power to the EDFA obtained with EDFA R0302 @ 160 mA (=2.5) and R0303 @ 160 mA (=2.8) (polarization splitter removed, N=560).....	105
Figure 6.9: BER curves as a function of the optical power at the OC12 receiver with the input power to the EDFA as a parameter. (EDFA R0302 @ 120 mA, G=25 dB, =2.4, polarization splitter removed, N=560).....	106
Figure 6.10: Comparison of the BER floors as a function of the input power to the EDFA obtained with EDFA R0302 operated with a pump current of 160 mA (G=28 dB) and 120 mA (G=25 dB).	107
Figure 6.11: Comparison between the BER curves measured as a function of the optical power at the receiver obtained when the EDFA R0302 is operated in the linear and the saturated regimes. (power splitter removed N=560).....	108
Figure 6.12: BER curves as a function of the optical power at the OC12 receiver with the input power to the EDFA as a parameter using the EDFA R0302 @ 120 mA and the output Queensgate QMF filter. (gain G=25 dB, noise factor =2.4, polarization splitter re	109

Figure 6.13: Comparison of the BER floor as a function of the number of modes for an input power to the EDFA of about -36 dBm using the EDFA R0302 @ 120 mA (gain G=25 dB, noise factor =2.4, polarization splitter removed)	110
Figure 5A.1: Veritech VMA3k10C-232 amplifier frequency response	140
Figure 5B.1: Mas-Tech LED E15D1-002 power spectrum.....	141
Figure 5B.1: Simplified version of the Mas-Tech LED driver	143
Figure 5B.2(a): Thermistor bridge . (b) TEC comparator	143
Figure 5C.1: BT&D photodetector electrical frequency response	145
Figure 5C.2: SHF 90 P amplifier frequency response.....	146
Figure 5C.3: Mini-Circuit SLP-850 filter frequency response	147
Figure 5E.1: Schematic of TR Labs EDFA packages.....	149
Figure 5F.1: Schematic of the BNR OC12 receiver.	150
Figure 5F.2: BNR OC12 receiver frequency response. (Bruce Beggs, BNR Ottawa)....	151

List of Symbols

$a(t)$:	Birth rate
$b(t)$:	Death rate
B :	Bit rate
B_o :	Optical bandwidth; Optical filter bandwidth
B_e :	Detection bandwidth; electrical bandwidth
B_{EDFA} :	EDFA gain bandwidth
B_{LED} or $\Delta\nu_{LED}$:	LED optical bandwidth
B_{OF} or $\Delta\nu_{OF}$:	Optical filter bandwidth
$B(n, N, \bar{n})$:	Negative binomial PDF
$c(t)$:	Immigration rate
e or q :	Electron Charge
F :	Fabry-Perot finesse
G :	EDFA gain
G_o :	Small signal gain
$g(\tau)$:	Normalized autocorrelation function
$G(\tau)$:	Autocorrelation function
$G_{in}(z)$	PGF of the input of the BDI medium
$G(z, t)$:	PGF of the output of the BDI medium
$G_{BD}(z, t)$:	PGF of the birth and death processes
$G_I(z, t)$:	PGF of the immigration process
h :	Planck's constant = 6.63×10^{-34} J.s
$h(t)$:	BDI medium function
$h_d(t)$:	Photodetector impulse response function
$h_r(t)$:	Optical receiver impulse response function
$H(f)$:	Optical receiver transfer function
$i(t)$:	Detector photocurrent
$\langle i \rangle$:	Average photocurrent
I_s :	Signal equivalent mean photocurrent
I_{sp} :	Spontaneous emission equivalent mean photocurrent
I_{th} :	Thermal noise equivalent mean photocurrent
$I(r, t)$:	Light intensity
k :	Boltzmann's Constant = 1.381×10^{-23} J/K
$k(t)$:	BDI medium function

l :	EDFA length
L :	Optical fiber loss
m , or ρ :	Polarization coefficient
n :	Number; photon number
$\langle n \rangle$ or \bar{n} :	Mean number; mean photon number
$n(r, t)$:	Photon flux density
\bar{n}_{in} :	Mean number of particles at the input of the BDI medium
$\bar{n}_{on}, \bar{n}_{off}$:	Average number of photon for the On and Off states, respectively
$\bar{n}(t)$:	Mean number of particles at the output of the BDI medium
N :	Number of modes
N_{ex} :	Excess noise equivalent mean square photocurrent
N_{sp} :	Spontaneous emission or noise factor
N_{shot} :	Shot noise equivalent mean square photocurrent
N_{s-sp} :	Signal-spontaneous beat noise equivalent mean square photocurrent
N_{sp-sp} :	Spontaneous-spont. beat noise equivalent mean square photocurrent
N_{th} :	Thermal noise equivalent mean square photocurrent
$p(n)$:	PDF; photon number distribution
$p_{in}(n)$:	PDF of the input of the BDI medium
$p(n, t)$:	PDF of the output of the BDI medium
$P(t)$:	Optical power
P_{av} :	Average optical power
P_m :	Minimum power of fundamental limit of detection
P_r :	Received optical power
P_s or P_{sig} :	Signal power
P_{sp} or P_{ASE} :	Amplified spontaneous emission power
P_{LED} :	LED optical power
P_{in} :	EDFA input power
P_{sat} :	EDFA saturation power
P_{total} :	Total power
Q :	Parameter of the Gaussian approximation for the BER
r :	Position in space; extinction ratio
R_L :	Equivalent optical receiver noise resistor
s :	Ratio of the input to the output BDI medium standard deviation
S :	Signal equivalent mean square photocurrent
$S(\nu)$:	Power spectral density or power spectrum
$S_{LED}(\nu)$:	LED power spectrum

$S_{OF}(v)$:	Optical filter transmittance
t :	Time; interaction time of particles in BDI medium
T :	Detection or observation time; bit time; temperature
$T(v)$:	Fabry-Perot filter transmittance
T_m :	BER measurement time
T_{max} :	Fabry-Perot maximum transmittance
$u(r, t)$:	Optical field
$U(r, t)$:	Complex function describing the optical field
W :	Mean photon number arriving in time interval $(0, T)$
$Z(z, t; \tau)$:	PGF of the BDI medium
α :	Proportionality constant
β :	Roll-off factor
$\delta(W)$:	Delta function
$\Delta\lambda$:	Linewidth; optical bandwidth in term of wavelength
$\Delta\nu$:	Linewidth; FWHM optical bandwidth; optical bandwidth in term of frequency
$\Delta\nu_{ER}$:	Equivalent rectangular bandwidth
$\Delta\nu_c$:	Bandwidth defined as the inverse of the coherence time
γ_o :	Decision threshold
λ :	Wavelength
μ_{in}, μ_{out} :	Input and output EDFA coupling coefficients, respectively
η :	Detector quantum efficiency
τ_c :	Memory or coherence time
σ_n^2 :	Variance; photon number variance
ν :	Frequency
ν_F :	Free spectral range
$\sigma^2(t)$:	BDI output variance
σ_i^2 :	Photocurrent variance

List of Abbreviations

AGC	Automatic Gain Control
AC	Alternating Current
ASE	Amplified Spontaneous Emission
BDI	Birth-Death-Immigration
BER	Bit Error Rate
BERT	Bit Error Rate Tester
DC	Direct Current
DFB	Distributed Feedback
DIP	Dual In-Line Package
DM	Direct Modulator
DWDM	Dense Wavelength Division Multiplexing
EDFA	Erbium Doped Fiber Amplifier
EM	External Modulator
FC/APC	Fiber Connector/ Angular Physical Contact
FDM	Frequency Division Multiplexing
FSR	Free Spectral Range
FWHM	Full Width Half Maximum
GPIB	General Purpose Interface Bus
IF	Intermediate Frequency
LED	Light Emitting Diode
NRZ	Non-Return-to-Zero
OC12	Optical Carrier 12
OOK	On-Off Keying
OPM	Optical Power Meter
PDF	Probability Density Function
PGF	Probability Generating Function
PIN	P-Intrinsic-N
PSD	Power Spectral Density
RZ	Return-to-Zero
SNR	Signal-to-Noise Ratio
TEC	Thermoelectric Cooler
VOA	Variable Optical Attenuator
WDM	Wavelength Division Multiplexing or Multiplexer

1. Introduction

Spectral slicing of a broad incoherent light source was demonstrated for the first time in 1988 by Reeve et al. [1]. This technique was seen as a way to bypass the need for good quality laser sources acting as optical carriers for wavelength division multiplexing (WDM) or frequency division multiplexing (FDM) transmission. It consists of taking slices in the spectrum of a broad source by adequate filtering. Each slice then becomes an optical carrier that can be modulated at a high bit rate, multiplexed and sent through an optical fiber link. In their experiment, Reeve et al. achieved a four-channel system operating at 2 Mb/s over 2.2 km using a light emitting diode (LED) as a source. Recently, FDM transmission with as many as 100 channels modulated at several hundreds of Mb/s over tens of kilometers have been achieved using a set of distributed feedback (DFB) lasers [2]. Some experiments of the same kind but using spectrally sliced carriers combined with optical amplifiers have also been reported [3-4]. Although the fundamental limit of this method regarding the number channels that can be placed side by side before reaching an unacceptable signal-to-noise ratio (SNR) and/or bit error rate (BER) has been investigated [5], no complete explanation has yet been given. The aim of this work is to get a better understanding of spectral slicing as well as look at its fundamental limit.

This chapter gives an introduction to the vast and continuously growing field of optical communications and to spectral slicing. It is divided into four parts. First, an overview of the field of optical communication is presented. Then, a description of the project is given along with its motivations. In the third part, we explore different important aspects of spectral slicing that will have to be considered in our analysis. Finally, the chapter will be summarized with a conclusion.

1.1 Overview of Optical Communications

In principle, for a communication system, the greater the carrier frequency is, the larger the available transmission bandwidth and consequently, the larger its capacity for carrying information is. For example, communications at optical frequencies gives an increase in the potential usable bandwidth by a factor 10^4 over high frequency microwave transmission [6]. Furthermore, the development of optical fiber technology has provided a very good guiding medium for optical communications. Single-mode optical fibers have a low loss region extending over more than 30 THz [7]. From an

engineering point of view, this represents an incredible potential. For these reasons, a lot of effort has been made in the last decade to exploit this potential.

1.1.1 Types of Communication Systems

Optical communication systems can be classified according to the type of modulation they used. There are two basic types of modulation: field and intensity modulation. In the majority of optical fiber systems, semiconductor sources such as LEDs and laser diodes are used and intensity modulation is achieved by varying their injection current. This is called direct modulation. Another way to achieve intensity modulation is to use external modulators. These devices are also used in conjunction with semiconductor sources. They are essentially high-speed electro-optic shutters. The modulation can be analog or digital. In digital systems, signals are represented by a sequence of 0's and 1's called bits. If intensity modulation is used, each bit is represented by the presence or absence of a pulse of light. This type of modulation is called on-off keying (OOK). There exist other types of analog and digital modulation that can be impressed on either the amplitude, the frequency, the phase, or the polarization of light. For further details, the reader can consult the book by Stremler [8].

1.1.2 Multiplexed Transmission

One way to exploit the available optical bandwidth is to use multiplexed transmission. Multiplexing is defined as the transmission and retrieval of more than one signal through the same communication link. Multiplexing of signals can be performed in either the time or the frequency domain. In the time domain, different time slots are allocated to samples of the different signals while in the frequency domain, carriers of distinct frequencies are modulated by different signals. For optical systems based on intensity modulation and multiplexing in the frequency domain, three multiplexing techniques are being explored: Wavelength Division Multiplexing (WDM), Frequency Division Multiplexing (FDM) and Dense Wavelength Division Multiplexing (DWDM). Some distinctions are useful to make about these techniques. Brackett [7] indicates that it is common to refer to DWDM for systems when the wavelength spacing is on the order of 1 nm and to optical FDM for systems where the frequency spacing is on the order of the signal bandwidth or bit rate. He also mentions that WDM usually refers to systems where the channel bit rate is much smaller than the carrier spacing by typically several tens of nm. Those distinctions give a feel for the degree of complexity involved. For a good

review on FDM transmission and networks the reader can consult the paper by Brackett [7].

Multiplexed transmission in the frequency domain requires the allocation of one carrier per channel. These carriers must have a narrow bandwidth, be stable and their separation must match the multiplexer passband. Several good quality laser diodes designed to operate at precise frequencies matching the multiplexer can play the role of carriers. Several experiments using this technique have been reported [9-11]. The main disadvantage of this method is that it requires very high quality sources whose wavelengths must be selected to match the different multiplexer channels. In fact, as the number of signals increases and thus the spacing between carriers diminishes, the characteristics of the sources become critical. Those sources are commercially limited and consequently very expensive. Another technique known as spectrum slicing is also being explored. This consists of isolating narrow spectral slices from the emission spectrum of broad sources such as LEDs and SLDs (Superluminescent Diodes). The spectral slices are obtained by the wavelength division multiplexer (also called WDM) passband filters and are then modulated. This approach has the advantage of being very simple. However, spectrum slicing is inefficient from a power-budget standpoint since a very small fraction of the source power is coupled through the multiplexer [12].

1.1.3 Detection and Performance

There are two standard types of detection used in optical communication systems: coherent and direct (or incoherent) detection. Coherent detection involves the mixing of the incoming signal with a local optical oscillator to translate it into a baseband signal (homodyning) or into a signal at an intermediate frequency (IF) (heterodyning). This signal can then be processed using standard filtering techniques. Coherent detection usually requires knowledge of the phase and the frequency content of the incoming signal which is not easy to obtain in practice. For this reason, the majority of optical fiber communication systems use direct detection. In direct detection, only the variations in the optical power level (or intensity) are monitored and no information is carried by the phase and frequency of the signal.

The direct detection of an intensity modulated carrier is basically a photon counting process where each detected photon is converted to an electron-hole pair by a semiconductor photodetector. The random nature of the photogeneration and photodetection processes adds undesirable fluctuations to the useful signal. These fluctuations are commonly called noise. Consequently, the performance of a system

depends on the signal level relative to the noise. In analog systems, performance is defined in terms of Signal-to-Noise Ratio (SNR). In digital system, it is defined in terms of Bit Error Rate (BER), i.e. the probability of error per bit. In the best conditions, when an on-off keying (OOK) modulation is used, it takes at least 21 photons per bit to achieve a BER of 10^{-9} [13]. This is known as the quantum limit of direct detection. For less ideal conditions and especially in the presence of noise, this limit can be significantly higher.

1.1.4 Optical Amplifiers

There are two types of optical amplifiers: the semiconductor type and the fiber type. The fiber type optical amplifiers have an important advantage over the semiconductor type in that they are polarization insensitive. They simply consist of a length of silica fiber doped with rare earth ions. Rare earth doped and especially erbium doped fibers have recently received a growing attention from the scientific community because of their potential for low cost, easily produced sources and amplifiers at wavelengths of interest for optical communications [14]. When associated with silica, the erbium atom exhibits a broad fluorescence line of width about 40 nm centered near 1550 nm [15]. In addition, erbium has two absorption lines free from excited state absorption at 980 and 1480 nm which allow efficient pumping by semiconductor lasers. The amplification property of erbium doped fibers comes from stimulated atomic state de-excitation. By this process, a signal at a wavelength near 1550 nm is amplified as it travels through the fiber. Gain values as high as 37 dB can be achieved by design optimization [15]. In addition to the amplified signal, however, there is also a small amount of noise added which is due to the amplified spontaneous emission inside the amplification medium. More information on fiber amplifiers can be found in the papers by Urquhart [14], Desurvire [15] and Ainslie [16].

1.2 Project Description

In this project, the fundamental limit of spectral slicing is investigated. To accomplish this, we are going to study the noise characteristics of spectrally filtered LED emission before and after optical amplification by an erbium doped fiber amplifier (EDFA). The focus will be put on the properties of one single spectrally sliced optically amplified carrier. This will allow us to get a better understanding of both the spectral slicing process and the EDFA amplification mechanism and should determine if the spectral

slicing method can be used to generate optical carriers in an optical FDM or WDM application.

The motivation behind this project is to offer an alternative to the need for several semiconductor laser sources with very tight specifications on the operating frequency generally required in FDM systems.

This research project was supervised by Dr. Jan Conradi and took place at Telecommunications Research Laboratories (TRLabs). It was supported by the Natural Science and Engineering Research Council (NSERC), Bell Northern Research (BNR) and TRLabs through the NSERC/ BNR/TRLabs Chair in Fiber Optic Communication at the University of Alberta.

1.3 Spectral Slicing

The principle of spectral slicing is illustrated in Figure 1.1. It consists generating optical carriers by taking slices in the spectrum of a broad incoherent light source such as an LED using one or several optical filters. Each carrier can then be separately modulated at a high bit rate, multiplexed and transmitted through an optical fiber link. The optical filtering can be accomplished by a series of optical filters or by a Fabry-Perot type filter which has a periodic transmittance as illustrated in Figure 1.1.

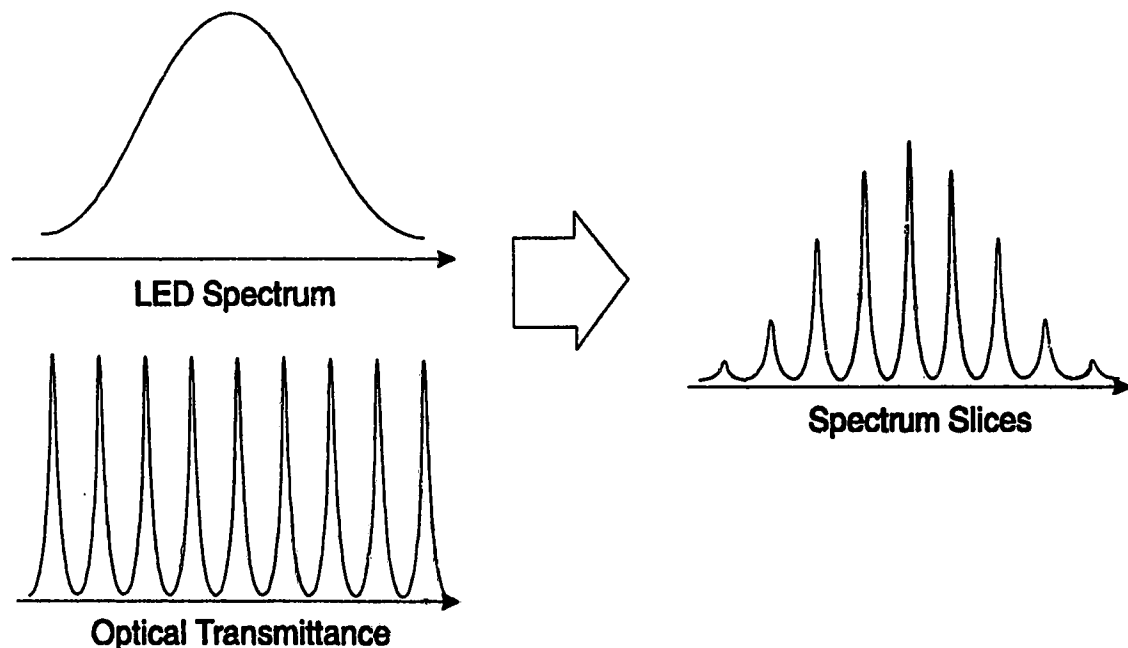


Figure 1.1: Illustration of spectral slicing. Here an optical filter having a periodic transmittance is used to generate a series of slices from the spectrum of a broad LED.

1.3.1 Optical FDM System

Figure 1.2 shows the general block diagram of an optical FDM system using spectral slicing. It is composed of a carrier generator, a demultiplexer, a series of modulators and a multiplexer, on the transmission side, and a demultiplexer and a series of receivers on the reception side. The carrier generator provides a set of optical carriers using the technique described above. Then, each of these carriers is separated from the others by a demultiplexer and intensity modulated with an external modulator. The N resulting outputs are then recombined by a multiplexer and transmitted through an optical fiber link. On the reception side, the N outputs are demultiplexed and detected by a series of optical receivers.

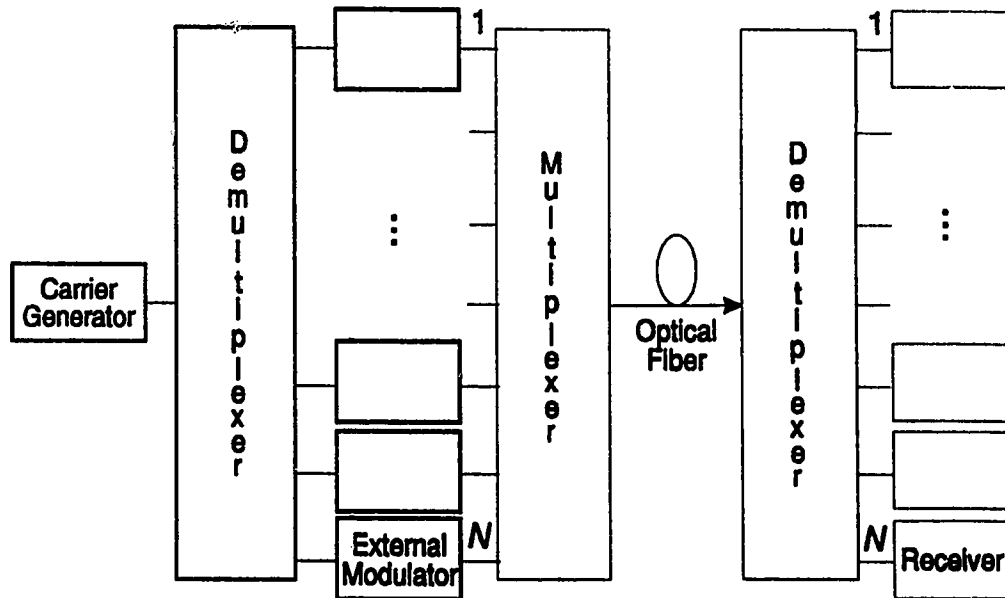


Figure 1.2: General block diagram of a FDM system.

1.3.2 Carrier Generator

The carrier generator is the most important part in this project because it is where the spectral slicing occurs. It is composed of three parts: an LED, an EDFA, and an optical filter as shown in Figure 1.3.

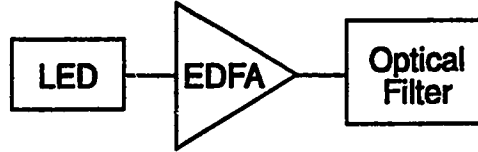


Figure 1.3: Block diagram of the carrier generator

LED Source

The source used for the carrier generator is an LED. It is a forward-biased semiconductor p-n junction with a large radiative recombination rate arising from externally injected carriers. It is essentially a device that converts current into light. It is called an incoherent light source since its emission is just composed of spontaneous emission of photons. LEDs are available in a variety of wavelengths including around 1.3 and 1.55 μm in either surface-emitting or edge-emitting configurations. Typical LEDs can couple a few tens of microwatts in a single mode optical fiber. Devices operating in the 1.3 μm range generally offer more power than those operating in the 1.55 μm . Their optical spectrum is approximately Gaussian with a FWHM (Full Width Half Maximum) bandwidth in the range of 70 to 100 nm. The reader may consult the book by Saleh and Teich [13] and by Petermann [17] for more information on LEDs.

EDFA

An EDFA is used in the carrier generator to increase the LED output power before it is filtered. As mentioned earlier, EDFAs are fiber traveling wave optical amplifiers for which their amplification properties come from their erbium dopant. When light signals pass through EDFAs, amplification occurs and a small amount of amplified spontaneous emission is added. This amplified spontaneous emission (ASE) occurring inside the gain medium adds noise to the signal when detected. The ASE power can be calculated as follows:

$$P_{sp} = m_p N_{sp} (G-1) h\nu B_o \quad (1.1)$$

where m_p is called the polarization coefficient, N_{sp} is the EDFA noise factor, $h\nu$ is the photon energy in Joule and B_o , the EDFA optical bandwidth. The noise factor is a very important parameter for an optical amplifier. It plays the role of noise figure. The parameter m_p accounts for the polarization of light. It can take a value between 1 and 2. In the detection of an optically amplified signal, additional noise is created by the beating

of the signal with the ASE. This phenomenon has been extensively studied by Olsson [19]. The gain of an EDFA is determined by the input signal power and a parameter called the saturation power. It can be approximated by the following transcendental equation:

$$G = G_o \exp \left[(1-G) \left(\frac{P_{in}}{P_{sat}} \right) \right] \quad (1.2)$$

where G_o is the small signal gain, P_{in} is the input signal power and P_{sat} is the saturation power. The saturation power depends on the fiber length, the erbium concentration, the pump power. For small input signal power, the gain is a constant equal to G_o . In this case, the EDFA is said to operate in the linear regime. For inputs greater than the saturation power, the gain decreases and the EDFA is said to operate in saturation. Several other properties of EDFAs are treated in the book edited by France [20].

Optical Filter

The optical filter is used to slice the LED spectrum. Several types of optical filters can be used to accomplish the spectral slicing. However, the most interesting is the Fabry-Perot because of its periodic transmittance. This is essentially a resonant cavity most often air-filled with partially reflecting mirrors at both ends. Light entering the cavity makes a series of round trips and, at every pass, it is partially transmitted. The total transmission is determined by summing the transmitted light amplitudes. The transmittance of such filters is defined as a function of frequency as follows [13]:

$$T(\nu) = \frac{T_{max}}{1 + (2F/\pi)^2 \sin^2(\pi\nu/\nu_F)} \quad (1.3)$$

where F is called the finesse, and ν_F is the free spectral range (FSR). T_{max} is the maximum transmission and depends on the reflection and transmission coefficients of the mirrors. It also indicates the insertion loss of the filter. The FSR defines the spectral spacing between the adjacent transmission peaks and depends on the cavity length and the refractive index of the cavity. The FWHM bandwidth $\Delta\nu$ of the transmission peaks is related to the FSR and the finesse by the following formula:

$$\Delta\nu = \frac{\nu_F}{F} \quad (1.4)$$

Tunable devices are available with bandwidth as narrow as a few tens of kilohertz and very low insertion loss. More information about Fabry-Perot filters can be found in the papers by Gornall [21] and Miller [22]

1.3.3 Optical Receiver

The optical receiver is used to detect the modulated optical carriers generated by filtering the EDFA amplified LED emission. It is an important sub-system of our project since it is where the detection process occurs. As shown in Figure 1.4, the optical receiver is composed of three parts: a photodetector, one or more amplifiers and an electrical filter.

A photodetector is generally a semiconductor device that converts a photon flux to an electron flux or electric current. It accomplishes essentially the inverse function of a semiconductor source. A photodetector is characterized by three factors: its responsivity, electrical bandwidth and its noise current. The responsivity describes how efficient the photodetector is in converting an optical signal to a photocurrent or equivalently, photons to electrons. Good photodetectors have responsivity of 0.7 to 0.8 A/W. The electrical

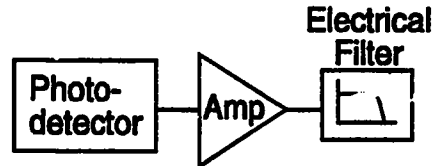


Figure 1.4: Block diagram of the optical receiver.

bandwidth of a photodetector is a measure of how fast it responds to a change in the optical signal. The larger the bandwidth, the better the photodetector is. Today, photodetectors with bandwidths of several gigahertz are available commercially. Finally, the noise current specifies the limit on the lower detectable power level of the photodetector.

The photodetector is generally followed by an amplification stage and an electrical filter. The overall performance of this set of components is given by the receiver sensitivity. It is the power level required at the photodetector to achieve a certain performance criterion. In digital communications, the criterion commonly used is a BER of 10^{-9} for a given bit rate. The sensitivity is generally limited by the noise of the electrical components of the receiver. Several configurations can be adopted for the receiver including high, low and transimpedance front ends to optimize the performance in a particular application. This is treated in detail by Williams [23]. For more information about semiconductor devices, the reader may consult the book by Kressel [24].

1.3.4 Detection of Light

The random nature of the photon emission process creates undesirable fluctuations in the optical signal which upon detection add to the useful signal. Additional fluctuations are created by the movement of electrical charges in circuit elements of the optical receiver. These fluctuations are all regrouped under the term noise.

Electrical Noise

The electrical noise results from the thermal motion of charges in dissipative elements and transistors of an electrical circuit. It is generally gaussian in nature and is always present in an optical receiver. This is discussed in detail by Saleh[13, 25] and Teich. This noise degrades the sensitivity of the optical receiver and contributes to the degradation of the performance of the system.

Photon Noise

For large signal levels, the receiver noise can be neglected and the photon noise is dominant. This noise is due to the random arrival of photons on the photodetector. The statistical distribution of the number of photons arriving on a photodetector depends on the nature of the light source. For coherent light, for example, the arrival of photons can be seen as the independent occurrence of random events at a rate proportional to the optical power. In this case, the photon number statistics follows a Poisson distribution. However, for partially coherent or incoherent light, the arrival of photons is no longer a sequence of independent events; therefore, the photon statistics are different. This is the case, for example, of thermal light whose photon number statistics follows a Bose-Einstein distribution.

For coherent light flux, the number of photons n counted in an interval T follows a Poisson distribution given by:

$$p(n) = W^n \frac{e^{-W}}{n!},$$

where W represents the mean photon number arriving in a time interval $(0, T)$ and is defined as:

$$W = \frac{1}{h\nu} \int_0^T P(t) dt,$$

where

$P(t)$ is the optical power in Watts.

For partially coherent or incoherent light flux, the photon number will differ from the Poisson distribution. In particular, the photon number statistics of a spectrally sliced incoherent source such as an LED before and after amplification by an EDFA will probably differ from the Poisson distribution. This will be considered in detail in Chapters 2 and 3.

Quantum Limit

A simple calculation can be performed to determine the minimum power required in an optical carrier according to the quantum limit for detection. If we assume that the average number of photons at the detector in certain interval of time T (a pulse) is W , then the average power is given by:

$$P_{av} = h\nu \frac{W}{T} \text{ [Watts].}$$

As mentioned in Section 1.1.3, for a BER of 10^{-9} , the quantum limit for detection requires $W = 21$ photons. Assuming a digital system operating at $1.55 \mu\text{m}$ with a bit rate $B = 1/T = 1 \text{ Gb/s}$, the minimum power required is:

$$P_m \approx 3 \times 10^{-9} \text{ [Watts] (or -55 dBm).}$$

Multiplying this result by 10 provides margin of safety. Therefore, the minimum power required is 30 nW.

We can compare this result to the power of one spectral slice from an LED spectrum using an optical filter. Assuming that the optical filter FWHM $\Delta\lambda_{OF}$ is 0.5 nm, and that the LED has an output power P_{LED} of 10 μW and a FWHM $\Delta\lambda_{LED} = 100 \text{ nm}$, the power of one spectral slice P_{slice} can be approximated by:

$$P_{slice} \approx \frac{\Delta\lambda_{OF}}{\Delta\lambda_{LED}} P_{LED} \text{ [Watts].}$$

which gives:

$$P_{slice} = 50 \times 10^{-9} \text{ [Watts] (or -43 dBm).}$$

A slice power of 50 nW is more than the minimum power required by the quantum limit 30 nW. Therefore, based on this preliminary calculation, the method is feasible.

1.4 Conclusion

The first section of this chapter presented an overview of the vast and growing field of optical communications. This showed that scientists and engineers have tried to exploit the enormous potential of optical communications by using various techniques of

modulation, multiplexing and detection. In the second section, a description of the thesis project was given. The principal motivation behind the project is to offer an alternative to the semiconductor laser sources generally used as carriers in optical FDM systems. In the third section, the spectral slicing method was described along with the various components of the carrier generator using this technique. Then, we discussed the detection process and introduced the notion of noise with a special emphasis on photon noise. It was stated that the statistical distribution of the number of photons depends on the nature of the light source. Also, a simple calculation allowed the comparison of the power contained in one generated carrier using the proposed method to the minimum power for detection required by the quantum limit.

In conclusion, even though the simple calculation performed in the last section of this chapter showed the feasibility of the proposed method, further examinations are necessary in order to determine if this is a viable option to the currently used technology.

2. Statistics of Filtered Incoherent Light Sources

This chapter presents a review of the study of the statistical properties of light, a topic often referred to as the Theory of Optical Coherence [25]. A special emphasis is put on the case of filtered incoherent light which represents filtered LED emission. Most of the work on the Theory of Optical Coherence was accomplished in the late 50's and early 60's by pioneers like Mandel, Glauber, Wolf, Bédard and also Jakeman and Pike [26]. But the subject has re-emerged with the development of optical communications and since, several good books and review articles were published on this subject [13, 25-29].

The chapter is divided into three sections. First, the concept of randomness in light is introduced. Second, the statistics of some common light sources are discussed and in particular the case of filtered thermal light. Finally, a conclusion summarizes the chapter.

2.1 Statistical Properties of Light

Randomness in light is caused by inherent fluctuations of the source and/or of the medium through which light propagates. However, in this report, we are only interested in the fluctuations of the source and therefore, we assume no additional fluctuation caused by the medium. Depending on the nature of the source, light obeys a certain set of probabilistic laws which can be characterized by statistical averages. This section introduces the concept of randomness in light along with a set of useful statistical averages to characterize its behavior. The major part of this section is drawn from Chapters 10 and 11 of the book by Saleh and Teich [13].

2.1.1 Coherent and Partially Coherent Sources

Light sources that exhibit no fluctuations do not exist in reality. However, in the case where their fluctuations are negligible, they are called coherent sources and their electric fields are said to be deterministic. All other sources that exhibit fluctuations have a variable degree of coherence and are called partially coherent sources. These sources are said to have stochastic fields which can be represented by random functions of time and space.

An optical field can be defined as:

$$u(r, t) = \text{Re}\{U(r, t)\}, \quad (2.1)$$

where $U(r,t)$ is a complex function,
 r is the position in space,
 t is time,
and $\text{Re}\{.\}$ represents the real part.

$U(r,t)$ can take different forms depending on the nature of the light source. For example, for a perfectly coherent source (deterministic monochromatic light):

$$U(r,t) = U(r) \exp(j2\pi\nu t), \quad (2.2)$$

where ν is the light frequency,
and $U(r)$ is a deterministic function.

For a partially coherent source (random light), $U(r,t)$ is a random function of time and space but it can be characterized by a set of statistical averages.

2.1.2 Optical Intensity

The intensity of deterministic light is defined as the squared magnitude of the optical field:

$$I(r,t) = |U(r,t)|^2. \quad (2.3)$$

For monochromatic deterministic light, the intensity is independent of time but for random light, $U(r,t)$ is a complex random function and therefore the intensity is also random. In this case, the average intensity must be used and it is defined as:

$$I(r,t) = \langle |U(r,t)|^2 \rangle, \quad (2.4)$$

where $\langle . \rangle$ means ensemble average.

The optical intensity has the dimension of energy per (time \times area). It can therefore be associated to a photon flux density. Assuming that each photon carries an energy $h\nu$, the photon flux density $n(r,t)$ is:

$$n(r,t) = \frac{I(r,t)}{h\nu}, \quad (2.5)$$

where h is the Planck's constant (6.63×10^{-34} J.s).

Note that this equation represents the link between the classical and quantum theory of light.

2.1.3 Temporal Coherence and Spectrum

The autocorrelation function of a stationary complex random function $U(r,t)$ evaluated at a fixed point in space is defined as:

$$G(\tau) = \langle U(t) U(t+\tau) \rangle, \quad (2.6)$$

where, here again, $\langle \cdot \rangle$ means statistical average.

This function is also called temporal coherence function and is related to the optical intensity in the following way:

$$I = G(0). \quad (2.7)$$

Therefore one can define a normalized autocorrelation function which is insensitive to the intensity:

$$g(\tau) = \frac{G(\tau)}{G(0)} \quad \text{and} \quad 0 < g(\tau) < 1. \quad (2.8)$$

This function is a measure of the degree of temporal coherence of the optical field. The function $U(t)$ can also be characterized by a time scale representing its 'memory'. Fluctuations at points separated by a time interval longer than the memory time are considered independent. The function appears smooth over its memory time and exhibits fluctuations when observed over longer time intervals. The memory time also called the coherence time is defined as:

$$\tau_c = \int_{-\infty}^{\infty} |g(\tau)|^2 d\tau. \quad (2.9)$$

It is a common way to indicate the degree of temporal coherence of a field.

Another important statistical average that is the frequency domain equivalent of the autocorrelation function is the power spectral density (PSD) or simply spectrum. It is defined as the Fourier transform of the autocorrelation function:

$$S(\nu) = \int_{-\infty}^{\infty} G(\tau) \exp(-j2\pi\nu\tau) d\tau. \quad (2.10)$$

The PSD gives the frequency distribution of the power contained in an electrical field. Its relation to the autocorrelation function is illustrated for two different types of light source in Figure 2.1. In (a), the case of a light source having a short coherence time is depicted. As we can see, a short coherence time results in a broad spectrum. The case of a light source having a longer coherence time is shown in (b). A long coherence time corresponds to a narrow spectrum. We also notice that within the coherence time, the electric field appears to be correlated, i. e., each value is similar to its adjacent neighbors.

For the majority of optical fields, the spectrum of light occupies a more or less narrow band around a central frequency ν_0 . The spectral width or linewidth $\Delta\nu$ of a field is proportional to the inverse of its coherence time τ_c but can have several definitions. One

Removed due to copyright restrictions

Figure 2.1: Relation between the autocorrelation function and the power spectral density (Taken from Saleh and Teich [13]). The electric field, the autocorrelation function and the spectrum are shown for the case of a light source having a short coherence time in (a) and a longer one in (b)

common definition is the spectrum full width half maximum (FWHM). Another common one is the equivalent noise or rectangular bandwidth. It is defined as follows:

$$\Delta\nu_{ER} = \frac{P_{total}}{S_0} = \frac{\int_{-\infty}^{\infty} S(\nu) d\nu}{S_0} \quad (2.11)$$

where P_{total} is the total power contained in the field, $S(\nu)$ is the PSD of the field and S_0 its peak value. Another convenient definition for the linewidth of an optical field is as follows:

$$\Delta\nu_c = \frac{\left[\int_{-\infty}^{\infty} S(\nu) d\nu \right]^2}{\int_{-\infty}^{\infty} S^2(\nu) d\nu} \quad (2.12)$$

With this definition the linewidth $\Delta\nu_c$ is always equal to the inverse of the coherence time τ_c regardless of the shape of the optical spectrum $S(\nu)$ [13]. The relation between $\Delta\nu_{FWHM}$, $\Delta\nu_{ER}$, $\Delta\nu_c$ and τ_c is given in Appendix 2A for different spectrum shapes.

2.1.4 Spatial Coherence and Polarization

Just as for temporal coherence, a set of functions can be derived to characterize the coherence of an optical field in space. However, this will not be considered in our analysis.

In an optical communication system, we only observe the temporal effect of the photoelectrons as they are produced over the entire detector area [27]. Consequently, in the following, only the occurrences of the photon will be studied and the intensity $I(r, t)$ will be noted $I(t)$. In addition, the electric field will always be assumed to be either linearly polarized in one direction or simply unpolarized. An unpolarized electric field can be seen as a field having a random polarization.

2.1.5 Photon Number

The mean photon flux is associated with the optical intensity as follows:

$$n(t) = \frac{\int_A I(t) dA}{h\nu} = \frac{AI(t)}{h\nu} = \frac{P(t)}{h\nu}, \quad (2.13)$$

where A is the detection area and $h\nu$ is the photon energy.

For deterministic monochromatic light, the intensity is constant in time ($I(t) = I$) and $n(t)$ is given by:

$$n(t) = \frac{AI}{h\nu} = \frac{P}{h\nu}. \quad (2.14)$$

For non-monochromatic light, ν must be replaced by $\bar{\nu}$ representing the central light frequency.

The mean number of photons \bar{n} detected in the area A and during the observation time T is obtained by performing the following integral:

$$\bar{n} = \int_0^T n(t) dt. \quad (2.15)$$

For deterministic light, the optical intensity does not depend on time and \bar{n} is simply:

$$\bar{n} = n(t) T. \quad (2.16)$$

Due to its quantum nature, even if the intensity of light $I(t)$ is constant, the time of arrival of photons is governed by probabilistic laws. If a source emits photons at a constant rate (deterministic and monochromatic light), the probability density of detecting one photon at a certain point in space and during the observation time T is proportional to the intensity $I(t)$ at that point. The intensity $I(t)$ determines the mean photon flux density $n(t)$ and the properties of the light source determine the fluctuations in $n(t)$. If, for example, the optical power $P(t)$ varies with time, the density of random photon detections will follow the function $P(t)$ (see Figure 2.2). The mean photon flux is given by Equation (2.13) but the times at which photons are detected are random. Where the power is large,

Removed due to copyright restrictions

Figure 2.2: (a) Constant optical power and the corresponding random photon arrival times.(b) Time varying optical power and the corresponding random photon arrival times. (Taken from Saleh and Teich [13])

there are more photons arriving, on average, in a given time interval and where the power is small, there are less. Even if the power is constant, the times at which photons are detected are random and determined by the statistics of the source.

For a perfectly coherent source (deterministic and monochromatic light), the arrival of photons can be seen as the independent occurrences of random events at a rate proportional to the optical power (see derivation by Gagliardi and Karp [27], Chap. 4). In this case, the photon number is described by the well-known Poisson distribution given by:

$$p(n) = \frac{W^n \exp(-W)}{n!}, \quad (2.17)$$

where W is defined as:

$$W = \frac{1}{h\nu} \int_0^T P(t) dt = \frac{1}{h\nu} \int_0^T \int_A I(t) dA dt. \quad (2.18)$$

For coherent light, the quantity W (the normalized integrated intensity) is a constant and represents the mean number of photons \bar{n} in the interval of time $(0,T)$. But, for a partially coherent or incoherent light source, the intensity itself fluctuates randomly in time (and/or space) as does the optical power. This results in the integral W also being

random; therefore, additional averaging over W is required to determine the mean number of photons. In this case, the photon arrivals cannot always be considered as a sequence of independent events and the photon number distribution may differ from Poisson. If the fluctuations in the mean photon number W are described by a probability density function $p_w(W)$, the unconditional photon counting distribution for incoherent light can be obtained by averaging the conditional photon counting distribution $p(n|W)$:

$$p(n|W) = \frac{W^n \exp(-W)}{n!} \quad (2.19)$$

weighted by the probability density $p_w(W)$ over all the permitted values of W :

$$\begin{aligned} p(n) &= \int_0^{\infty} p(n|W)p_w(W)dW \\ &= \int_0^{\infty} \frac{W^n \exp(-W)}{n!} p_w(W)dW. \end{aligned} \quad (2.20)$$

This formula was first derived by Mandel [30] in 1958 and is known as Mandel's Formula. It is also referred to as the conditional [26] or doubly stochastic Poisson distribution [25, 26] because of the two sources of randomness that contribute to it; i.e., the quantum nature of photons (which behave according to a Poisson distribution) and the intensity fluctuation arising from the incoherence of the light source. This same equation is sometimes called the Poisson Transform [25] or the Photodetection Equation [29]. This integral is very difficult to evaluate in practice. A great deal of work has been done in trying to evaluate Mandel's formula for different light sources [29]. The photon number mean and mean square are given by:

$$\begin{aligned} \langle n \rangle &= \sum_n n p(n) = \langle W \rangle \\ \langle n^2 \rangle &= \sum_n n^2 p(n) = \langle W \rangle + \langle W^2 \rangle, \end{aligned} \quad (2.21)$$

where $\langle \cdot \rangle$ signifies statistical average.

From this, the variance is found to be:

$$\sigma_n^2 = \langle n \rangle + \sigma_w^2, \quad (2.22)$$

where σ_w^2 is the variance of W .

The photon number variance is the sum of two contribution; the first term is the basic contribution of the Poisson distribution and the second is an additional contribution caused by the fluctuations of the source.

2.2 Statistics of some Light Sources

In this section, the statistics of the most common light sources are discussed in order to derive their respective photon number distributions. The majority of the material in this section is drawn from the book by Saleh [25] and the review article by Metha [26].

2.2.1 Ideal Laser (Coherent) Light

Laser light is characterized by stimulated emission. This means that an ideal laser source emits photons that have the same frequency and same phase. Such a source does not exhibit any field amplitude fluctuations and is often referred to as a perfectly coherent source (deterministic and monochromatic light). In this case, the integral W is a constant or equivalently a random variable with an impulse function as probability distribution:

$$p(W) = \delta(W - \langle W \rangle). \quad (2.23)$$

The evaluation of Mandel's formula becomes very simple in this case. Using Equation (2.20), we obtain:

$$\begin{aligned} p(n) &= \int_0^{\infty} \frac{W^n \exp(-W)}{n!} \delta(W - \langle W \rangle) dW \\ &= \frac{\bar{n}^n \exp(-\bar{n})}{n!}, \end{aligned} \quad (2.24)$$

where $\langle W \rangle$ has been replaced by \bar{n} .

This is the Poisson distribution with mean and variance:

$$\begin{aligned} \langle n \rangle &= \bar{n} \\ \sigma_n^2 &= \bar{n}. \end{aligned} \quad (2.25)$$

As seen earlier, due to the quantum nature of light, even when the source emits totally deterministic monochromatic light, there is still randomness in the photon number.

For real (non-ideal) laser light, which is not characterized by pure stimulated emission, additional randomness is added causing the photon number to deviate slightly from the Poisson distribution. A common model used for predicting the photon number distribution of real laser light is to consider the laser output to be an ideal laser field on

which is superimposed another wide spectrum field having random amplitude fluctuations described by a Gaussian distribution. In that case, the photon number can be expressed in terms of the Laguerre polynomials [31].

2.2.2 Thermal (Incoherent) Light

Thermal light represents light emitted by a thermal source, i.e. a resonator whose walls are maintained at a temperature in equilibrium with its surroundings. It can also represent light created by the spontaneous emission from a large number of atoms; each of them acting independently. Photons are therefore released randomly at various frequencies and at different phases. Light sources characterized by these phenomena are usually called incoherent and their output can be modeled by a field with amplitude fluctuations described by a Gaussian distribution and with various spectrum shapes or widths. The instantaneous intensity of a linearly polarized thermal source is described by an exponential distribution given by:

$$p(I) = \frac{1}{\langle I \rangle} \exp\left(-\frac{I}{\langle I \rangle}\right). \quad (2.26)$$

Narrowband Thermal Light

As discussed in Section 2.1.3, there is a correspondence between the linewidth $\Delta\nu$ of an optical field and its time of coherence τ_c . It is given by:

$$\Delta\nu = \alpha \times \frac{1}{\tau_c}, \quad (2.27)$$

where α is a proportionality constant. In the case where the definition (2.12) is used for the linewidth, this proportionality constant α is equal to unity. In addition, the symbol B_o will now be used to designate the linewidth or *optical* bandwidth specifically. In the same manner, the symbol B_e will be used for the *electrical* bandwidth associated with an observation or detection time T . Thus, an optical field having a small bandwidth B_o compared to the detection bandwidth B_e is said to be a narrowband field. Equivalently, we can also say that a narrowband field has a long coherence time τ_c compared to the detection time T .

When the coherence time τ_c of the source is very long compared to the detection time T ($\tau_c \gg T$), the intensity of light $I(t)$ can be considered as a constant in the interval

T and W is then, approximately $\frac{AI(t)T}{h\nu}$. Consequently, the probability distribution of W is exponential:

$$p(W) = \frac{1}{\langle W \rangle} \exp\left(-\frac{W}{\langle W \rangle}\right), \quad (2.28)$$

where $\langle W \rangle = \frac{A\langle I \rangle T}{h\nu}$.

By evaluating Mandel's formula (Equation (2.20)) with the above probability distribution, one obtains the following photon number distribution:

$$p(n) = \frac{1}{(\bar{n} + 1)} \left(\frac{\bar{n}}{\bar{n} + 1}\right)^n, \quad (\tau_c \gg T) \text{ or } (B_o \ll B_c). \quad (2.29)$$

This corresponds to the Bose-Einstein distribution [25] which has a mean and variance given by:

$$\begin{aligned} \langle n \rangle &= \bar{n} \\ \sigma_n^2 &= \bar{n} + \bar{n}^2. \end{aligned} \quad (2.30)$$

If we compare these two expressions to those obtained for the Poisson distribution (Equation (2.25)), we find that the only difference is in the additional term \bar{n}^2 in the variance of the Bose-Einstein distribution. This results in a larger fluctuation in the photon number for the case of a narrowband thermal source than for the case of an ideal laser source even if both are monochromatic. This comes from the fact that a thermal source has random intensity fluctuations whereas an ideal laser source has none. For comparison, the Poisson and Bose-Einstein distributions are shown in Figure 2.3 (a) and (b), respectively. In this figure, both the Poisson and the Bose-Einstein distributions are plotted with the mean number \bar{n} as a parameter. This mean \bar{n} can be associated with the average number of photons during a bit time T in a digital intensity modulated communication system. We notice that for the Poisson distribution (Figure 2.3 (a)), the highest probability of finding photons is always near the mean \bar{n} while it is always at zero in the case of the Bose-Einstein distribution (Figure 2.3 (b)). We notice also that the variance of the Bose-Einstein distribution is significantly larger than that of the Poisson distribution.

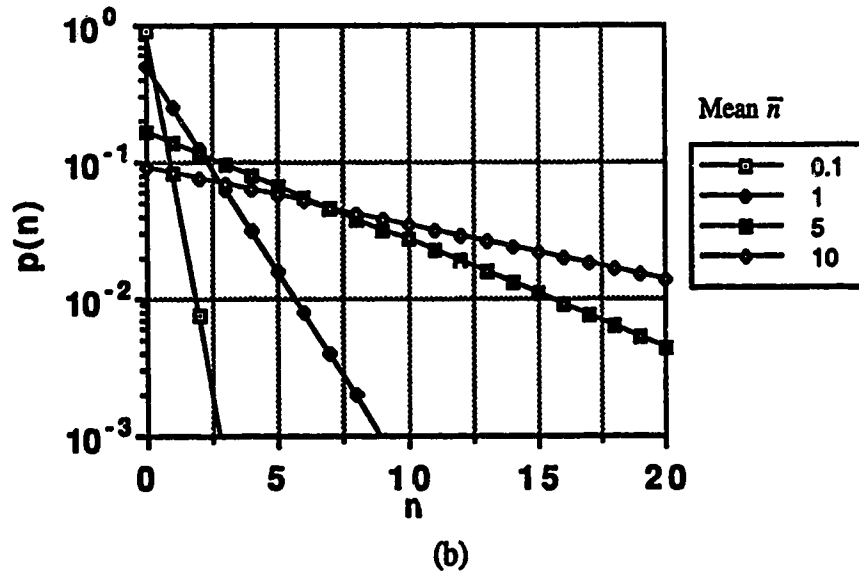
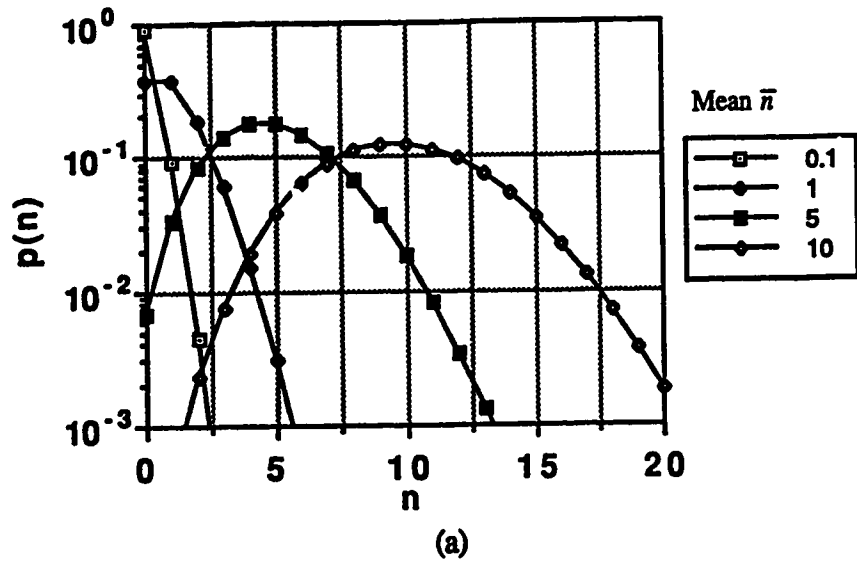


Figure 2.3: Poisson (a) and Bose-Einstein (b) distributions plotted with the mean number of photons \bar{n} as a parameter.

Wideband Thermal Light

On the other hand, when τ_c is small compared to T ($\tau_c \ll T$), the interval T can be divided into a large number of sub-intervals of the order of τ_c and the contributions to W from each of these sub-intervals are random variables that can be considered statistically independent. From the central limit theorem, W is found to be Gaussian distributed. But in

the limit where the ratio $\tau_c/T \rightarrow 0$ (source with infinite linewidth), the fluctuations in the intensity are smoothed out by the integration and the distribution of W tends to an impulse function as in the case of ideal laser light:

$$p(W) = \delta(W - \langle W \rangle). \quad (2.31)$$

In that case, the evaluation of Mandel's formula gives a Poisson distribution for the photon number:

$$p(n) = \frac{\bar{n}^n \exp(-\bar{n})}{n!}, \quad (\tau_c \ll T) \text{ or } (B_o \gg B_c). \quad (2.32)$$

and again, the mean and the variance are:

$$\begin{aligned} \langle n \rangle &= \bar{n} \\ \sigma_n^2 &= \bar{n}. \end{aligned} \quad (2.33)$$

This result is quite surprising. It means that one can obtain the same photon number statistics by either using a perfectly coherent source (ideal laser) or a totally incoherent source having an extremely large frequency spectrum.

2.2.3 Filtered Thermal Light

The two cases treated above are the simplest. When arbitrary spectrum shapes with variable widths are assumed, for example, the derivation of the photon number probability distribution is more complicated and closed forms often simply do not exist. For a filtered polarized thermal source having an arbitrary spectrum shape an approximate formula was derived for the photon number distribution. The probability distribution of W was suggested by Rice [32]:

$$p(W) = \frac{a^N}{2^N} \frac{W^{N-1}}{(N-1)!} \exp(-\frac{1}{2}aW), \quad (2.34)$$

where the constants a and N are defined in the following way:

$$N = \frac{T^2}{2 \int_0^T (T-\tau) |g(\tau)|^2 d\tau}, \quad (2.35)$$

$$a = \frac{2N}{\langle W \rangle}, \quad (2.36)$$

where $g(\tau)$ is the normalized autocorrelation function of the optical field and $\langle W \rangle$ the integrated light intensity.

Using Mandel's formula (Equation (2.20)), we obtain:

$$p(n) = \frac{\Gamma(n+N)}{n! \Gamma(N)} \frac{1}{(1+\bar{n}/N)^N} \frac{1}{(1+N/\bar{n})^n}, \quad (2.37)$$

where $\Gamma(\cdot)$ is Euler's gamma function. The parameter \bar{n} is the mean of the distribution and N is called the number of modes and is defined by Equations (2.35) and (2.36).

This photon number distribution was obtained for the first time by Mandel [33] in 1959. It is known as the negative binomial distribution [25]. If N is an integer the Equation (2.37) can be rewritten in terms of the Newton's binomial formula as follows:

$$p(n) = \binom{n+N-1}{n} \frac{1}{(1+\bar{n}/N)^N} \frac{1}{(1+N/\bar{n})^n}. \quad (2.38)$$

The factorial moments of the negative binomial distribution are given by:

$$\frac{\langle n^r \rangle}{\langle n \rangle^r} = \frac{\Gamma(N+r)}{\Gamma(N)N^r}, \quad (2.39)$$

where r is the moment order.

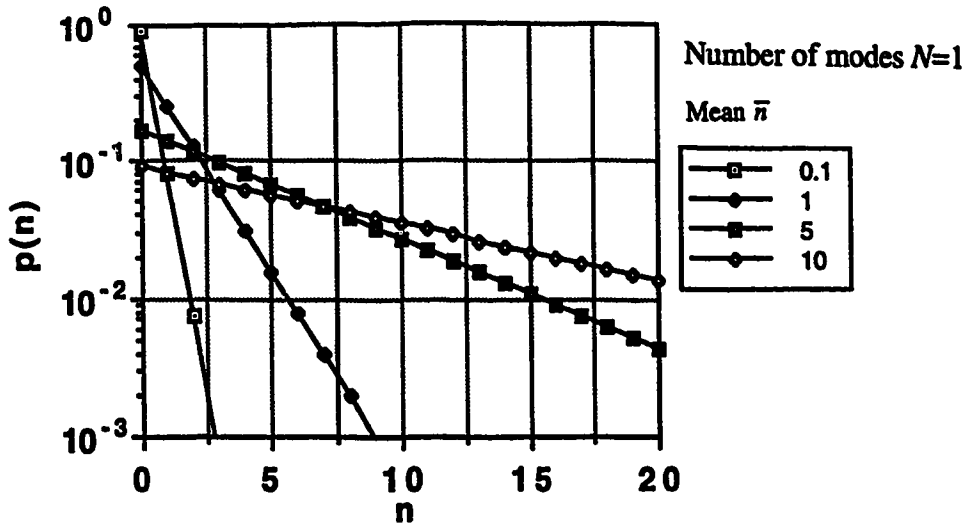
In particular, for $r=2$, we have, using the identity $\Gamma(x+1) = x\Gamma(x)$:

$$\frac{\langle n^2 \rangle}{\langle n \rangle^2} = \frac{\Gamma(N+2)}{\Gamma(N)N^2} = \frac{(N+1)N\Gamma(N)}{\Gamma(N)N^2} = \frac{N+1}{N}. \quad (2.40)$$

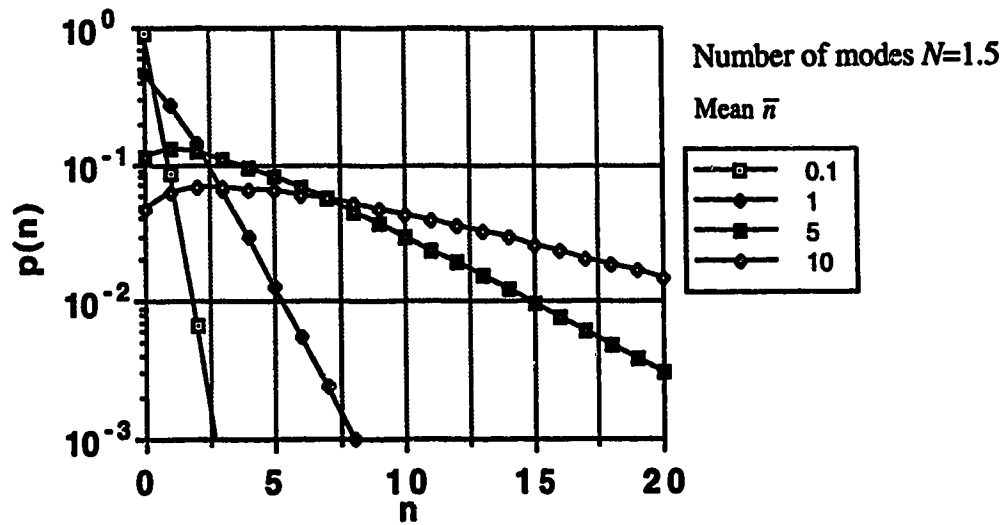
From this, the variance is found to be:

$$\sigma_n^2 = \bar{n} + \frac{\bar{n}^2}{N}. \quad (2.41)$$

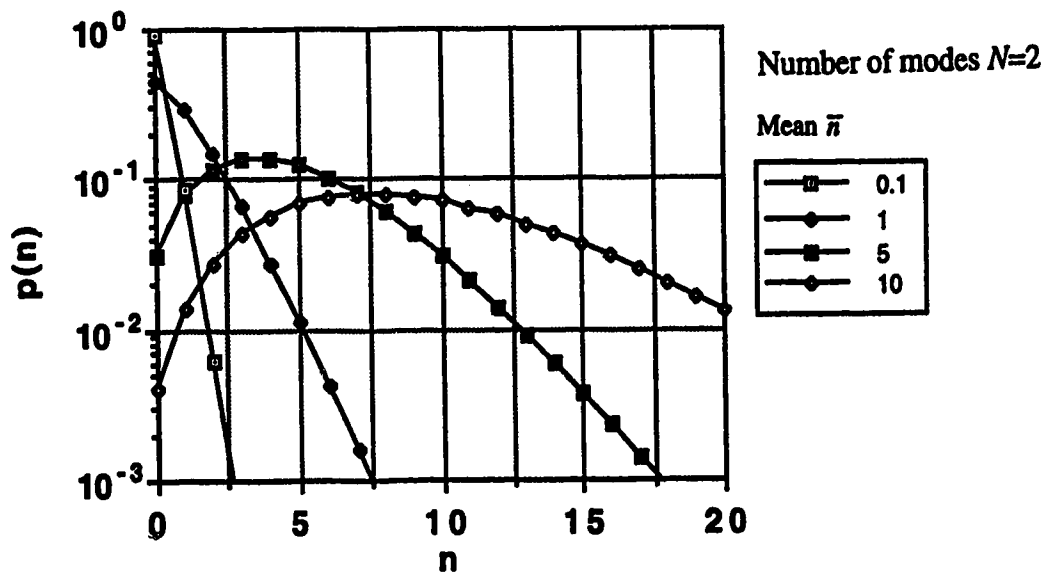
The distribution of Equation (2.37) is plotted in Figure 2.4 with the number of modes N and the mean \bar{n} as parameters. This figure shows five different plots labeled (a) to (e). Each plot is obtained for a constant number of modes and four different values of the mean. The values taken for the number of modes and for the mean are $N=1, 1.5, 2, 5, 100$ and $\bar{n}=0.1, 1, 5, 10$, respectively.



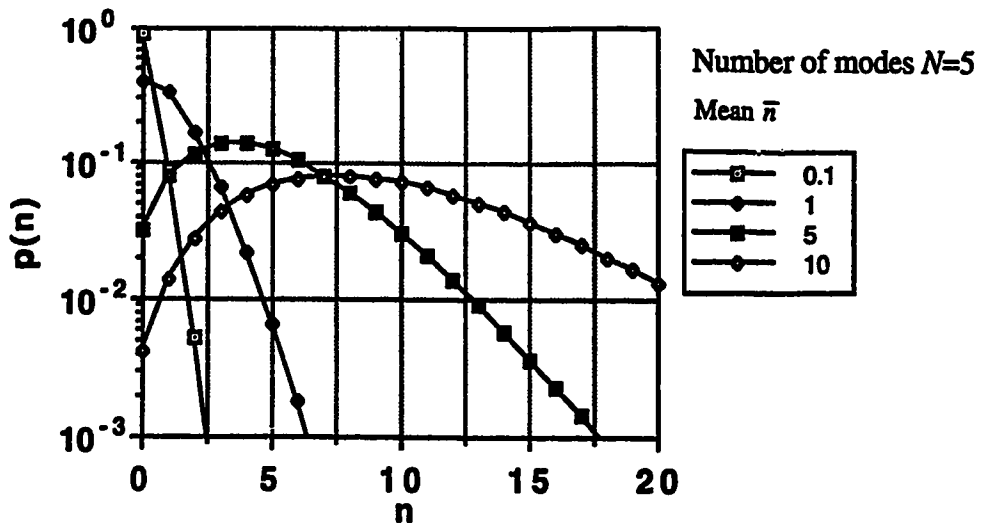
(a)



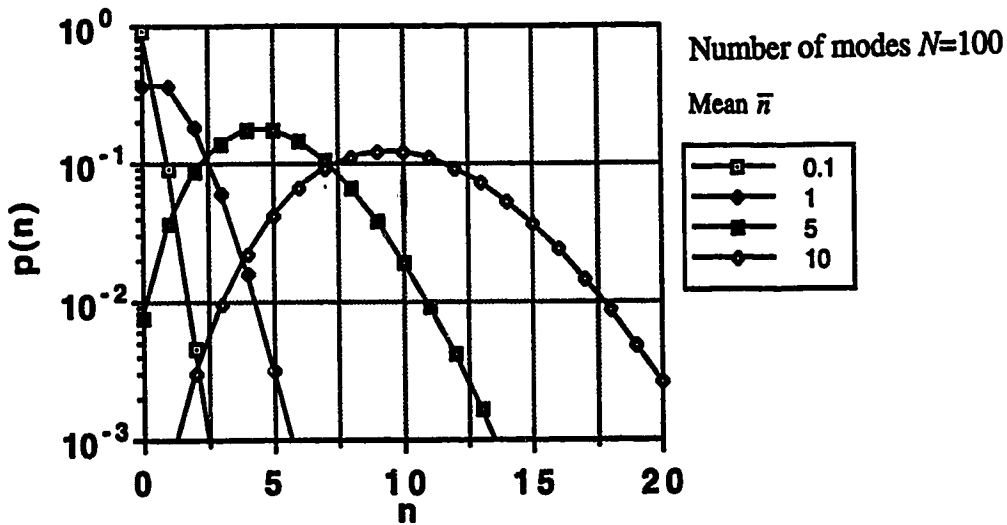
(b)



(c)



(d)



(e)

Figure 2.4: Negative binomial distribution plotted with \bar{n} and N as parameters. (a) $N=1$, (b) 1.5, (c) 2, (d) 5, (e) 100.

As we can see from this figure, the increase of the mean broadens the distribution. The increase of the number of modes shifts the point of highest probability of the distribution towards the value of the mean. The distribution is narrower and more symmetric as the number of modes increases. For $N=1$, the highest point of the distribution is located at $n=0$ for all values of the mean whereas for $N=100$, it is approximately located at $n=0, 1, 5$ and 10 . For $N=1$, the negative binomial distribution reduces to a Bose-Einstein distribution. This can easily be seen by comparing Figure 2.4 (a) and 2.3 (b). For large values of N , however, the negative binomial tends towards a Poisson distribution.

The plot of Figure 2.4 (e) obtained for $N=100$ can be compared to Figure 2.3 (a). They are practically identical.

If we compare the expression for the variance of the negative binomial distribution (Equation (2.41)) with that of the Poisson distribution (Equation (2.25)), we see that they differ by the term \bar{n}^2/N . This term is called the *excess noise term* and is due to the incoherency of the source. [34]

As we can see by looking at Equation (2.35), the number of modes N depends on the autocorrelation function of the optical field and therefore, on its spectrum shape and width. It also depends on the detection time T and consequently on the shape of the electrical frequency response. The expression for the parameter N is given for different optical spectrum shapes and a detection time T in Appendix 2B. If we define the detection time T as the inverse of the total electrical bandwidth B_e , T can be replaced by $1/B_e$ in the expressions of Table 2B.1 and we can plot the number of modes N as a function of the ratio B_o/B_e . This has been done in Figure 2.5. From this figure, we can see that when the ratio B_o/B_e becomes large, that is when the optical spectrum width B_o is large compared to the electrical bandwidth B_e , the number of modes N essentially becomes equal to the ratio B_o/B_e . In that case the variance becomes:

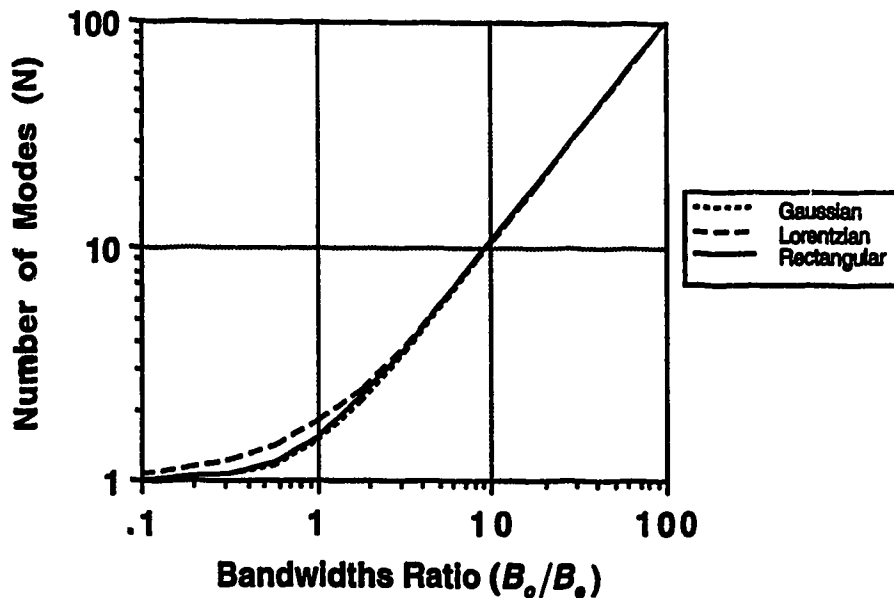


Figure 2.5: Plots of the parameter N as a function of the ratio B_o/B_e .

$$\sigma_n^2 \approx \bar{n} + \bar{n}^2 \left(\frac{B_c}{B_o} \right) \quad (B_c \ll B_o), \quad (2.42)$$

This simplified expression for the variance allows us to investigate the effect of the source spectrum on the photon number statistics and particularly the optical filtering effect in the case of spectral slicing. The expression of Equation (2.42) was obtained by Hodara [34] in 1965.

The case of an arbitrarily polarized thermal source can be viewed as an extension of the linearly polarized case. In fact, the light intensity can be divided into its two polarization parts which are statistically independent. Consequently, we have:

$$I(t) = I_1(t) + I_2(t) \quad (2.43)$$

$$\text{with} \quad \langle I_1 \rangle = \frac{1}{2}(1+\rho)\langle I \rangle \text{ and } \langle I_2 \rangle = \frac{1}{2}(1-\rho)\langle I \rangle. \quad (2.44)$$

where ρ is called the polarization coefficient. This parameter is equal to 1 when the light is linearly polarized and to 0 when the light is unpolarized. The resulting photon number distribution is a convolution between two negative binomial distribution. The results can be express as follows [28]:

$$p(n) \approx \left[1 + \frac{\bar{n}(1+\rho)}{2N} \right]^{-N} \left[1 + \frac{\bar{n}(1-\rho)}{2N} \right]^{-N} \\ \times \sum_{k=0}^n \frac{\Gamma(N+k)\Gamma(N+n-k)}{k!(n-k)![\Gamma(N)]^2} \left[1 + \frac{2N}{\bar{n}(1+\rho)} \right]^{-k} \left[1 + \frac{2N}{\bar{n}(1-\rho)} \right]^{-n+k}. \quad (2.45)$$

The mean and variance of Equation (2.44) are:

$$\langle n \rangle = \bar{n} \\ \sigma_n^2 = \bar{n} \left[1 + \frac{(1+\rho)}{2N} \bar{n} \right]. \quad (2.46)$$

Equation (2.45) reduces to a single negative binomial distribution (Equation 2.37) for $\rho=1$ which represents the linearly polarized case and for $\rho=0$ which is the unpolarized case. However, the number of modes N becomes $2N$ in Equation (2.37) in the unpolarized case. This result allows us to treat both linearly polarized and unpolarized thermal light the same way since both have the same photon number distribution. It suffices to remember the factor of two in the number of modes.

2.3 LED Statistics

As mentioned in the Introduction, an LED is a forward biased semiconductor p-n junction with a large radiative recombination rate arising from externally injected carriers. Its output light just consists of spontaneous emission of photons (generally unpolarized) which results from random electron-hole recombination in the semiconductor material. The photons are emitted independently of each other with a frequency and phase that are independent of those of other photons [35]. Since spontaneous emission essentially behaves like thermal light [17], we will assume that the statistics of a filtered LED follow those of a filtered unpolarized thermal source (negative binomial) as described in the previous section. This assumption is a very important one since it will be the basis for the rest of our work.

2.4. Conclusion

The first part of this chapter introduced the concept of randomness in light with a set of statistical averages to help characterize this randomness. In the second part, the statistics of some common light sources were discussed and their photon number distributions were given. In particular, the photon number distribution of a filtered thermal source was found to be a negative binomial. This distribution is characterized by a mean count \bar{n} and a number of modes N . The variance of the negative binomial contains an additional term that depends on the number of modes. This additional term is called *excess noise term* and is due to the incoherency of the source. The number of modes is related to the bandwidths of both the photodetector (electrical, B_e) and the optical field (B_o). Finally, we found that both linearly and randomly polarized filtered thermal sources could be described by a negative binomial with a different number of modes.

In the next chapter, a statistical model for optical amplifiers will be introduced. This model will allow us to obtain the photon number distribution of their output.

3. Birth-Death-Immigration Processes Applied to Optical Amplifiers

Birth-death-immigration (BDI) media have been known for long time. As early as 1957, Shimoda et al. [36] used them to model the amplification of photons inside a maser amplifier. Their work remained unused for almost thirty years. More recently, Teich et al. [37-39] revived the subject in trying to apply the BDI theory to linear optical amplifiers, that is optical amplifiers operating in the linear regime. This chapter is an introduction to BDI media and to their use in the modeling of the statistical output of optical amplifiers and in particular of EDFAs (erbium doped fiber amplifiers).

There are four main divisions in the chapter. First, the theory of BDI media is introduced. Second, the mathematical expression for the output of a BDI medium is obtained for some simple inputs as well as for an input characterized by negative binomial distribution which describes filtered incoherent light sources such as LEDs. Third, a series of observations is made in which the BDI parameters are related to the physical quantities of EDFAs. In particular, the well-known beat noise terms encountered in optically amplified signals are identified in the BDI output variance. Finally, the chapter is summarized in the conclusion.

3.1 BDI Theory

Many books on probability and statistics treat BDI processes [40, 41]. In this section, the BDI medium parameters is defined as well as the mathematical equations describing it. The Probability Generating Function (PGF) method will also be introduced as an aid to solve the BDI medium equations.

3.1.1 Description

A BDI medium is characterized by a set of four parameters: a birth rate per particle $a(t)$ and a death rate per particle $b(t)$, an immigration rate $c(t)$, and a depth or time of traversal t . Each particle inside a BDI medium can either generate another particle (birth), do nothing or disappear (death). The probability of generating another particle or disappearing is weighted by the birth and death rates, $a(t)$ and $b(t)$, respectively. In addition, there is a probability that some particles be spontaneously created inside the medium (immigration). This probability is determined by the immigration rate $c(t)$. These

processes are very similar to the those encountered in the amplification of optical signals. The birth, death and immigration rates can be associated with the stimulated emission, the absorption and spontaneous emission of photons, respectively, inside an optical amplifier operating in the linear regime. The optical amplifier noise caused by its ASE (amplified spontaneous emission) can be treated as an immigration-birth process, i.e., a birth for which the initial particle is a spontaneously emitted photon. The parameter t can be related to the interaction time of photons inside the optical amplifier. In the case of an EDFA, for instance, this time is given by the ratio of the length of doped fiber to the speed of light.

Figure 3.1 illustrates the processes discussed above in the case of three photons entering an EDFA of length l modeled by a BDI medium. In the figure, the EDFA has been divided into six equal sections. The count for the number of births, deaths and immigrations as well as for the total number of photons is provided after each section of the amplifier. After having gone through the entire EDFA length, a total of 7 births, 4 deaths and 6 immigrations have been recorded. The total number of photons at the output is 12. Note that the photon labeled n_2 goes straight through the EDFA without giving any birth.

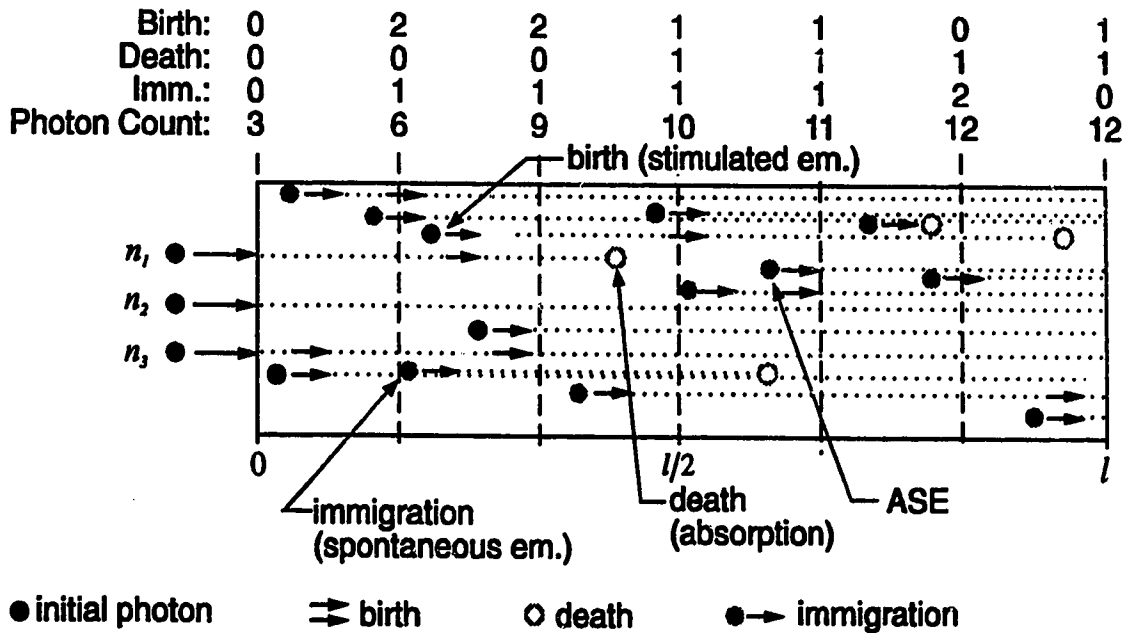


Figure 3.1: Illustration of the birth, death and immigration processes of a BDI medium and their physical correspondence in EDFA amplification.

3.1.2 BDI Equations

A BDI medium is mathematically described by a differential equation. If the probability (meaning the probability density function (PDF)) of having n particles at the input of the BDI medium is $p_{in}(n)$, then the probability $p(n,t)$ that n particles are present in the BDI medium after a time t , satisfies the Forward Kolmogorov difference-differential equation given by:

$$\begin{aligned} \frac{\partial p(n,t)}{\partial t} = & [(n-1)a + c]p(n-1,t) \\ & + [(n+1)b]p(n+1,t) \\ & - [n(a+b) + c]p(n,t). \end{aligned} \quad (3.1)$$

It is possible to solve Equation (3.1) and obtain the PDF of the output of the BDI medium in terms of the PDF of the input. This is not easy to do in practice but there exist some methods to facilitate the task. In the next section, we introduce one of these methods called the Probability Generating Function (PGF) method. The derivation leading to the Equation (3.1) as well as its solution can be found in a paper by Diament and Teich [37]. The major part of the rest of this section is drawn from this paper.

3.1.3 Probability Generating Function

The PGF of the BDI medium is defined as follows:

$$G(z,t) = \langle z^n \rangle = \sum_{n=0}^{\infty} p(n,t)z^n, \quad (3.2)$$

It is basically the z-transform (or Laplace transform) of the PDF $p(n,t)$. The PGF satisfies the partial differential equation:

$$\frac{\partial G(z,t)}{\partial t} = [z-1] \left[(az-b) \frac{\partial G(z,t)}{\partial z} + cG(z,t) \right], \quad (3.3)$$

which has for its solution, in the general case of varying birth, death and immigration rates [37]:

$$G(z,t) = G_{in}(Z(z,t;0),0) \exp \left\{ \int_0^t [Z(z,t;\tau) - 1] c(\tau) d\tau \right\}, \quad (3.4)$$

where
$$Z(z, t; \tau) = 1 + \frac{(z-1)h(\tau)}{h(t) - [z-1][k(t) - k(\tau)]}, \quad (3.5)$$

$$h(u) = \exp\left[\int_0^u (b(t) - a(t)) dt\right], \quad (3.6)$$

$$k(u) = \int_0^u [h(t)a(t)] dt \quad (3.7)$$

and $G_{in}(z)$ is the PGF of the input.

Equation (3.4) can be rewritten as function of a birth-death (BD) process and an immigration (I) process [40]:

$$G(z, t) = G_{in}(G_{BD}(z, t))G_I(z, t), \quad (3.8)$$

where
$$G_{BD}(z, t) = Z(z, t; 0) \quad (3.9)$$

and
$$G_I(z, t) = \exp\left\{\int_0^t [Z(z, t; \tau) - 1]c(\tau) d\tau\right\}. \quad (3.10)$$

The mean number of particles at the output of the BDI medium is:

$$\bar{n}(t) = \frac{1}{h(t)} \left[\bar{n}_{in} + \int_0^t h(\tau)c(\tau) d\tau \right], \quad (3.11)$$

where \bar{n}_{in} is the initial mean number of particles at the input. \bar{n}_{in} and $\bar{n}(t)$ can be associated with the average number of photons found in an interval of time T at the input and output of an EDFA, respectively and the parameter $1/h(t)$, with the EDFA small signal gain.

The case of constant birth, death and immigration rates greatly simplifies the mathematics. The Equations (3.6), (3.7) and (3.10) become:

$$h(t) = \exp((b-a)t) \quad (3.12)$$

$$k(t) = [a/(b-a)][h(t) - 1] \quad (3.13)$$

$$G_I(z, t) = [1 - (z-1)k(t)/h(t)]^{-c/a}. \quad (3.14)$$

In this case, the PGF of the BDI medium $G(z, t)$ simplifies to:

$$G(z, t) = \frac{G_{in}(Z(z, t; 0))}{[1 - (z-1)k(t)/h(t)]^{c/a}} \quad (3.15)$$

with
$$Z(z, t; 0) = 1 + \frac{(z-1)}{h(t) - (z-1)k(t)}. \quad (3.16)$$

The mean and the variance of the output become:

$$\bar{n}(t) = \frac{\bar{n}_{in} + (c/a)k(t)}{h(t)} \quad (3.17)$$

$$\sigma^2(t) = \frac{\sigma_{in}^2 - \bar{n}_{in} + (2k(t) + h(t))\bar{n}_{in} + (c/a)k(t)(\frac{1}{2}k(t) - h(t))}{h^2(t)}. \quad (3.18)$$

The assumption of constant birth, death and immigration rates allows us to obtain non-integral expressions for the PGF (Equation (3.15)) as well as for the output mean (3.17) and variance (3.18). For an EDFA, the stimulated emission and absorption rates as well as the spontaneous emission rate are expected to be dependent on the amplifier length l and consequently on the interaction time t . This is mainly due to the pumping mechanism which is generally nonuniform throughout the length of the EDFA. For instance, if the pump and the input signal are co-propagating, the stimulated emission rate will most likely be larger at the input end whereas the absorption rate is expected to be larger at the output end. This means that EDFA amplification would be best represented by a BDI medium with variable birth, death and immigration rates. However, only the case of constant birth, death and immigration rates will be considered in the subsequent sections. This is equivalent to assuming that the pumping is uniform throughout the EDFA length.

In the case of no input, $p_{in}(n) = \delta(n)$ and the PGF, $G_{in}(z)$, becomes equal to 1. From Equation (3.15), we obtain:

$$G(z, t) = [1 - (z-1)k(t)/h(t)]^{-c/a} = G_l(z, t) \quad (3.19)$$

This PGF is of the form:

$$G(z, N, \bar{n}) = [1 - (z-1)(\bar{n}/N)]^{-N} \quad (3.20)$$

and describes a negative binomial PDF:

$$B(n, N, \bar{n}) = \frac{N^N \Gamma(n+N)}{n! \Gamma(N)} \frac{\bar{n}^n}{(\bar{n} + N)^{n+N}} \quad (3.21)$$

with mean $\bar{n} = (c/a)[k(t)/h(t)]$ and number of modes $N = (c/a)$. As seen in the previous chapter, the variance of this PDF is given by:

$$\sigma_n^2 = \bar{n} + \frac{\bar{n}^2}{N} \quad (3.22)$$

In the previous chapter, we discussed the negative binomial PDF and we found that it characterized the statistics of LED emission. The output of an EDFA for which there is no signal at the input just consists of ASE. Consequently, the result of Equation (3.21) shows that the statistical behavior of ASE is characterized by the same photon

number distribution as for an LED. Here the mean \bar{n} can represent the average number of photons that were produced by the ASE and that are detected over an interval of time T . The number of modes N , here given by (c/a) , is as defined in Chapter 2. It is related to the ratio of the optical to the electrical bandwidths. Finally, as discussed also in Chapter 2, the negative binomial PDF reduces to the Poisson distribution in the limit of $N \rightarrow \infty$ and to the Bose-Einstein distribution when $N = 1$.

3.2 Some Input Distributions

In the previous section, we introduced the PGF method which was used to solve the BDI equations. The use of this method greatly simplifies the task. In this section, the PGF method is used to determine the PDF of the output of a BDI medium for various inputs.

As it is often done in electrical engineering and in mathematics in general, we can treat a BDI medium as a system that simply applies a transformation on the function at its input [37]. The PGF of the BDI medium (Equation 3.15) simply becomes its transfer function. This is illustrated in Figure 3.2. Since it is usually simpler to work with the PGF than with the PDF, the entire calculations can be performed in the PGF domain and the final PDF can be obtained by taking the inverse z or Laplace-transform of the resulting PGF. In general, the input can be deterministic or probabilistic. In the following, the output PDF of a BDI medium is obtained for the case where the input is a fixed number of particles and for the cases where the input has either a Poisson or a negative binomial PDF.

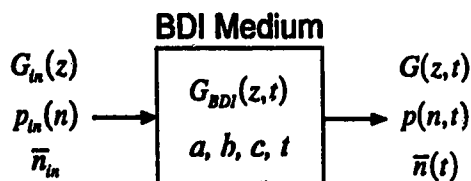


Figure 3.2: Input-output relationship for a BDI medium treated as a system.

3.2.1 Deterministic Input

The case of no input was discussed in the previous section. The result for the PDF of the output was found to be a negative binomial. Now, if the input is one particle, then $p_{in}(n) = \delta(n-1)$ and $G_{in}(z) = z$. In this case, Equation (3.15) reduces to:

$$G(z, t) = \frac{Z(z, t; 0)}{[1 - (z-1)k(t)/h(t)]^{c/a}} \quad (3.23)$$

$$= \frac{[1 + (z-1)/(h(t) - (z-1)k(t))]}{[1 - (z-1)k(t)/h(t)]^{c/a}}$$

$$= \frac{[1 + (z-1)(1-k(t))/h(t)]}{[1 - (z-1)k(t)/h(t)]^{(c/a+1)}} \quad (3.24)$$

Since a factor of z in the PGF means a shift by one count in the PDF, the PDF of the output is:

$$p(n, t) = [1 - (1-k(t))/h(t)]B(n, N, N(k(t)/h(t)))$$

$$+ [(1-k(t))/h(t)]B(n-1, N, N(k(t)/h(t))), \quad (3.25)$$

where $N = (c/a) + 1. \quad (3.26)$

For the case of \bar{n}_{in} initial particles, $p_{in}(n) = \delta(n - \bar{n}_{in})$ and $G_{in}(z) = z^{\bar{n}_{in}}$. Equation (3.15) gives:

$$G(z, t) = \frac{(Z(z, t; 0))^{\bar{n}_{in}}}{[1 - (z-1)k(t)/h(t)]^{c/a}} \quad (3.27)$$

$$= \frac{[1 + (z-1)(1-k(t))/h(t)]}{[1 - (z-1)k(t)/h(t)]^{(c/a + \bar{n}_{in})}}. \quad (3.28)$$

The resulting output PDF is a convolution between two negative binomial PDFs:

$$p(n, t) = B(n, N, N(k(t)/h(t))) * B(n, \bar{n}_{in}, -\bar{n}_{in}(1-k(t))/h(t)), \quad (3.29)$$

where $N = (c/a) + \bar{n}_{in}. \quad (3.30)$

3.2.2 Poisson Input

As mentioned in the previous chapter, the Poisson PDF characterizes the photon number distribution of a perfectly coherent light source (an ideal laser). In the same way as for the deterministic input, we can use the PGF method to determine the BDI medium output for the case of a Poisson PDF input. The PGF of a Poisson PDF with mean \bar{n}_{in} is given by [25]:

$$G_{in}(z) = \exp[\bar{n}_{in}(z-1)]. \quad (3.31)$$

$G_{in}(Z(z, t; 0))$ becomes:

$$G_{in}(Z(z, t; 0)) = \exp\left[\frac{(\bar{n}_{in}/h(t))(z-1)}{[1-(k(t)/h(t))(z-1)]}\right]. \quad (3.32)$$

Using Equation (3.15), we find:

$$G(z, t) = \exp\left[\frac{\bar{n}_{in}/h(t)(z-1)}{[1-(z-1)k(t)/h(t)]}\right] [1-(z-1)k(t)/h(t)]^{-(c/a)}. \quad (3.33)$$

This PGF corresponds to a noncentral negative binomial PDF which is given by [37]:

$$p(n, t) = \frac{(k(t)/h(t))^n}{((k(t)/h(t))+1)^{n+(c/a)}} \exp\left[-\frac{(k(t)/h(t))(\bar{n}_{in}/k(t))}{((k(t)/h(t))+1)}\right] \times L_n^{((c/a)-1)}\left(-(\bar{n}_{in}/k(t))/((k(t)/h(t))+1)\right), \quad (3.34)$$

where $L_n^k(\cdot)$ is an associated Laguerre polynomial. Note that here, the quantity (c/a) must be an integer.

The output mean and variance of this PDF are:

$$\begin{aligned} \bar{n}(t) &= \bar{n}_{in}/h(t) + (c/a)[k(t)/h(t)] \\ \sigma^2(t) &= (\bar{n}_{in}/h(t))[2(k(t)/h(t))+1] + (c/a)(k(t)/h(t))[k(t)/h(t)+1]. \end{aligned} \quad (3.35)$$

3.2.3 Negative Binomial Input

The case of negative binomial PDF input is interesting because as we saw in the previous chapter, this PDF characterizes the emission a filtered LED. In addition, we can obtain both the Poisson and the Bose-Einstein distributions in its limits.

The PGF of a negative binomial PDF with a mean \bar{n}_{in} and number of modes N_{in} , is given by [25]:

$$G_{in}(z) = [1-(z-1)(\bar{n}_{in}/N_{in})]^{-N_{in}} \quad (3.36)$$

In this case, $G_{in}(Z(z, t; 0))$ becomes:

$$G_{in}(Z(z,t;0)) = \left[1 - \left[\left(1 + \frac{(z-1)}{(h(t) - (z-1)k(t))} \right) - 1 \right] (\bar{n}_{in}/N_{in}) \right]^{-N_{in}} \quad (3.37)$$

$$= \left[\frac{1 - (z-1)(k(t) - (\bar{n}_{in}/N_{in}))/h(t)}{1 - (z-1)k(t)/h(t)} \right]^{-N_{in}} \quad (3.38)$$

Using Equation (3.15), we obtain for the PGF:

$$G(z,t) = \left[1 - (z-1)(k(t) + (\bar{n}_{in}/N_{in}))/h(t) \right]^{-N_{in}} \left[1 - (z-1)k(t)/h(t) \right]^{-(c/a) + N_{in}}. \quad (3.39)$$

This PGF corresponds to a convolution between two negative binomial PDFs:

$$p(n,t) = B(n, N_{in}, (N_{in}k(t) + \bar{n}_{in})/h(t)) * B(n, N, N(k(t)/h(t))), \quad (3.40)$$

where

$$N = (c/a) - N_{in}. \quad (3.41)$$

The mean and the variance of this PDF are given by Equations (3.17) and (3.18), respectively.

The PDF obtained in Equation (3.40) describes the statistical behavior of the output of a system composed of an LED followed by an EDFA operating in the linear regime, an optical filter and a photodetector. As discussed earlier, the number of modes is related to the filtering by the ratio of the optical to the electrical bandwidths. Since all the photons are detected by the same photodetector, the electrical filtering is the same for both the LED and the EDFA. Consequently, the parameter N_{in} is determined by the optical filtering applied to the LED and (c/a) that is applied to the EDFA. In addition, a small number of modes can be seen as narrow optical filtering and a large number as broader filtering. In a system composed of an LED followed by an EDFA, the filtering applied after the EDFA will determine the number of modes for both the input PDF and the BDI medium.

In the case where the number of modes is the same for both the input negative binomial PDF and the BDI medium, that is for $N_{in} = (c/a) = N$, the second term in Equation (3.39) becomes unity and Equation (3.40) reduces to a simple negative binomial PDF with a mean and variance given by the following two expressions:

$$\bar{n}(t) = \frac{\bar{n}_{in} + Nk(t)}{h(t)} \quad (3.42)$$

$$\sigma^2(t) = \bar{n}(t) + \frac{\bar{n}^2(t)}{N}. \quad (3.43)$$

In order to get some insight into the statistical behavior of the output of this system, the PDF of Equation (3.40) is plotted as a function of the photon number as the interaction time t , the average input number of photons \bar{n}_{in} and the number of modes N are consecutively varied. For the calculation, we assume a constant birth rate a of 7, a constant death rate b of 6 and a constant immigration c of 8. Figure 3.3 shows the plot of the PDF of Equation (3.40) for an average input number of photons $\bar{n}_{in}=8$, a number of modes $N=7.5$ and for four values of the parameter t . These values are $t=0, 0.14, 0.29$ and 0.57 . As mentioned earlier, the parameter t is given by the ratio of the EDFA length to the speed of light. Varying the value of the parameter t effectively means changing the length and consequently the gain of the EDFA. The gain values can be calculated using Equation (3.12). They are 1, 1.15, 1.3 and 1.8 for $t=0, 0.14, 0.29$ and 0.57 , respectively. As we can see from Figure 3.3, the BDI medium broadens the initial PDF and this effect increases with larger values of the interaction time t . The mean is also shifted upward. This is due in part to the fact that an increase of the parameter t causes an increase of the gain and therefore, an increase of the average output number of photons. In addition, some ASE is added to the output amplified signal which contribute to the shift of the mean. To measure the relative broadening of the output PDF compared to the input, we define the parameter s as the ratio of the output to the input standard deviations:

$$s = \frac{\sigma(t)}{\sigma_{in}}. \quad (3.44)$$

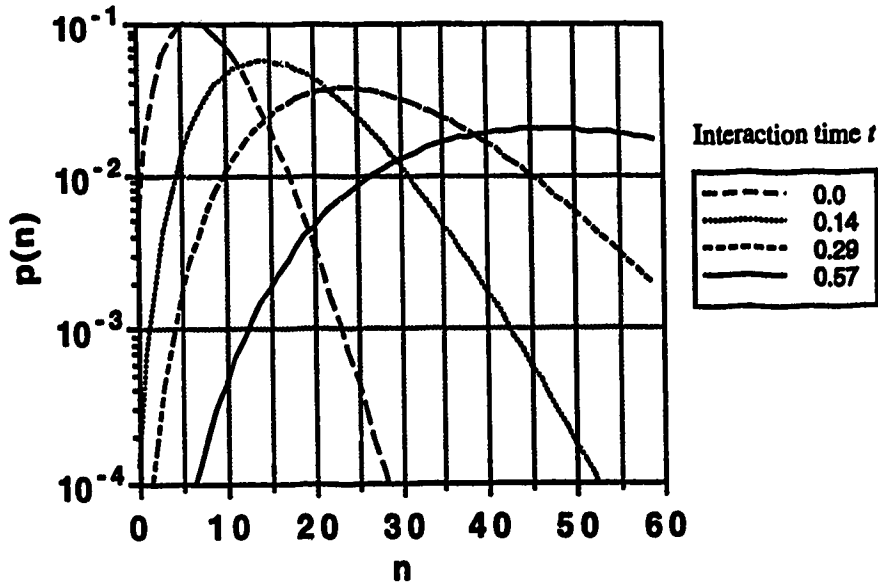


Figure 3.3: Plot of Equation (3.40) for $N=7.5$ and $\bar{n}_{in}=8$ with the interaction time t as a parameter.

The ratio s is plotted as a function of the interaction time t in Figure 3.4. This ratio increases with increasing value of t to finally reach a factor of slightly over 3.5 at $t=0.55$. This can be explained in part by the fact that as per Equation (3.18) the variance is proportional to the square of the gain $1/h(t)$.

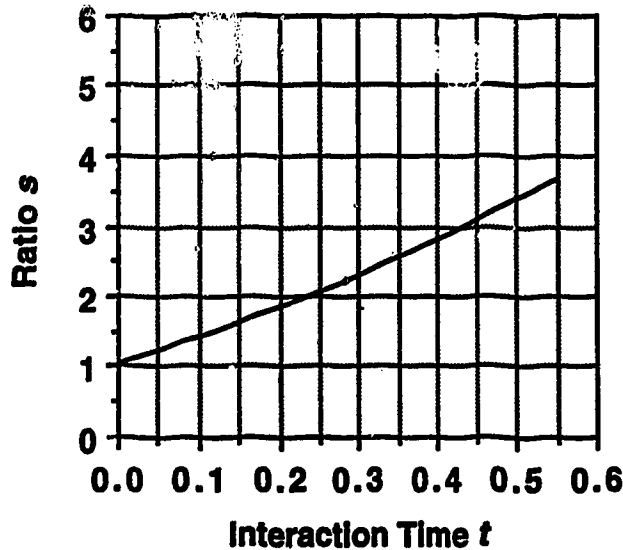


Figure 3.4: Plot of the ratio of the output to the input standard deviations for the case where $N=7.5$ and $\bar{n}_in=8$ as a function of the interaction time t .

The effect of the average input number of photons can also be examined. Figure 3.5 shows the output PDF for a gain of 1.3 ($t=0.29$), a number of modes $N=7.5$ and for different values of the average input number of photons \bar{n}_in . From this figure, we see that the PDF appears broader with increasing values of \bar{n}_in but this broadening is not all due to the BDI medium. In fact, the variance of the input negative binomial PDF also increases with the average input number of photons \bar{n}_in . The ratio of the output to the input standard deviations s is plotted as a function of the interaction time t with the average input number of photons as a parameter in Figure 3.6. By looking at this figure, we realize that the overall increase in the output standard deviation is smaller as the value of \bar{n}_in gets larger.

Finally, the effect of the number of modes on the output PDF is illustrated in Figure 3.7. This plot is obtained for an average input number of photons $\bar{n}_in=8$ and for a gain of 1.3 ($t=0.29$). Each PDF curve of the plot is obtained for a constant value for the number of modes N which is varied from 1 to 7.5. We see that the main effect of the

increase of the number of modes on the PDF is to shift the point of highest probability. This point is approximately located at $n=0, 7, 14$ and 22 for $N=1, 2, 4$ and 7.5 , respectively. Figure 3.8 shows the plot of the ratio s as a function of the interaction time t with the number of modes N as a parameter. We find, from this figure, that the increase in the output standard deviation is minimum for a number of modes equal to unity. On the other hand, the PDF of the input is the largest for $N=1$.

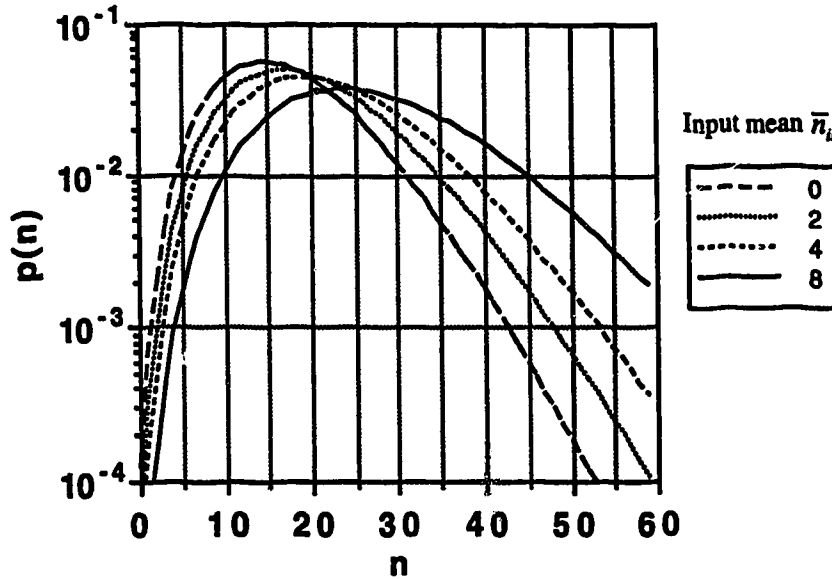


Figure 3.5: Plot of Equation (3.40) for $t=0.29$ and $N=7.5$ for different values of the input mean \bar{n}_{in} .

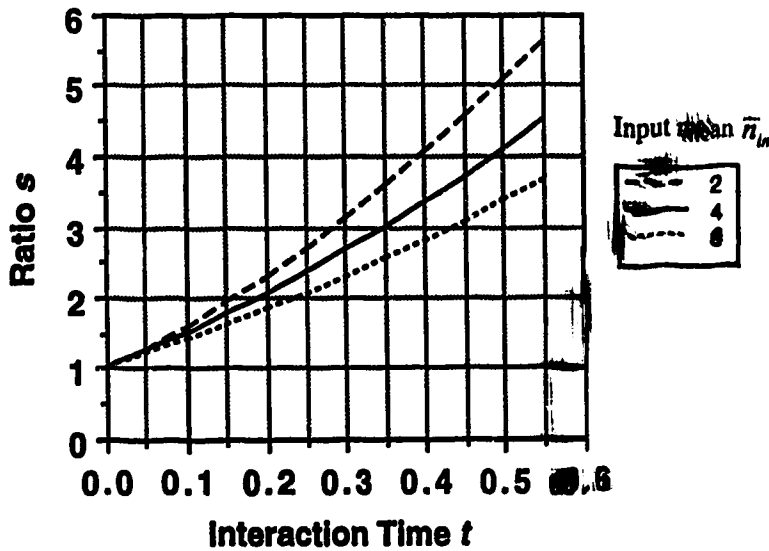


Figure 3.6: Plot of the ratio of the output to the input standard deviations as a function of the interaction time t for $N=7.5$ with the input mean \bar{n}_{in} as a parameter.

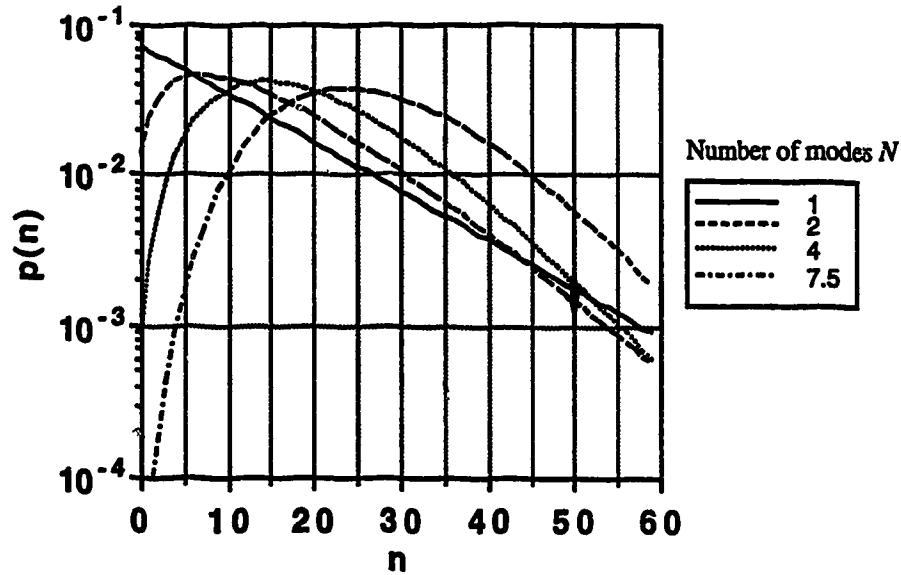


Figure 3.7: Plot of Equation (3.40) for $t=0.29$ and $\bar{n}_{in}=8$ for different values of the number of modes N .

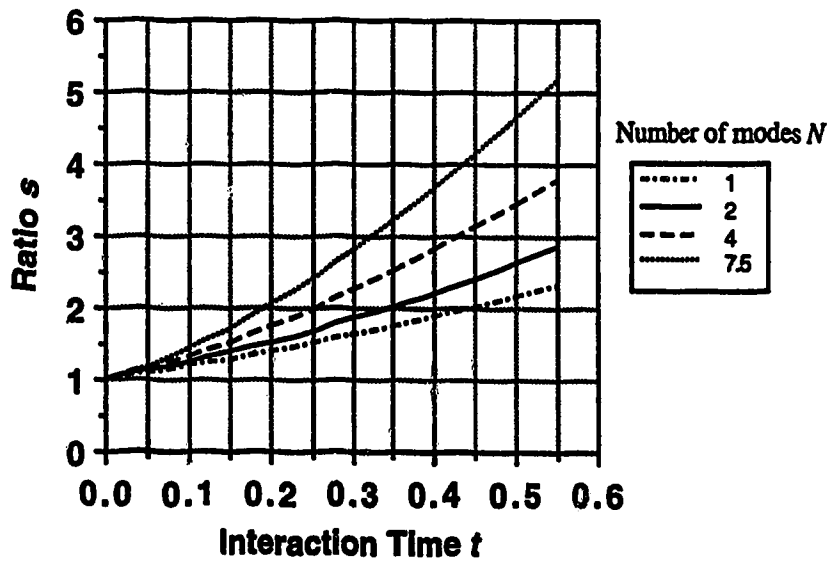


Figure 3.8: Plot of the ratio of the output to the input standard deviations as a function of the interaction time t for $\bar{n}_{in}=8$ with the number of modes N as a parameter.

The last two cases are combined in a unique plot shown in Figure 3.9. In this plot, the ratio of the output to the input standard deviations s is plotted as a function of the average input number of photons \bar{n}_{in} for different number of modes N . This figure makes

easier the comparison of the effect of these two parameters. The ratio s increases as the number of modes N increases but for a large average input number of photons, this ratio tends asymptotically to the value of amplification gain.

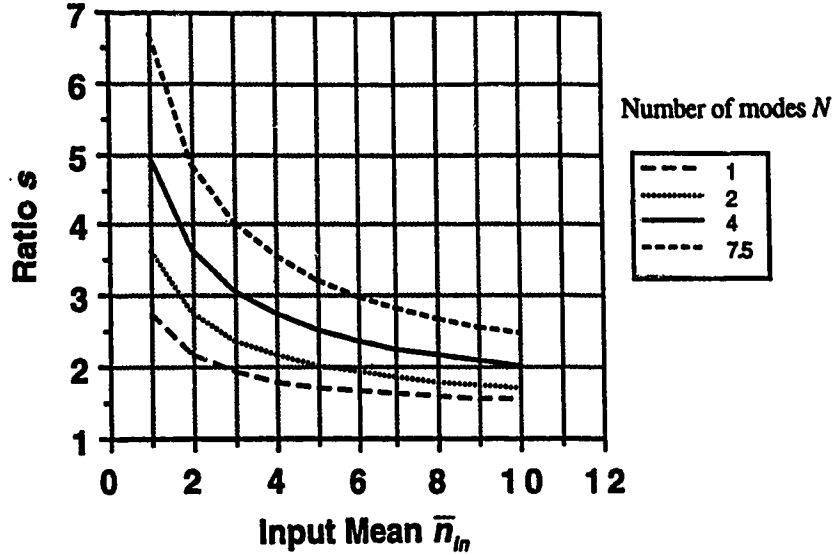


Figure 3.9: Plot of the ratio of the output to the input standard deviations as a function of the input mean \bar{n}_{in} for $t=0.29$ with the number of modes N as a parameter.

3.3 EDFA Noise Terms

In this section, the BDI medium is compared to Olsson's model for optical amplifiers [19]. This will allow us to relate the BDI parameters to such quantities as the noise factor, the optical bandwidth and optical gain which characterize EDFAs. For a better comparison, Olsson's noise terms are repeated here for the case of optically amplified laser light. Linearly polarized light is assumed in his model. The noise terms are all given in terms of their equivalent mean square photocurrent except for Equation (3.45) and (3.46) which represents the ASE power and its equivalent photocurrent.

ASE power:
$$P_{sp} = N_{sp} (G-1) h\nu B_o \quad (3.45)$$

ASE Equivalent photocurrent:
$$I_{sp} = P_{sp} e / h\nu = e N_{sp} (G-1) B_o \quad (3.46)$$

Shot noise:
$$N_{shot} = 2 B_e \mu_{out} L (G I_s \mu_{in} + I_{sp}) \quad (3.47)$$

Signal-spontaneous noise:
$$N_{s-sp} = 4 G I_s \mu_{in} \mu_{out}^2 I_{sp} L^2 B_e / B_o \quad (3.48)$$

Spontaneous-spont. noise:
$$N_{sp-sp} = (I_{sp}\mu_{out}L)^2 B_e (2B_o - B_e) / B_o^2 \quad (3.49)$$

Thermal noise:
$$N_{th} = I_{th}^2 \quad (3.50)$$

The various parameters are defined as follows:

- I_s is the equivalent laser signal photocurrent,
- N_{sp} , the spontaneous noise factor,
- G , the optical gain,
- e , the electron charge,
- μ_{in} and μ_{out} , the input and output coupling factors,
- L , the fiber loss before the photodetector,
- B_o , the total EDFA optical bandwidth,

and B_e , the single-sided electrical bandwidths. (the total electrical bandwidth is $2B_e$)

As discussed at the end of Section 3.1, the output mean of the BDI medium (Equation 3.17) when there is no input can be associated with the average number of photons generated by the ASE inside an EDFA. To compare it with Equation (3.46), it must first be converted into an equivalent photocurrent. Assuming that each photon detected generates a corresponding photoelectron, the equivalent photocurrent of the ASE average output number of photons is obtained by multiplying Equation (3.17) evaluated at $\bar{n}_{in}=0$ by the electron charge e and by the total electrical bandwidth $2B_e$. We therefore have:

$$\bar{n}(t)|_{\bar{n}_{in}=0} \times 2eB_e = \left(\frac{c}{a}\right) \frac{k(t)}{h(t)} (2eB_e) = \left(\frac{c}{a}\right) \left(\frac{a}{a-b}\right) [1/h(t)-1] (2eB_e). \quad (3.51)$$

As mentioned earlier in this chapter, the ratio (c/a) can be seen as the number of modes of the BDI medium and it is approximately equal to the ratio of the optical to the electrical bandwidths, here $B_o/(2B_e)$. Assuming $(c/a) = B_o/(2B_e)$, Equation (3.51) becomes:

$$\left(\frac{B_o}{2B_e}\right) \left(\frac{a}{a-b}\right) [1/h(t)-1] (2eB_e) = e \left(\frac{a}{a-b}\right) [1/h(t)-1] B_o \quad (3.52)$$

This expression can now be compared with Olsson's ASE equivalent photocurrent (Equation (3.46)):

$$e \left(\frac{a}{a-b}\right) [1/h(t)-1] B_o = I_{sp} = eN_{sp} (G-1) B_o \quad (3.53)$$

We find that the gain G corresponds to $1/h(t)$ and the noise factor N_{sp} to the quantity $a/(a-b)$. The first result was known from the previous sections but not the second one.

This result indicates that the noise factor is determined uniquely by the birth (stimulated emission) and death (absorption) rates and is not affected by the immigration (spontaneous emission) rate. In addition, from Equation (3.12), we can relate the quantity $(a-b)$ the EDFA optical bandwidth B_o [36].

By substituting these findings in the expression for the output variance for the case of $N_{in} = (c/a) = N$ (Equation 3.43), we can identify the various beat noise terms encountered in the detection of amplified light. Repeating Equation (3.43):

$$\sigma^2(t) = \bar{n}(t) + \frac{\bar{n}^2(t)}{N}$$

and substituting the expression for the output mean $\bar{n}(t)$ (Equation (3.42)), we get:

$$\sigma^2(t) = \left(\frac{\bar{n}_{in} + Nk(t)}{h(t)} \right) + \left(\frac{\bar{n}_{in}^2 + 2\bar{n}_{in}Nk(t) + N^2k^2(t)}{Nh^2(t)} \right). \quad (3.54)$$

Replacing $1/h(t)$ by G , $a/(a-b)$ by N_{sp} , we obtain for the first term:

$$\left(\frac{\bar{n}_{in} + Nk(t)}{h(t)} \right) = \underbrace{(G\bar{n}_{in})}_{\text{Signal Shot Noise}} + \underbrace{N_{sp}(G-1)N}_{\text{Spontaneous Shot Noise}}, \quad (3.55)$$

and for the second term:

$$\left(\frac{\bar{n}_{in}^2 + 2\bar{n}_{in}Nk(t) + N^2k^2(t)}{Nh^2(t)} \right) = \underbrace{G^2(\bar{n}_{in}^2/N)}_{\text{Excess Noise Term}} + \underbrace{2N_{sp}G\bar{n}_{in}(G-1)}_{\text{Signal-Spont. Beat Term}} + \underbrace{N_{sp}^2(G-1)^2N}_{\text{Spont.-Spont. Beat Term}}. \quad (3.56)$$

To obtain the equivalent mean square photocurrent for these noise terms, we must multiply the Equation (3.54) and (3.55) by $(2eB_e)^2$. Comparing the equivalent mean square photocurrent of the last term of Equation (3.56) with Equation (3.49), we have, for μ_{in} , μ_{out} and L equal to unity:

$$N_{sp}^2(G-1)^2N(2eB_e)^2 = N_{sp-sp} = (eN_{sp}(G-1)B_o)^2 B_e(2B_o - B_e)/B_o^2 \quad (3.57)$$

From this equation, we have:

$$N = \frac{(2B_o - B_e)}{4B_e} \quad (3.58)$$

In our case, the optical bandwidth is always much larger than the electrical bandwidth ($B_o \gg 2B_e$) and the expression of Equation (3.58) reduces to:

$$N \approx \frac{B_o}{2B_e} \quad (B_o \gg 2B_e) \quad (3.59)$$

This result is almost identical to the one found in Chapter 2. The factor of two in front of the electrical bandwidth B_e comes from the fact that B_e is defined here as the single-sided bandwidth whereas in Chapter 2, it was defined as the two-sided one.

Conversely, the BDI parameters a , b , c and t can now be expressed in terms of N_{sp} , B_o , B_e and G . They are given by:

$$a = N_{sp}(2B_o), \quad (3.60)$$

$$b = a - (2B_o) = 2B_o(N_{sp} - 1), \quad (3.61)$$

$$c \approx \left(\frac{B_o}{2B_e} \right) a = N_{sp} \left(\frac{B_o^2}{2B_e} \right) \quad (3.62)$$

and, with the help of Equation (3.12),:

$$t = \ln[G]/B_o. \quad (3.63)$$

3.3.1 Discussion

For the rest of this work, we will assume that the filtering is the same on both the LED and the EDFA. This means that both the negative binomial PDF representing the LED photon emission and the BDI medium modeling the EDFA have the same number of modes. In addition, the optical bandwidth will always be assumed larger than the electrical bandwidth. This allows us to approximate the number of modes directly by the ratio of these two bandwidths. Also, we have to remember that the BDI medium described here can be used to model linear optical amplifiers only. Consequently, the EDFA will be assumed to always operate in the linear regime. Although there are some ways [42-44] to include the saturation they are not considered here. In addition, we have to remember that the assumption of constant birth, death and immigration rates for the BDI medium is equivalent to assuming the uniform pumping throughout the EDFA length. Finally, the equivalent mean square noise photocurrent defined in Equations (4.45) to (4.50) are defined for linearly polarized light at the photodetector. This effectively means that there is a polarizer in front of the photodetector. Although the signal can have some degree of polarization, the ASE is not. Consequently, if this polarizer is removed from the link, the ASE power doubles. The polarization can be accounted for by introducing a parameter

noted m , in front of the expression of the ASE power. This parameter will be equal to 1 for linearly polarized ASE and 2 for unpolarized ASE.

3.4. Conclusion

After having defined the parameters and the mathematical equations describing a BDI medium, we calculated its output for different inputs using a method called PGF method. In particular, we calculated the output PDF of a BDI medium for a negative binomial PDF at its input. From the result of these calculations, we made some observations in order to relate BDI parameters to characteristic quantities of EDFAs. We identified the various beat noise terms encountered in the detection of optically amplified light in the BDI output variance.

In the next chapter, the performance of spectral slicing of an LED followed by a EDFA and an optical filter will be examined theoretically for a digital fiber optic transmission. To do that, we will use the statistical models described in the this chapter and in the previous one. The performance will be studied in terms of both the SNR (signal-to-noise ratio) and BER (bit-error rate).

4. Theoretical Performance of Spectral Slicing with and without the Use of EDFAs

In Chapter 2, we studied the statistics of various light sources to find their corresponding photon number distribution. We found that the photon emission of a filtered LED is characterized by a negative binomial PDF. In Chapter 3, we introduced the BDI medium and we found that the filtered output of an LED optically amplified by EDFA is also a negative binomial PDF in the case where the same optical filtering is applied to both the EDFA and the LED. In this chapter, the performance of spectral slicing is examined using the theory described in Chapters 2 and 3. The focus will be put on one slice or carrier only.

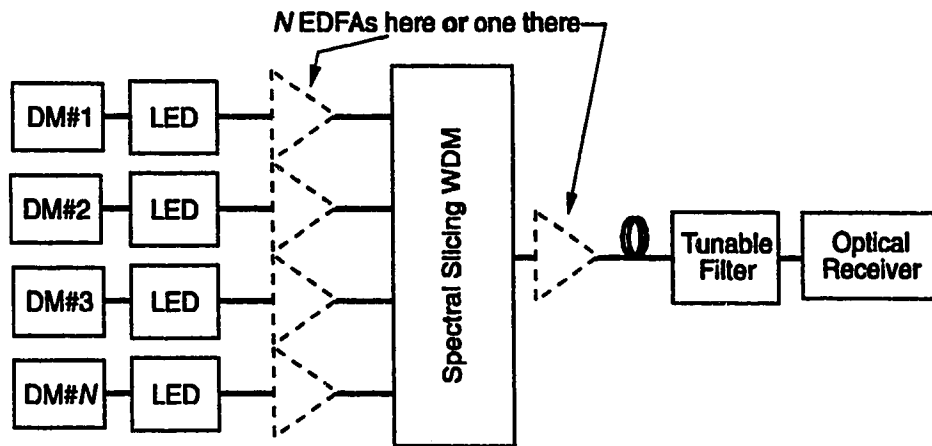
The chapter is divided into four parts. In the first part, we describe the spectral slicing system. Second, the performance of one single spectral slice is examined based on both the SNR and the BER. Then the performance of spectral slicing is evaluated in a WDM application. Finally, the chapter ends with a conclusion.

4.1 System Description

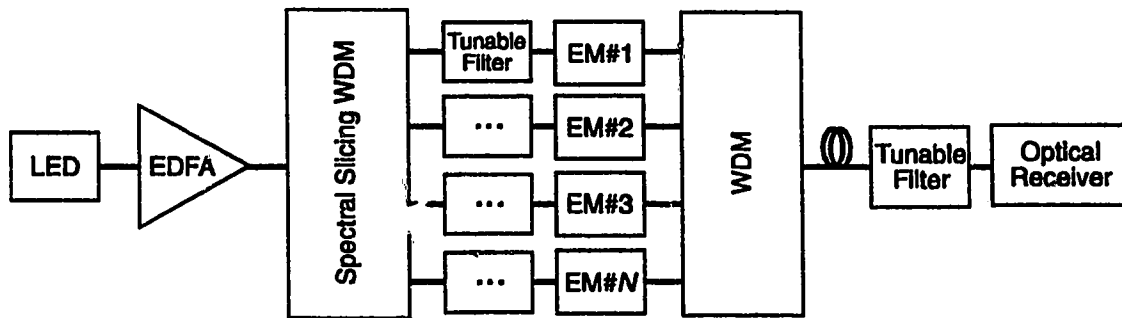
Figure 4.1 shows two designs of WDM systems using spectral slicing. The first one uses a series of LEDs that are directly modulated. Their output power is then optically amplified by EDFAs, filtered and optically multiplexed by a WDM, transmitted and detected. A WDM is basically a frequency sensitive coupler composed of a set of filters and a set of wavelength sensitive combiners. Note that the set of EDFAs following the LEDs could also be replaced by a single one after the WDM. The second design utilizes only one LED and one EDFA but a series of external modulators (EMs) between two WDM filters back to back. The main idea behind the second design is that all the optical carriers are generated using only one source.

For the purposes of examining the impact of filtering on the behavior of a transmission system, we are interested only in the study of one single carrier. Thus, the actual system under study reduces to an LED, followed by an EDFA, optical filter and an optical receiver as shown in Figure 4.2. In addition, we assume that the carrier impinging on the photodetector is linearly polarized. In the figure, a polarizer designated by an arrow standing up is used just before the optical receiver to ensure that the light impinging on the

photodetector is linearly polarized. The coil designates the optical fiber and its associated loss.



(a)



(b)

Figure 4.1: Two designs of WDM transmission systems using spectral slicing. In (a) LEDs are directly modulated (DMs) and in (b) external modulators (EMs) are used.

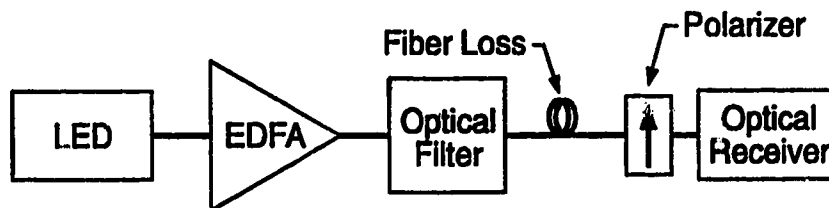


Figure 4.2: Spectral slicing system under study. It is composed of an LED, an EDFA, an optical filter and an optical receiver.

4.1.1 Signal Power

The signal power is the optical power contained in one spectral slice or carrier. It is obtained by taking the integral over all frequencies of the product of the LED power spectrum $S_{LED}(\nu)$ and the optical filter transmittance $S_{OF}(\nu)$. It can be calculated as follows:

$$P_s = \int_{-\infty}^{\infty} [S_{LED}(\nu)S_{OF}(\nu)]d\nu \quad (4.1)$$

The LED power spectrum is approximately Gaussian in shape with a FWHM bandwidth that can be as large as 100 nm (~13 THz). This bandwidth is several times larger than that of the spectral slicing optical filter. Consequently, the LED power spectrum can be assumed essentially flat over the optical filter bandwidth. This is illustrated in Figure 4.3 where a broad LED is filtered by a narrow optical filter. The LED and the optical filter FWHM bandwidths are identified by $\Delta\nu_{LED}$ and $\Delta\nu_{OF}$, respectively, on the figure. ν_o and ν_{OF} designate the LED and the optical filter center frequencies, respectively.

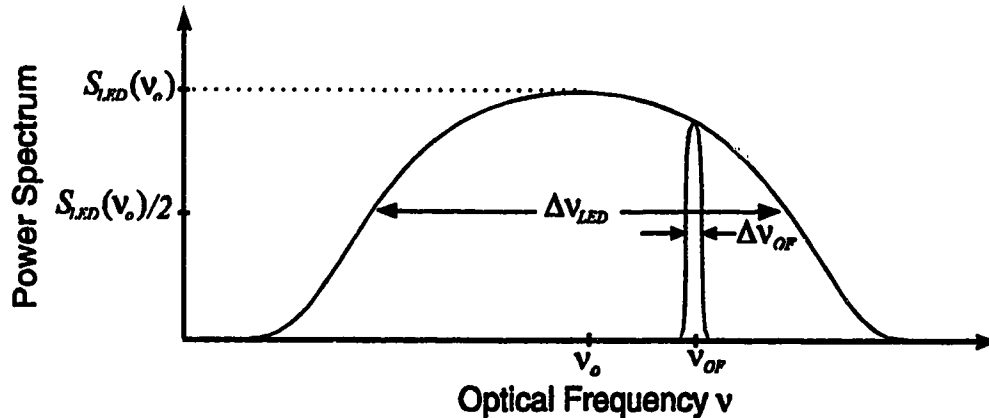


Figure 4.3: Illustration of spectral slicing of a broad LED with a narrow optical filter .

Assuming a Gaussian power spectrum for the LED $S_{LED}(\nu)$, we have:

$$S_{LED}(\nu) = \frac{P_{LED}}{\sqrt{2\pi}\sigma} \exp\left(-\frac{(\nu-\nu_o)^2}{2\sigma^2}\right) \quad (4.2)$$

where the parameter σ defines the linewidth of the LED. Its relationship with the FWHM and the equivalent rectangular bandwidth is given in Table 2B.1. With the assumption that

the LED spectrum is flat over the optical filter bandwidth, the average power contained in a carrier can be calculated as follows:

$$P_s = S_{LED}(v_{OF}) \int_{-\infty}^{\infty} S_{OF}(v) dv \quad (4.3)$$

In the case where the optical filter is centered exactly at the spectrum peak of the LED, that is when $v_{OF} = v_o$, Equation (4.3) reduces to:

$$P_s = \frac{P_{LED}}{\sqrt{2\pi}\sigma} \int_{-\infty}^{\infty} S_{OF}(v) dv \quad (4.4)$$

If the optical filter has no insertion loss, the integral of Equation (4.3) is effectively the equivalent rectangular bandwidth of the optical filter B_{OF} . We therefore get for the signal power:

$$P_s = \frac{P_{LED}}{\sqrt{2\pi}\sigma} B_{OF} = \frac{P_{LED}}{B_{LED}} B_{OF} \quad (4.5)$$

where B_{LED} is the equivalent rectangular bandwidth of the LED. As for the LED, the EDFA gain spectrum is generally very broad. Although it can not usually be approximated by a simple function, it can be made fairly flat over the entire bandwidth with the use of some dopants like aluminum [15]. Consequently, the amplified signal power can simply be obtained by multiplying the expression of Equation (4.5) by the gain of the EDFA at the optical filter center frequency, i.e., $G(v_{OF})$.

4.1.2 Modulation

The modulation applied to the optical carrier can be analog or digital. Digital signals are represented by a sequence of zeros and ones called bits. The rate at which the bits occur is called the bit rate and is noted B and is inversely related to the duration of a bit T , i.e., $B=1/T$. When OOK intensity modulation is used, a large number of photons is associated with the *on* states and a small number with the *off* states. One can define the extinction ratio as follows:

$$r = \frac{\text{average \# of photons during on state}}{\text{average \# of photons during off state}} \quad (4.6)$$

An extinction ratio of infinity represents the best case and is not achievable in practice. More realistic values are on the order of 10 to 100. The average number of photons during the *on* and *off* states is defined as [19]:

$$\bar{n}_{off} = (P_{av}/(2h\nu B_e)) \left(\frac{2}{r+1} \right). \quad (4.7)$$

$$\bar{n}_{on} = (P_{av}/(2h\nu B_e)) \left(\frac{2r}{r+1} \right) \quad (4.8)$$

where P_{av} is the average signal power, $h\nu$, the photon energy and B_e , the single-sided electrical bandwidth. In our case, P_{av} is given by P_s which is defined in Equation (4.1).

Two types of digital signals can be used in OOK modulation: non-return-to-zero (NRZ) and return-to-zero (RZ). NRZ signals have a 100 % duty cycle whereas RZ signals have a 50 % duty cycle. The NRZ and RZ signals are illustrated in Figure 4.4 for the same bit rate. We see that the NRZ signal occupies the full duration T of a bit while the RZ occupies only half. This results in that an RZ signal requires twice the electrical

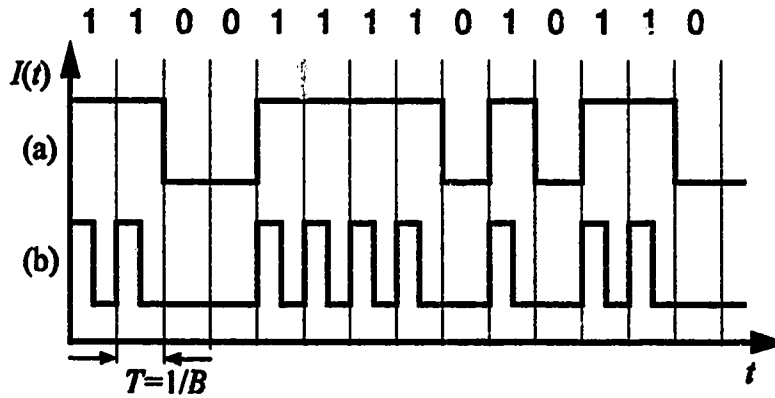


Figure 4.4: (a) NRZ and (b) RZ signals.

bandwidth of an NRZ signal. NRZ and RZ OOK modulation can be applied by directly varying the injection current of the LED or by the use of external modulators.

4.1.3 Photodetection

The photodetector essentially converts a flux of photons to a corresponding photocurrent. The process by which a photon stream is converted to a photocurrent is called photodetection. It can be modeled in the following equation [27]:

$$i(t) = \sum_{m=1}^{n(0,t)} h_d(t-t_m), \quad (4.9)$$

where $h_d(t)$ is the photodetector impulse response function. The area of the photodetector impulse response function is equal to the electron charge. t_m is the time of release of the m th photoelectron and $n(0,t)$ is the number photoelectrons released during the time interval $(0,t)$. The photodetector is always followed by an electric circuit to form an optical receiver. Consequently, it is more appropriate to use the impulse function of the $h_r(t)$ of the optical receiver. The transfer function of the optical receiver $H_r(f)$ can be obtained by the Fourier transform of its impulse response function $h_r(t)$. It can have different shapes to serve different purposes. One shape commonly used in digital communication is the raised-cosine because it minimizes the intersymbol interference [8]. Its magnitude is defined as follows:

$$|H_r(f)| = \begin{cases} 1 & \text{for } |f| < B - B_e \\ \cos^2\left(\frac{\pi}{4} \frac{|f| + B_e - B}{B_e - B/2}\right) & \text{for } (B - B_e) < |f| < B_e \\ 0, & \text{for } |f| > B_e. \end{cases} \quad (4.10)$$

B_e is the single-sided absolute receiver (electrical) bandwidth and is given by:

$$B_e = \frac{1}{2}(1 + \beta)B, \quad (4.11)$$

where β is the roll-off factor and B , the bit rate. The roll-off factor changes the shape and the bandwidth of of the optical receiver transfer function $|H_r(f)|$. This is illustrated in Figure 4.5. For $\beta=0$, for instance, $|H_r(f)|$ is perfectly rectangular and the single-sided electrical bandwidth B_e is half the bit rate. For digital communication systems using OOK-NRZ modulation, a receiver bandwidth slightly larger is usually assumed. [6]

Assuming that each photon generates a corresponding photoelectron at the photodetector, the average photocurrent $\langle i \rangle$ produced by the detection of a OOK-NRZ modulated signal can be obtained by multiplying the average photon number recorded during the duration of a bit by the electron charge q and the total (double-sided) receiver (electrical) bandwidth $2B_e$. We obtain:

$$\langle i \rangle = 2q\bar{n}B_e. \quad (4.12)$$

In the same manner, the variance of the photocurrent is obtained by multiplying the variance of the photon number by $(2qB_e)^2$ as follow:

$$\sigma_i^2 = (2qB_e)^2 \sigma_n^2. \quad (4.13)$$

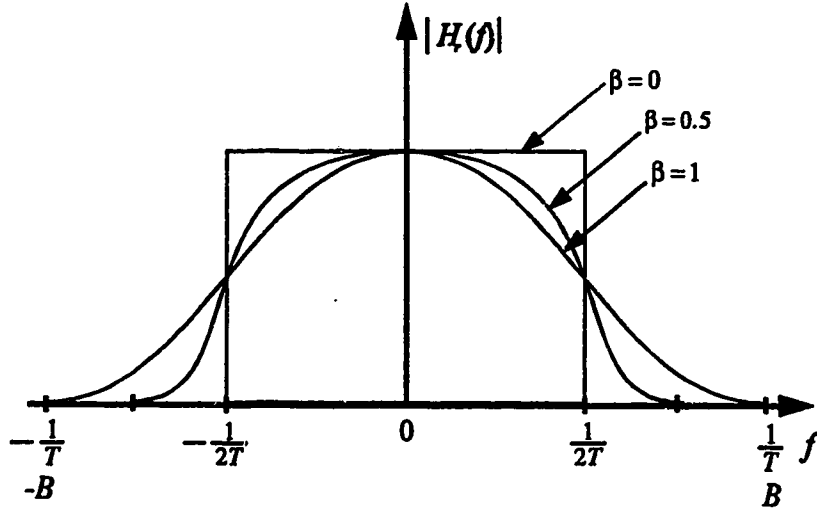


Figure 4.5: Plot of the receiver transfer function $|H_r(f)|$ for different values of the roll-off factor.

In a real photodetector, the efficiency of the conversion of photons to electrons is not 100%. It is scaled by a factor (usually denoted η) called the quantum efficiency. Therefore, the real average photocurrent would be obtained by multiplying the average photon number by $\eta(2qB_e)$ instead of only $(2qB_e)$. Also, for the moment, we will assume that the receiver circuit is noiseless, i.e., no thermal noise is added to the fluctuations of the signal. This is a reasonable approximation when the signal level is large. The impact of the thermal noise will be discussed later.

With the help of Equation (4.12) and (4.13), we can rewrite the various noise terms encountered in the detection of linearly polarized optically amplified signals identified in Chapter 3 (see Equations (3.55) and (3.56)) in terms of their equivalent mean square photocurrents. They are as follows:

ASE :
$$I_{sp} = P_{sp}(\eta q) / (h\nu) = \eta q m_r N_{sp} (G-1) (2B_e) N \quad (4.14)$$

Signal:
$$I_s = \bar{n} (2\eta q B_e) \quad (4.15)$$

Signal squared:
$$S = ((GI_s) \mu_{in} \mu_{out} L)^2 \quad (4.16)$$

Shot noise:
$$N_{shot} = (2\eta q B_e \mu_{out} L) (\mu_{in} (GI_s) + I_{sp}) \quad (4.17)$$

Signal-spontaneous noise:
$$N_{s-sp} = (2(GI_s) \mu_{in} \mu_{out}^2 I_{sp} (L^2)) / N \quad (4.18)$$

Spont.-spont. noise:
$$N_{sp-sp} = (\mu_{out} L I_{sp})^2 / N \quad (4.19)$$

Excess noise:
$$N_{ex} = (\mu_{in}\mu_{out}L(GI_s))^2 / N \quad (4.20)$$

where η is the quantum efficiency of the photodetector, μ_{in} and μ_{out} are the input and output coupling factors and L is the fiber loss between the optical filter and the optical receiver. The parameter m , in Equation (4.14) takes into account the polarization of the detected ASE. In our case, a polarizer is used in front of the optical receiver and m , becomes equal to 1. The Equation (4.15) defines the average photocurrent of the signal and \bar{n} is the average number of photons representing the signal. N is the number of modes as defined in Chapter 2 by Equation (2.35) and as we discussed in this chapter, it can be approximated by the ratio of the optical to the electrical bandwidths in the case of large N . Here the optical bandwidth B_o is that of the optical filter and the electrical bandwidth is the double-sided optical receiver bandwidth $2B_e$. Consequently, N is given by:

$$N \approx \frac{B_o}{2B_e} \quad (4.21)$$

The sum of the various noise terms is:

$$N_{tot} = N_{shot} + N_{sig-sp} + N_{sp-sp} + N_{ex}. \quad (4.22)$$

Note that N_{tot} is equal to the variance of the equivalent mean square photocurrent (Equation (4.13))

4.2 Performance

The performance of a transmission system depends on the signal level relative to noise. When analog modulation is used, the signal is a continuous waveform and the performance of the system is given in terms of SNR. When we use digital modulation, the signal is represented by a series of zeros and ones called bits and the performance is given in terms of BER. There exists a relationship between the SNR and the BER, however, this relationship is not always obvious. Although the SNR is not appropriate to evaluate the performance of a digital system, it can provide some insight into the understanding of the system behavior. Consequently, in the following, the performance of the system of Figure 4.2 will be studied in terms of both the SNR and the BER.

4.2.1 SNR in Absence of Thermal Noise

The general expression for the SNR is:

$$\begin{aligned}
SNR &= \frac{\text{Signal power}}{\text{Noise power}} \\
&= \frac{\text{Mean square signal photocurrent}}{\text{Mean square noise photocurrent}}.
\end{aligned} \tag{4.23}$$

Since we assume an optical receiver with no thermal noise, the noise of the system is caused by the fluctuations in the photon number only (photon noise). These fluctuations can be evaluated by the photon number variance σ_n^2 or equivalently by its equivalent mean square photocurrent N_{tot} . The SNR becomes:

$$SNR = \frac{S}{N_{tot}} = \frac{S}{N_{shot} + N_{s-sp} + N_{sp-sp} + N_{ex}} \tag{4.24}$$

First, we consider the system of Figure 4.2 in the case where the LED is directly OOK modulated with a NRZ signal and without the EDFA (i.e., $G = (1/h(\tau)) = 1$). Assuming a unity quantum efficiency for the photodetector ($\eta=1$) and no fiber loss ($L=1$), the SNR is given by:

$$SNR = \frac{S}{N_{shot} + N_{ex}} = \frac{\bar{n}^2}{\bar{n} + (\bar{n}^2/N)} = \frac{N\bar{n}}{N + \bar{n}}. \tag{4.25}$$

Here, \bar{n} can be defined as the average number of photons per bit as follows:

$$\bar{n} = \frac{1}{2}(\bar{n}_{on} + \bar{n}_{off}) \tag{4.26}$$

where \bar{n}_{off} and \bar{n}_{on} are the number of photons during the *on* and *off* states, respectively and are defined by the Equations (4.7) and (4.8), respectively. The Equation (4.25) has two limiting cases:

$$(1) \quad \text{for } \bar{n} \ll N, \quad SNR \approx \bar{n}, \tag{4.27}$$

$$(2) \quad \text{for } \bar{n} \gg N, \quad SNR \approx N. \tag{4.28}$$

Using Equation (4.21), these two cases can be rewritten as:

$$(1) \quad \text{for } \bar{n} \ll \frac{B_o}{2B_c}, \quad SNR \approx \bar{n}, \tag{4.27*}$$

$$(2) \quad \text{for } \bar{n} \gg \frac{B_o}{2B_c}, \quad SNR \approx \frac{B_o}{2B_c}. \tag{4.28*}$$

This result was found by Morkel et al [45].

Now, if the EDFA is incorporated and the LED is still directly OOK modulated with an NRZ signal, we have:

$$SNR = \frac{S}{N_{tot}} = \frac{S}{N_{shot} + N_{s-sp} + N_{sp-sp} + N_{ex}} \quad (4.29)$$

For large gain G , we have two limiting cases:

$$(1) \quad \text{for } \bar{n} \ll N, SNR \rightarrow \frac{S}{N_{sp-sp}} \approx \frac{\bar{n}^2}{N_{sp}^2 N}, \quad (4.30)$$

$$(2) \quad \text{for } \bar{n} \gg N, SNR \rightarrow \frac{S}{N_{ex}} \approx N. \quad (4.31)$$

As we can see, from Equation (4.28) and (4.31), the excess noise of the LED ultimately limits the SNR which becomes entirely determined by the number of modes even in the case where an EDFA is used. However, as the number of modes N becomes large compared to the signal power \bar{n} , the SNR becomes limited by the signal power and by the EDFA characteristics.

4.2.2 BER in Absence of Thermal Noise

The BER is defined as the weighted sum of the probabilities of mistaking a zero for a one and vice versa because of the presence of noise. In the case of a perfect extinction ratio ($r = \infty$), the BER is simply found by determining the probability of having zero photons during an *on* state [13]. As said in the Introduction, this gives an average number of photons per bit of 21. (This assumes a Poissonian photon number distribution (best case) and equiprobable zeros and ones.) This is known as the fundamental limit for direct detection. The determination of the BER for $r \neq \infty$ is more complicated and must make use of the formalism of the Decision Theory [46]. In this case, photons can be recorded even during the *off* state. Consequently, there is a region where the PDFs for the *on* and *off* states overlap and in the case where the zeros and ones are equiprobable, the BER is given by half the total overlapping area. This is illustrated in Figure 4.6. Mathematically, we must find a decision threshold γ_o , which fixes a boundary between the detection of ones and the zeros. The bits containing a number of photons that is greater than the threshold number are detected as ones and the others as zeros. Then, the BER is obtained by integrating (taking the sum for discrete PDFs) the overlapping region of the PDF of the *on* and *off* states delimited by the decision threshold and divide by two.

The mathematical expressions for the BER are:

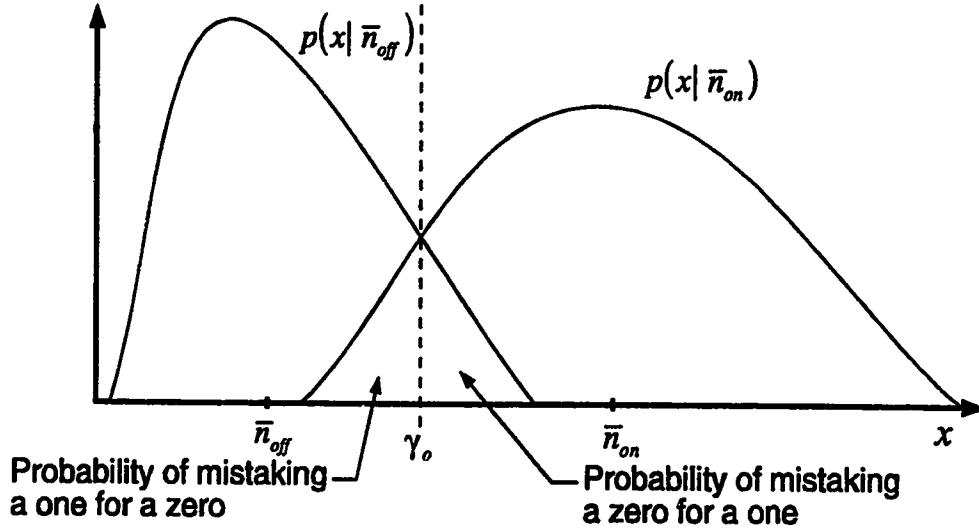


Figure 4.6: Illustration of the method for calculating the BER.

$$BER = \frac{1}{2} \left[\int_{-\infty}^{\gamma_o} p(x|\bar{n}_{on}) dx + \int_{\gamma_o}^{\infty} p(x|\bar{n}_{off}) dx \right] \text{ (for } x \text{ continuous)} \quad (4.32)$$

$$BER = \frac{1}{2} \left[\sum_{x=0}^{\gamma_o} p(x|\bar{n}_{on}) + \sum_{x=\gamma_o}^{\infty} p(x|\bar{n}_{off}) \right] \text{ (for } x \text{ discrete)} \quad (4.33)$$

where $p(x|\bar{n}_{off})$ and $p(x|\bar{n}_{on})$ are the PDFs for the *off* and *on* states, respectively. The variable x here represents the photon number.

Assuming NRZ OOK modulation with \bar{n}_{off} and \bar{n}_{on} representing the mean number of photons during the *off* and *on* states respectively and in the case where the noise has a negative binomial PDF, the optimum decision threshold can be found analytically. It is given by (see Appendix 4A for derivation):

$$\gamma_o = N \frac{\ln\left(\frac{(1+\bar{n}_{on}/N)}{(1+\bar{n}_{off}/N)}\right)}{\ln\left(\frac{(1+N/\bar{n}_{off})}{(1+N/\bar{n}_{on})}\right)} \quad (4.34)$$

and since the photon number is a discrete variable, the BER is obtained with the use of Equation (4.33)

An approximation of the BER can be obtained if the noise is assumed to be Gaussian distributed with a variance given by the sum of the noise terms N_{tot} , as defined in

Equation (4.22). In this case, the BER is related to the complementary error function [6, 19] as follows:

$$BER = \frac{1}{\sqrt{\pi}} \int_0^{\infty} \exp(-t^2) dt = \frac{1}{2} \operatorname{erfc}\left(\frac{Q}{\sqrt{2}}\right) \quad (4.35)$$

where

$$Q = \frac{\sqrt{S(on)} - \sqrt{S(off)}}{\sqrt{N_{tot}(on)} + \sqrt{N_{tot}(off)}} \quad (4.36)$$

This approximation is commonly used for digital intensity modulated system [19]. The parameter Q can be seen as a kind of SNR for a digital system and can be related to the SNR defined in Section 4.2.1. Note that with the Gaussian approximation, a BER of 10^{-9} is obtained for a Q equal to about 6.

The BER is usually plotted as a function of the optical power just before the receiver and the curves obtained follows a waterfall-like behavior. In the case of system of Figure 4.2 where the LED is directly modulated with an NRZ-OOK signal, this power is the average amplified signal power plus the ASE power. This corresponds to the average output number of photons after optical amplification and filtering multiplied by the photon energy and the bit rate. Substituting the EDFA parameters in the expression for the output number of the BDI medium (Equation (3.42)) and multiplying it by $h\nu B$, we obtain:

$$\begin{aligned} P_r &= \bar{n}(t)h\nu B \\ &= (G\bar{n} + P_{sp})h\nu B \end{aligned} \quad (4.37)$$

where \bar{n} is defined by (4.26). The optical power is often given in dB relative to one milliwatt or dBm. The power can be converted from Watts to dBm by the following formula:

$$P \text{ in dBm} = 10 \log\left(\frac{P \text{ in Watts}}{10^{-3}}\right) \quad (4.38)$$

4.2.3 Numerical Calculations

In this section, the BER performance of the system of Figure 4.2 is studied for the case where the LED is directly NRZ-OOK modulated at a bit rate B of 1 Gb/s. The EDFA is assumed to operate in the linear regime and its pumping is uniform throughout its length. The value 0.8 is taken for the EDFA coupling factors μ_{in} and μ_{out} . In addition, the spectral slicing is assumed perfect, i.e., the optical filter has a rectangular linewidth and no insertion loss. We assume that the optical receiver has no thermal noise and that its single-

sided bandwidth B_c is equal to 0.6 times the bit rate [6], i.e., $B_c=600$ MHz. The value 0.8 is taken for the quantum efficiency η of the photodetector. Finally, the number of modes N is approximated by the ratio of $B_o/2B_c$ for values of this ratio greater than 10.

Our study consists of varying the various system parameters, i.e., the LED power, the optical filter bandwidth, the gain and the noise factor of the EDFA and the LED extinction ratio, and observing the their effect on the BER performance. The BER is calculated using Equation (4.33) with the negative binomial PDF representing the noise at the optical receiver. For the calculations we used a very powerful mathematical software package called *Mathematica* [47]. The program listings can be found in Appendix 4B.

LED Power

To see the effect of the LED power on the BER performance of the system of Figure 4.2, the LED power was varied from 2 to 50 μ W (-27 to -13 dBm) while all the other parameters were kept constant. We assumed an extinction ratio r of 100 for the LED, a gain G of 30 dB with a noise factor N_{sp} of 1.5 for the EDFA and an optical filter bandwidth B_o of 0.5 nm (\sim 62 GHz). This gives about 53 for the number of modes. The BER is plotted as a function of the optical power at the receiver in Figure 4.7. This is

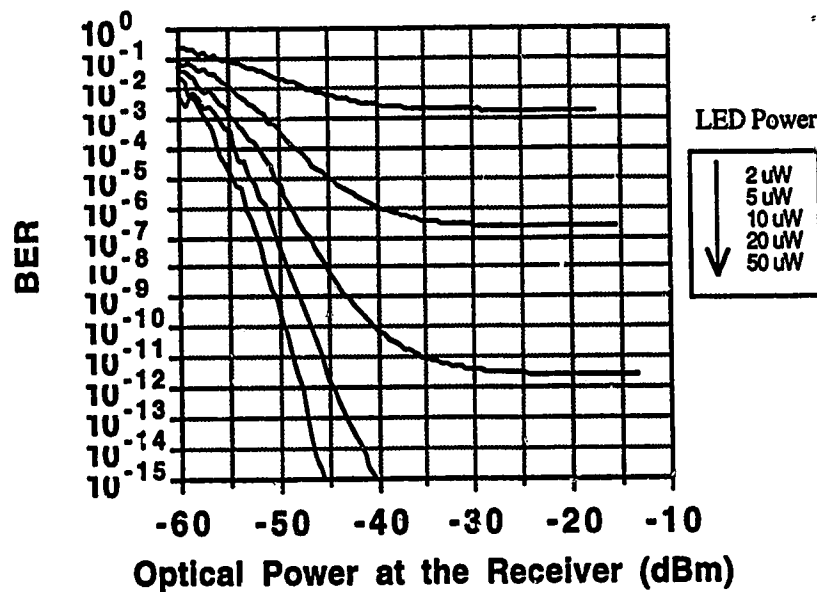


Figure 4.7: BER curves as a function of the optical power at the receiver for different LED power P_{LED} . ($r=100$, $G=30$ dB, $N_{sp}=1.5$ and $N\approx 53$)

obtained by varying the fiber loss L between the optical filter and the optical receiver in Figure 4.2. From Figure 4.7, we see that for a small amount of optical power at the receiver, the BER curves follow the usual waterfall-like behavior. However, we note that BER floors are reached for large power at the optical receiver and that they are shifted down for increasing values of LED power. The best sensitivity for our system is -50 dBm (10 nW) and is achieved for an LED power of 50 μ W (-13 dBm). This corresponds to an average of 65 photons per bit. As the LED power is reduced, the sensitivity degrades. For LED power less than 5 μ W for instance, the BER never reaches the 10^{-9} point. The BER floor is highly dependent on the LED power. To better see this effect, its value is plotted as a function of LED power in Figure 4.8. We see that a factor of two in input power creates a shift in the BER floor of about five orders of magnitude. In the rest of this section, the BER floor will be used as a point for comparison between the various parameters.

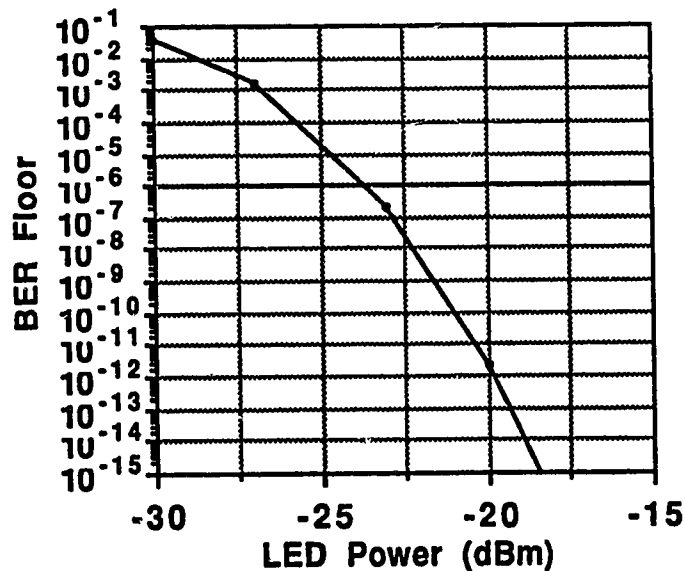


Figure 4.8: BER floor as a function of the LED power P_{LED} . ($r=100$, $G=30$ dB, $N_{sp}=1.5$ and $N=53$)

Because no simple relationship exists between the BER calculated with Equation (4.33) and the SNR, the BER floor is somewhat difficult to explain. However, it is possible to get some understanding of what is happening by looking at the expressions for the noise terms (Equations (4.14) to (4.20)) and the limiting cases for the SNR (Equations (4.30) and (4.31)). Amongst the noise terms, only that of the excess noise N_{ex} has a quadratic dependency on the average signal photocurrent I_s . As discussed in Section

4.2.1, this term dominates the SNR when the ratio of the average number of photon number per bit to the noise factor is larger than the number of modes. In our case, the BER is limited by the excess noise for all the values of LED power except for $2 \mu\text{W}$ where it is limited by the signal-spontaneous noise. The excess noise is due to the incoherency of the LED and it fixes the quality of the signal at the beginning of the system. The EDFA amplification can not improve this quality but can only degrade it because of its ASE.

Optical Filter Bandwidth (Number of Modes)

To look at the effect of optical filter bandwidth on the BER floors, we varied the number of modes N and kept all other parameters constant. For the calculations, we chose $10 \mu\text{W}$ (-20 dBm) for the LED power and 100 for the LED extinction ratio, 30 dB for the EDFA gain and 1.5 for the noise factor as before. The range of values for N is 30 to 70 and that corresponds to an optical filter bandwidth going from about 0.28 to 0.68 nm. Figure 4.9 shows the BER floor plotted as a function of the number of modes. As we can see, the number of modes also has an important effect on the BER floor. An increase of ten in the number of modes results in the BER floor being shifted down by two orders of magnitude. Here again, the system performance is dictated by the excess noise and the reason of the BER floor shift is due to the fact that the excess noise is inversely proportional to the number of modes. Eventually, for larger values of the number of modes, the signal-spontaneous and the spontaneous-spontaneous noises both overcome the excess noise and consequently also contribute to the degradation of the BER.

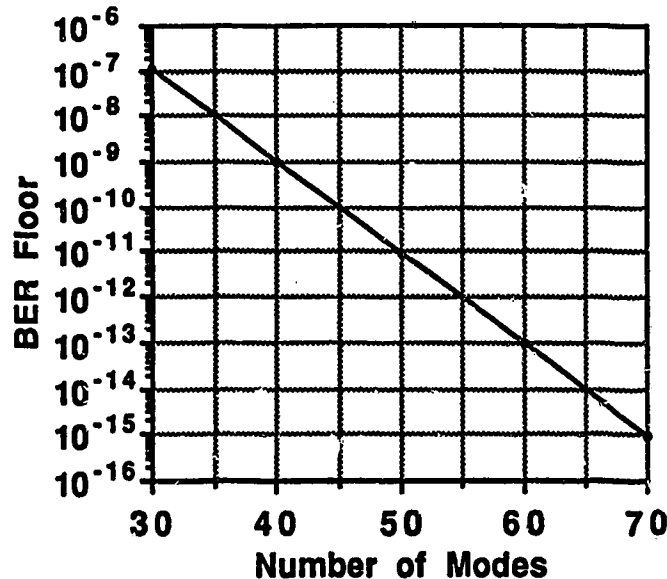


Figure 4.9: BER floor as a function of the number of modes N . ($P_{LED}=10 \mu\text{W}$, $r=100$, $G=30 \text{ dB}$ and $N_{sp}=1.5$)

EDFA Gain and Noise Factor

The effect of EDFA gain and noise factor on the BER floor was examined in the same way as the two previous cases. This result is presented in Figures 4.10 and 4.11, respectively. Figure 4.10 shows the BER floors obtained when the EDFA gain is varied from 10 to 30 dB and all other parameters are kept constant. Here we took $10 \mu\text{W}$ (-20 dBm) for the LED power and 100 for the LED extinction ratio, 53 for the number of modes and 1.5 for the noise factor. The effect of the EDFA gain on the BER floors is contrary to the two previous cases. The BER floors are shifted upwards as the gain increases but by a relatively small amount. As the gain goes from 10 to 30 dB, the BER floor goes from about 8×10^{-13} to about 2×10^{-12} . This was expected since the gain does not enter in any of the SNR expressions for large gain (see Equations (4.30) and (4.31)). In addition, we notice that the BER floor seems to reach a maximum value for large gain. This value is here also determined by the excess noise term.

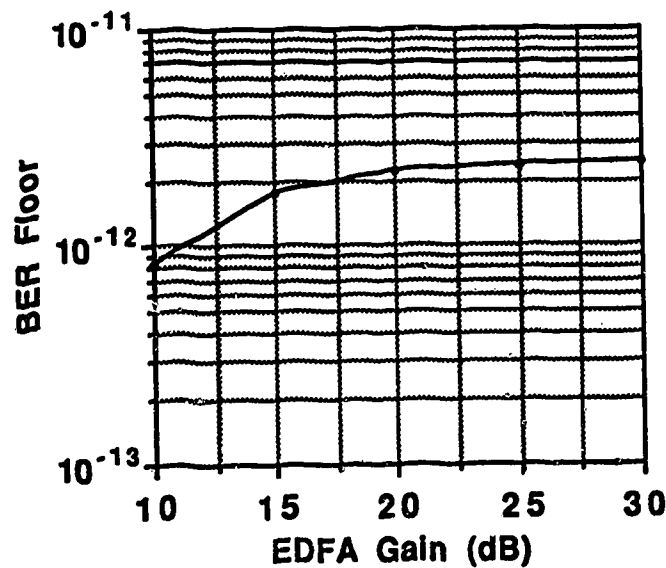


Figure 4.10: BER floor as a function of the EDFA gain G . ($P_{LED}=10 \mu\text{W}$, $r=100$, $N_{sp}=1.5$ and $N \approx 53$)

Figure 4.11 shows the variation of the BER floor values as the EDFA noise factor N_{sp} goes from 1 to 5. This was obtained for the same LED power, extinction ratio and number of modes as for the EDFA gain study above. In addition, we assumed 30 dB for the EDFA gain. As we can see, the noise factor largely affects the BER floor. An upward

shift of about 8 decades results in the BER floor as the noise factor goes from 1 to 5. The excess noise of the LED is here again responsible for the BER floors but the signal-spontaneous noise also affects the BER as N_{sp} goes up.

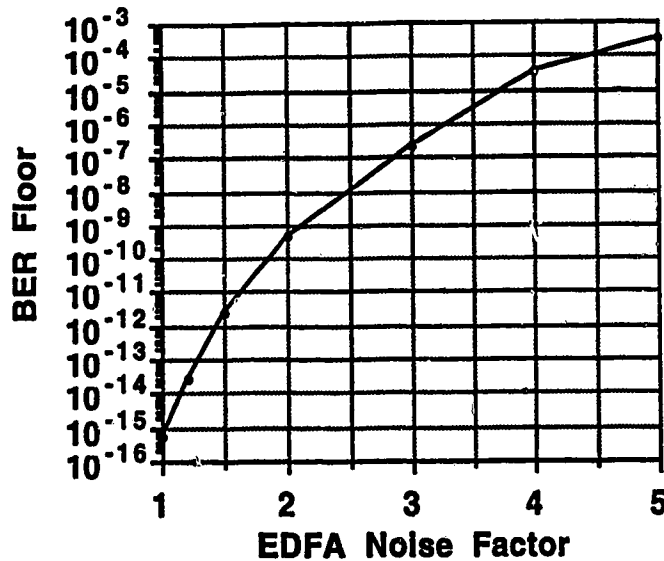


Figure 4.11: BER floor as a function of the EDFA noise factor N_{sp} . ($P_{LED}=10 \mu\text{W}$, $r=100$, $G=30 \text{ dB}$ and $N \approx 53$)

LED Extinction Ratio

Finally, the effect of the LED extinction ratio was also examined. To do so, we proceeded the same way as before and varied its value from 10 to 100 while keeping all other parameters constant. The noise factor value was reset to 1.5 and we kept all the other parameters identical as before. The effect of the LED extinction ratio on the BER floor is also quite important as shown in Figure 4.12. The BER floor is shifted down by almost five decades when the extinction ratio is increased from 10 to 100. The increase of the LED extinction ratio does not directly affect the SNR as defined in Section 4.2.1, it only affects the effective contrast between the zeros and the ones seen by the optical receiver. This contrast is however always limited by the ASE of the EDFA. Here, the system performance is again limited by the excess noise of the LED and as the LED extinction ratio increases, the minimum BER floor is determined by the number of modes.

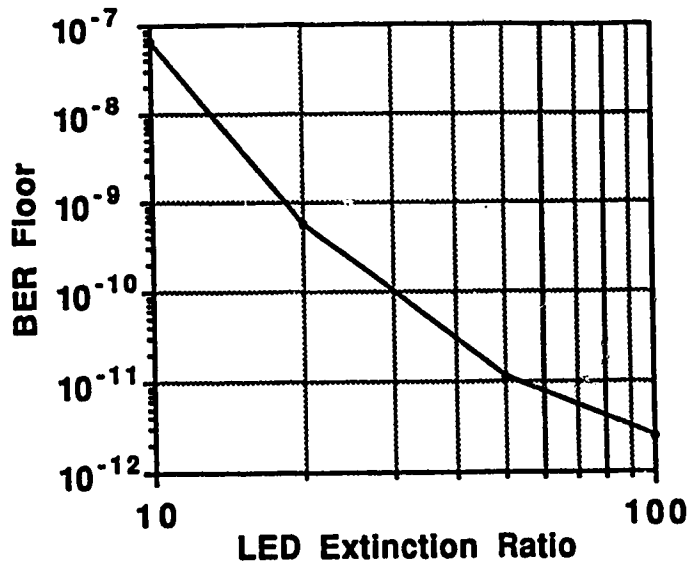


Figure 4.12: BER floor as a function of the LED extinction ratio r . ($P_{LED}=10 \mu\text{W}$, $G=30$ dB $N_{sp}=1.5$ and $N=53$)

Discussion

We can summarize the effect of the various parameters on the BER performance as follows. First, the best sensitivity is achieved for a high LED power. For a bit rate of 1 Gb/s, 64 photons per bit are required for an LED power of $50 \mu\text{W}$ with an extinction ratio of 100, a EDFA gain of 30 dB and an optical filter bandwidth of 0.5 nm. Second, BER floors are observed for large power at the optical receiver and their value is highly dependent on the LED power, the EDFA noise factor, the LED extinction ratio and the number of modes. These BER floors are caused by the excess noise of the LED which fixes the quality of the signal at the beginning of the system. For small LED power and large noise factor, the BER starts being affected by the signal-spontaneous and spontaneous beat noises. Third, since the LED power and the number of modes enters in the expression for the excess noise, they have a important effect on the BER floor. The EDFA noise factor and the LED extinction ratio are also important. The EDFA gain is the parameter that affects the least the value of the BER floors. Assuming that there is a sufficient amount power of power at the optical receiver, the BER performance consistently improves with increasing values of the number of modes, LED power and extinction ratio. On the other hand, increasing values of the EDFA gain and noise factor degrade the BER.

4.2.4 Comparison with the Gaussian approximation

As mentioned earlier, an approximation for the BER can be obtained by assuming that the fluctuations in the signal are Gaussian distributed with a variance given by the sum of the noise terms. In that case, the BER is given by Equation (4.35). The BER floors predicted using this approximation are compared to those of Figure 4.8. The comparison is shown in Figure 4.13 where the Gaussian approximation is designated by a dashed line. In this figure, the LED power is used as a parameter and is varied from -27 to -13 dBm (2 to 50 μ W). For small LED power, the two methods are very close however, they get further apart as the LED power increases. The BER floor calculated with the Gaussian approximation seems to reach minimum value for large LED power. This can be explained by the fact that the approximation of Equation (4.35) has the parameter Q as argument for the complementary error function. As mentioned earlier, this parameter can be seen as a kind of SNR. It becomes determined by the square root of the number of modes for large gain and large LED power. The minimum BER floor for the Gaussian approximation can be easily determined as:

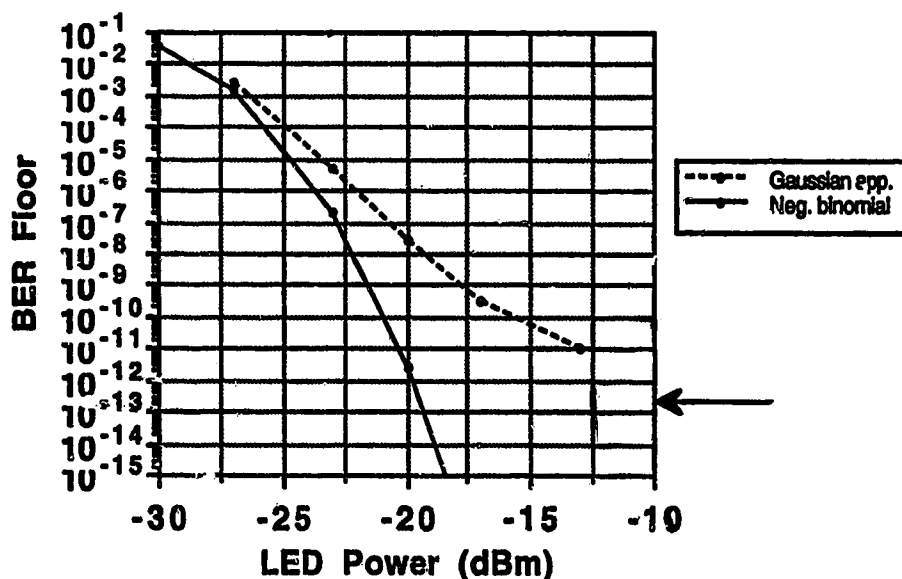


Figure 4.13: Comparison of the BER floors for different value of LED power P_{LED} . ($r=100$, $G=30$ dB, $N_{sp}=1.5$ and $N=53$)

$$BER \approx \frac{1}{2} \operatorname{erfc} \left(\frac{Q}{\sqrt{2}} \right) = \frac{1}{2} \operatorname{erfc} \left(\frac{\sqrt{N}}{\sqrt{2}} \right) \quad (4.39)$$

Since the plot of Figure 4.13 is obtained for a fixed number of modes of about 53, the minimum predicted BER floor for the Gaussian approximation is about 2×10^{-13} . This minimum value is indicated by an arrow in Figure 4.13.

The difference between the BER floor predicted according to the two methods for calculating the BER can be attributed to the fact that the Gaussian and the negative binomial PDFs are fundamentally different in shape. For instance, the Gaussian PDF is symmetric and entirely described by its mean and its variance. This means that its higher order moments are all zero. The negative binomial PDF has an asymmetry determined by its mean and its number of modes and its moments are given by Equation (2.39). Figure 4.14 illustrates the difference between the two distributions and their corresponding decision thresholds. The solid lines designate the negative binomial PDF and the dashed lines, the Gaussian PDF. The parameters used to generate the PDFs are indicated in the figure.

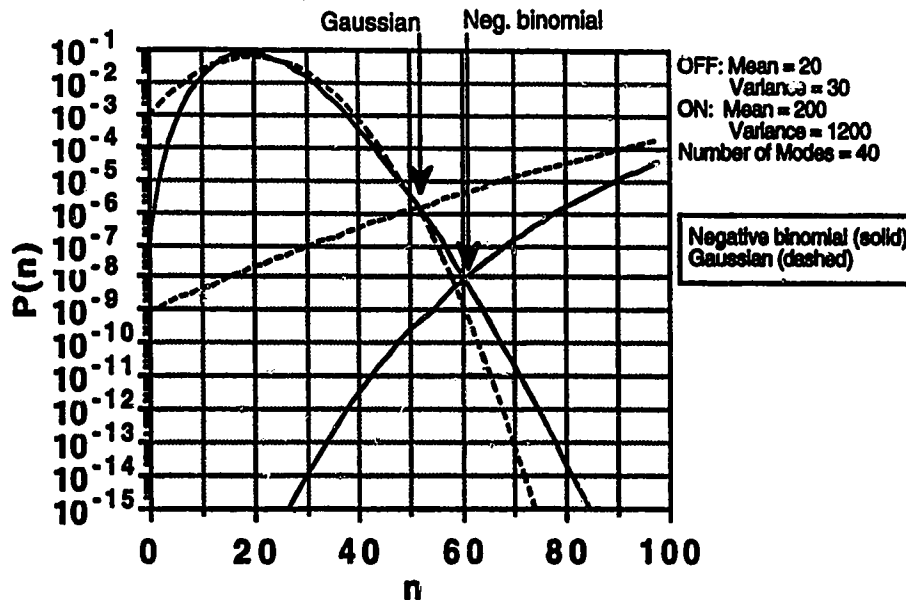


Figure 4.14: Negative binomial (solid) and Gaussian (dashed) PDFs and their decision thresholds.

The actual BER curves calculated with the two methods are compared as a function of LED power in Figure 4.15 where the number of modes is used as parameter. In the figure, the solid lines designate the BER calculated assuming a negative binomial

PDF and the dashed lines, the BER calculated with the Gaussian approximation. These BER curves were obtained for an LED extinction ratio of 100 and an EDFA gain and noise factor of 30 dB and 1.5, respectively. Also, we assumed that there was no fiber loss before the optical receiver. The BER floor values for the Gaussian approximation are easily predicted using Equation (4.39). The same comparison is presented but, this time, as a function of the number of modes and with the LED power as a parameter in Figure 4.16. This plot is very useful in that it allows us to determine quickly the minimum number of modes and consequently the minimum optical filtering required to achieved a given BER for given a LED power.

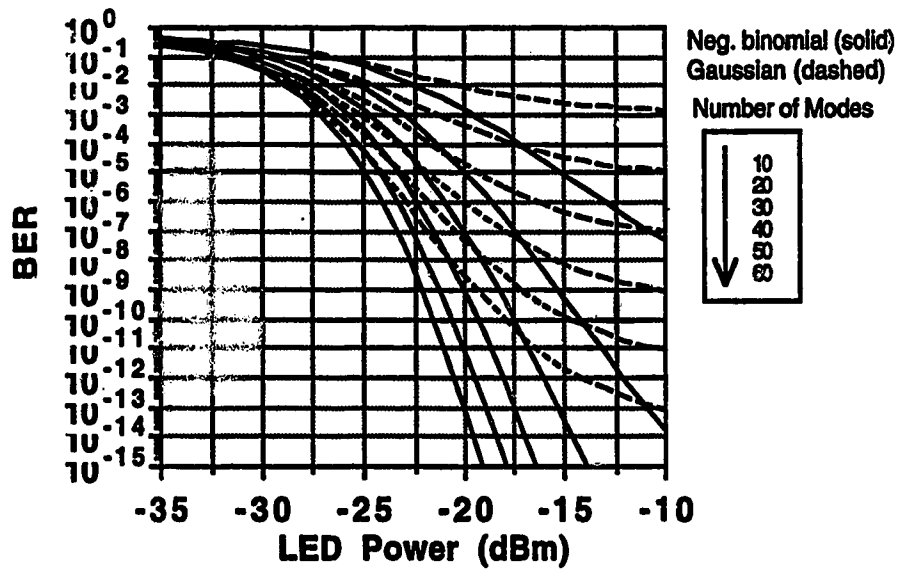


Figure 4.15: Comparison of the BER curves as a function of LED power with the number of modes as a parameter. Negative binomial (solid), Gaussian approximation (dashed) ($r=100$, $G=30$ dB, $N_p=1.5$)

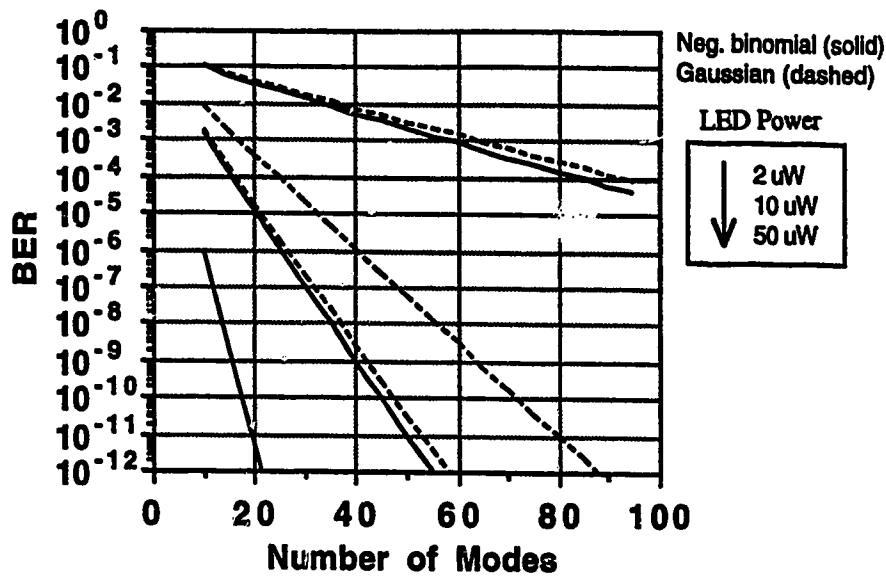


Figure 4.16: Comparison of BER curves as a function of the number of modes with this time the LED power as a parameter. ($r=100$, $G=30$ dB, $N_{sp}=1.5$).

4.3 Thermal Noise

So far, in our calculations, the optical receiver was assumed noiseless. In reality, however, there is always thermal noise added to the detected signal caused by the movement of charge in the optical receiver electrical circuit. The optical receiver thermal noise can be expressed as the mean square thermal noise current generated by an equivalent resistor R_L as follows:

$$N_{th} = \frac{4kTB_e}{R_L} \tag{4.40}$$

where k is the Boltzmann constants, T , the absolute temperature and B_e , the receiver electrical bandwidth. The resulting noise distribution at the optical receiver is then given by a convolution between the photon noise and the thermal noise PDFs. Thermal noise is Gaussian in nature and its effect is more important when a small amount of power hits the photodetector. In the limit of very small signal power, the noise distribution is essentially a Gaussian PDF. For high received power, the effect of thermal noise is generally negligible and we go back to a negative binomial PDF. Figure 4.17 shows the effect of thermal noise on the noise distribution for generic parameters. In the figure, the dotted line designates a negative binomial PDF with mean of 20, a variance of 60 and a number of modes of 10

and the solid line designates the same negative binomial PDF after its convolution with a Gaussian PDF symbolizing the optical receiver thermal noise. We assumed an effective variance of 16 for the thermal noise. The dashed line designates a Gaussian PDF with a mean and variance equal to that of the negative binomial. To perform the convolution, we took the inverse Fourier transform of the product of the PGF of the negative binomial PDF and the PGF of the Gaussian PDF. As we can see, the thermal noise not only broadens the initial negative binomial PDF but also changes its original shape.

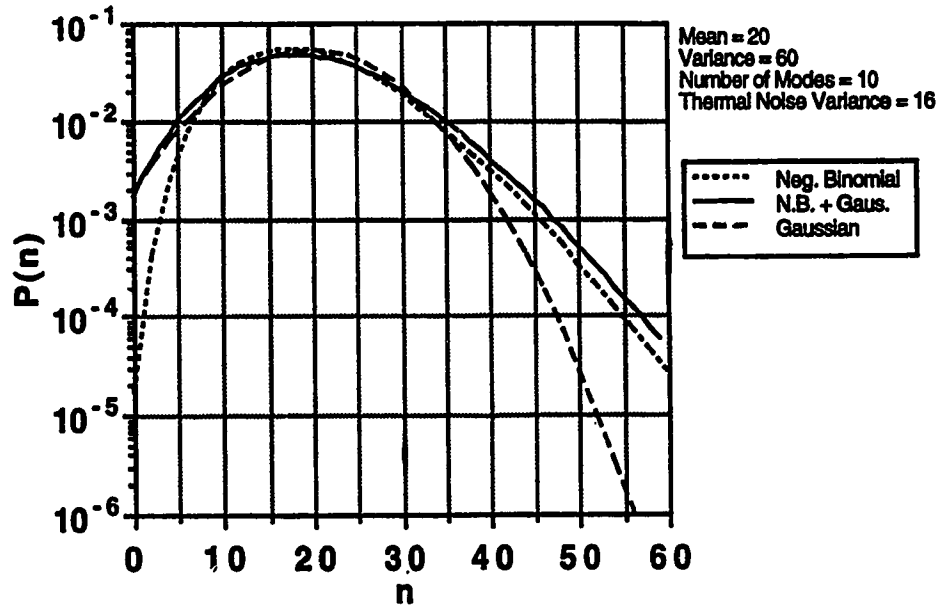


Figure 4.17: Effect of the thermal noise on the noise distribution.

4.4 Number of Channels in a WDM applications

In this section, we calculate the maximum number of channels possible for a WDM systems using spectral slicing such as the two shown in Figure 4.1. Since typical values for the FWHM bandwidths of the LED power spectrum B_{LED} and the EDFA gain spectrum B_{EDFA} are 100 (12.5 THz) and 30 nm (3.75 THz), respectively, we assume, to simplify the calculations, that the LED power spectrum is flat over the EDFA bandwidth. In addition, we assume that perfect spectral slicing can be accomplished with no guard band between adjacent channels. These assumptions are illustrated in Figure 4.18.

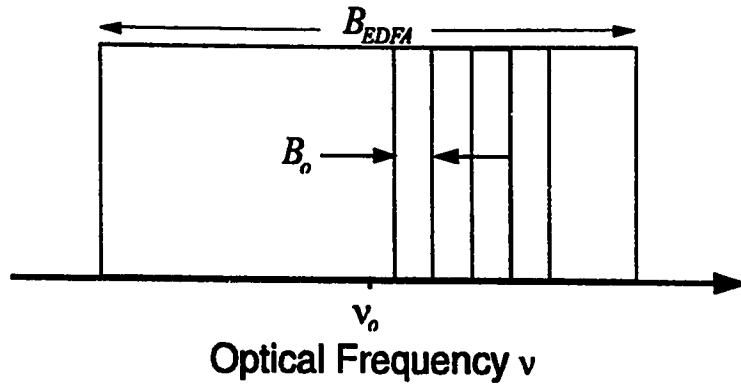


Figure 4.18: Illustration of perfect spectrum slicing of an LED followed by an EDFA in the case where the LED power spectrum is assumed flat over the EDFA bandwidth.

From this figure, the number of channels is given by:

$$\# \text{ of Channels} = \frac{B_{EDFA}}{B_o}, \quad (4.41)$$

where B_o here designates the optical filter bandwidth. Using the Gaussian approximation, we found in the previous section that a Q of at least 6 was required to achieve an BER of 10^{-9} . In addition, we found that the SNR was determined by the number of modes for large signal power and large EDFA gain. We therefore have:

$$SNR \approx Q^2 \approx N \approx \frac{B_o}{2B_e} \quad (4.42)$$

Substituting Equation (4.42) into (4.41) along with the values of the SNR to achieve a BER of 10^{-9} , we get:

$$\# \text{ of Channels} = \frac{B_{EDFA}}{72B_e}. \quad (4.43)$$

This formula was obtained by Liu [5]. Assuming that the optical receiver bandwidth $B_e = 0.6B = 0.6 \text{ Gb/s}$, we obtain a maximum number of channels of 86.

If we look now at Figure 4.16 for an LED power of $50 \mu\text{W}$, we find that a BER of 10^{-9} requires a number of modes of about 12. This gives:

$$\# \text{ of Channels} = \frac{B_{EDFA}}{24B_e}. \quad (4.44)$$

Using the same values for EDFA bandwidth and for the optical receiver bandwidth, we find that the maximum number of channels is now 260. This number is 3 time larger than the one predicted by the Gaussian approximation.

4.5 Conclusion

In this chapter, the performance of a spectral slicing system was examined. After having described the system, we studied the performance of one single optical carrier based on both the SNR and the BER. We found that the excess noise of the LED ultimately limits both the SNR and the BER of the system. This noise is also responsible for the BER floors observed when a large amount of power is at the optical receiver. Since this noise is a function of the LED power and the number of modes, these two system parameters have a very important effect on the BER floors. The EDFA amplification does not improve the system performance since the quality of the signal is fixed by the excess noise term at the beginning of the system. The performance is slightly degraded because of the ASE. We also found that the two methods used for calculating the BER give similar predictions for the BER floor for low LED power but start differing for large LED power. In fact, the BER floor predicted by the Gaussian approximation reaches a minimum value for large power due to the fact that the parameter Q saturates to a constant value in this regime. Finally, the performance of spectral slicing was evaluated in a WDM application. We found that the maximum number of channels predicted when the negative binomial distribution is assumed for the noise distribution is larger than the one predicted by the Gaussian approximation.

In the next two chapters, the performance of spectral slicing will be examined experimentally.

5. Experimental Setup

In the previous chapter, we looked at the performance of spectral slicing of an LED with and without the use of an EDFA from a theoretical point of view. We assumed good characteristics for the components and examined the effect of the various system parameters such as the LED power, the optical filter bandwidth (number of modes), the EDFA gain and noise factor and the LED extinction ratio. In reality, however, due to the reality of components, the performance is often worse than what is theoretically achievable.

In this chapter, an actual spectral slicing system is studied experimentally. The experimental system is first described and then, each of its components is characterized.

5.1 General Description

Before describing the experimental setup, we are going to say a word about the measurement apparatus.

For most of the measurements, we used two sets of apparatus: the Bit Error Rate Tester (BERT) and the Optical Power Meter (OPM) assemblies. Both sets are composed of a series of instruments made by the American manufacturer Hewlett-Packard (HP). The BERT assembly is used for waveform recording, (i.e., eye diagrams and rise and fall times) and error counting. It is composed of a HP 54120B Digitizing Oscilloscope, a HP 70004A Display, a HP70842A Error Detector for bit rates in the range of 0.1-3 Gb/s, a HP 54123A DC to 34 GHz Four Channel Test Set, a HP 70841A 0.1 to 3 Gb/s Pattern Generator and a HP 70322A 0.1 to 4.2 GHz Synthesized Signal Generator. The last two components of the BERT assembly are not used for measuring but for driving purposes. The OPM assembly is used to monitor the optical power at different points in the optical fiber link. It is composed of a HP 8153A Lightwave Multimeter used in conjunction with HP 81521B Optical Heads and HP 81533A Interfaces. The optical heads can operate in the wavelength range of 900 to 1700 nm with a dynamic range of -80 to +3 dBm. The OPM assembly absolute reading accuracy is 3.5 %. There are two OPM assemblies. They are labeled according to their GPIB addresses as #21 and #22. The OPM #22 is used for all measurement unless otherwise specified.

The experimental setup is composed of three major parts: the LED transmitter, the optical link and the optical receiver. The optical link is the part where the optical

amplification and the spectral slicing occur. The setup block diagram is shown in Figure 5.1. In the following, each part of the setup is described and characterized.

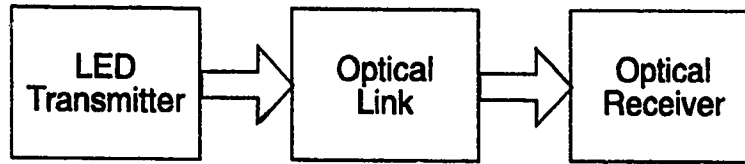


Figure 5.1: Block diagram of spectral slicing setup

5.2 LED Transmitter

The LED transmitter is composed of two parts: a Veritech microwave power amplifier and a Mas-Tech LED. Its block diagram is shown in Figure 5.2.

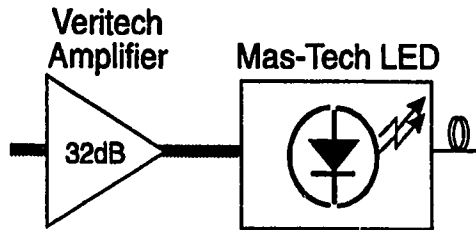


Figure 5.2: LED transmitter block diagram

The Veritech VMA3K10C-232 is a microwave power amplifier with a small signal gain of 32 dB and a noise figure of 8 dB. Its maximum output power in the linear regime is 17 dBm but it can be higher when operated in saturation. Saturation causes the Veritech output waveform to be distorted (the output waveform gets chopped at the top and bottom). The frequency response of the Veritech is approximately flat up to 10 GHz with a ripple of about ± 1 dB. It is shown in Appendix 5A along with its main characteristics.

The Mas-Tech E15D1-002 is powerful edge-emitting type LED that comes in a hermetically sealed 14 pin dual-in-line package (DIP) module with a thermoelectric cooler (TEC) and thermistor to provide temperature adjustment. When operated at a bias current of 100 mA, its emission peak is located around 1550 nm and its output optical power is about 20 μ W. The TEC and thermistor allow operation of the LED at the different temperatures. We made use of this feature to increase the LED output power. The optical and electrical characteristics of the Mas-Tech LED are examined in the following

subsections. The details on the temperature control, the LED driver circuits are given in Appendix 5B along with some more information on the Mas Tech LED characteristics.

5.2.1 Output Power

The curve obtained by plotting the optical output of semiconductor source versus bias current is called L-I curve. This has been done for the Mas-Tech LED for different temperatures. The measurement setup is shown in Figure 5.3 and the results are plotted in Figure 5.4. The measurement just consists of recording the LED output power with the OPM assembly for different bias current settings and temperatures. Note that in the conditions specified by the manufacturer, i.e., for a bias current of 100 mA at 25 °C, we measured an output power of about 23 μW for the LED. This corresponds to the device specifications.

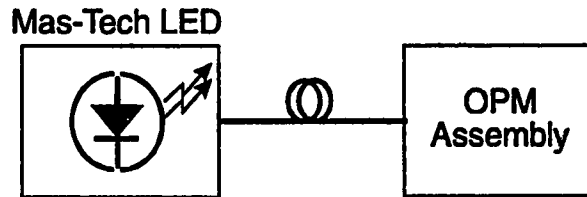


Figure 5.3: Setup for L-I curve measurements

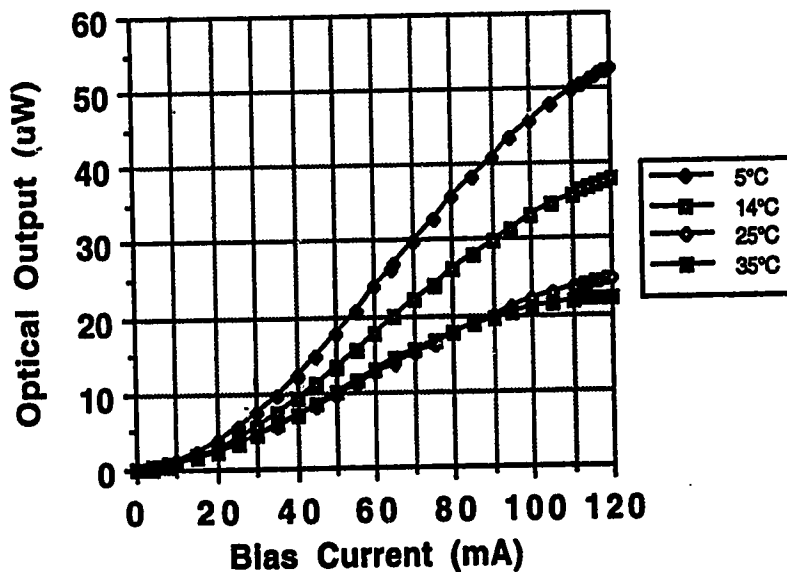


Figure 5.4: L-I curves of the Mas-Tech LED for different temperatures.

Digital OOK modulation is achieved by directly modulating the current of the LED. In our case, this is accomplished by biasing the LED at a DC current and by superimposing a pure AC current waveform to it. The L-I curves are fairly linear around their middle section but strongly non-linear at their ends. This can cause some distortion on the optical waveform and affect the actual optical extinction ratio. From Figure 5.4, we see that the L-I curve obtained for a temperature of 5°C provides the largest output power for the LED. Setting the DC bias at its inflexion point, i.e., 64 mA, we can choose a peak to peak current swing of 108 mA in order to take advantage of most of the linear section of the curve and avoid at the same time most of the non-linear region. From the L-I curves, this results in an LED extinction ratio of about 26 to 1, or 14 dB. In the remaining of the chapter, these settings will be referred to as the LED operating conditions.

5.2.2 Power Spectrum

To measure the LED optical spectrum, we used a Digikrom 240 monochromator. A monochromator is a device that makes use of a diffraction grating to decompose light into its frequency components. The Digikrom 240 has a minimum resolution of 0.07 nm and an insertion loss of about 8 dB. Combined with the OPM assembly, the power of each frequency component can be evaluated and the power spectral density can be determined. Both the monochromator and the OPM assembly were controlled by *LabVIEW* [48] which is a GPIB compatible laboratory instrument control software. Figure 5.5 shows the setup for spectrum measurements. The monochromator resolution was set to about 1 nm.

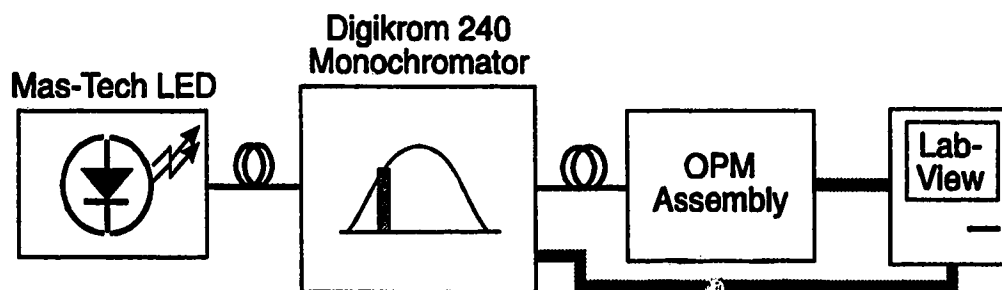


Figure 5.5: Setup for the LED power spectrum measurements

Figure 5.6 shows the LED power spectrum measured in two different conditions. In the conditions specified by the manufacturer, i.e., for a bias current of 100 mA at room temperature (25 °C), the LED spectrum peaks around 1521 nm and its FWHM bandwidth

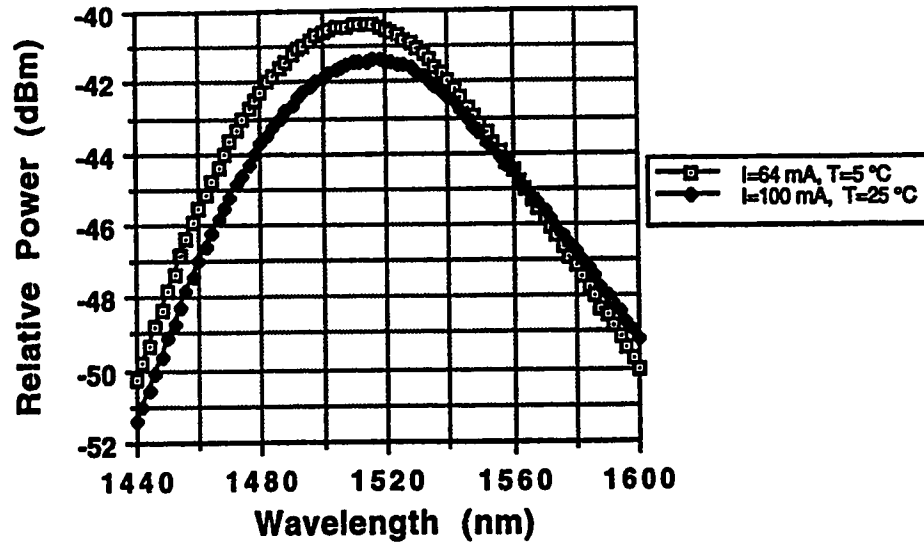


Figure 5.6: Mas-Tech LED spectra measured in the conditions specified by the manufacturer (100 mA, 25 °C) and in the operating conditions (64 mA, of 5 °C).

is approximately 90 nm. This value is slightly off compared to the specifications. This can be seen by comparing Figure 5.6 to Figure 5B.1 in Appendix 5B. In the operating condition, i.e., for a bias of 64 mA and a temperature of 5 °C, the LED spectrum peaks at 1517 nm and its FWHM bandwidth is about 80 nm. As we can see, the effect of cooling the LED increases its output power but also shifts its emission peak.

5.2.3 Electrical Response

The electrical response of a semiconductor source indicates how fast it can be modulated. We measured the electrical response of the Mas-Tech device using the setup shown in Figure 5.7. An HP 8753A Network Analyzer and an HP 85046A S-Parameter Test Set were used for the measurement. A BT&D model PDC4310 photodetector was used to convert the LED optical power back to an electrical signal for the network analyzer. The BT&D photodetector has a responsivity of 0.75 A/W and a fairly flat response up to several gigahertz. In addition, the BT&D is followed by an SHF 90P RF amplifier and a Mini-Circuit (MC) SLP-850 850 MHz low pass filter. The SHF amplifier has a small signal gain of 23 dB and a noise figure of 7 dB. Its frequency response is approximately flat up to 12 GHz with a ripple of about ± 1.5 dB. The SHF is used to boost the BT&D photocurrent which is too small for the network analyzer. The MC filter is there for noise

removal purposes. The BT&D, SHF and MC filter responses as well as their main characteristics are given in Appendix 5C. The Mas-Tech LED was biased at 64 mA at a temperature of 5°C. The network analyzer provides a sinusoidal waveform for which the amplitude can be adjusted. However, to avoid the distortion by the Veritech which has a maximum output of 17 dBm, the peak to peak current swing applied to the LED was limited to 64 mA.

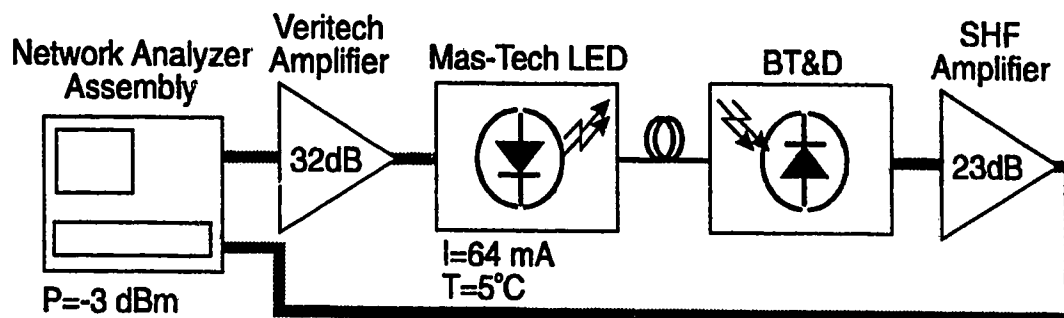


Figure 5.7: Setup for the frequency response measurement

The result for the measurements of the LED electrical response is shown in Figure 5.8. As we can see, the LED electrical response has a fairly shallow roll-off up to 400 MHz and then drops abruptly. Its maximum amplitude is down by 3 dB at around 225 MHz.

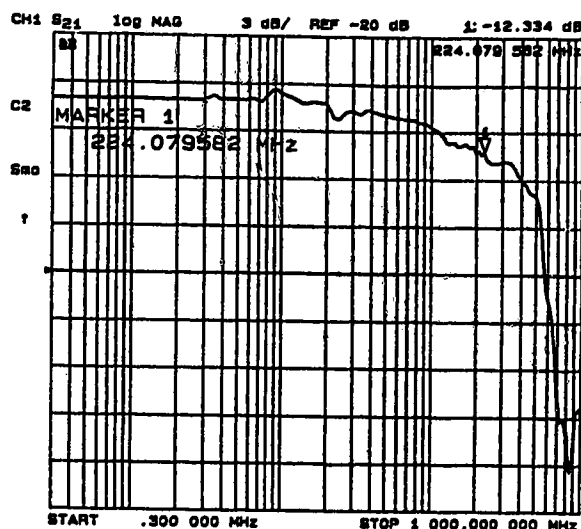


Figure 5.8: Mas-Tech LED frequency response.

When we applied the modulation, we noticed a small shift in optical power of about $2 \mu\text{W}$. This shift can be attributed to both the Veritech and LED distortion.

5.2.4 Optical Rise and Fall Times

The rise and fall time is also a measure of how fast a semiconductor source can be modulated. For digital modulation, they impose a limit on the minimum width of the pulses of light representing the bits. We measured the LED optical rise and fall times using the setup shown in Figure 5.9.

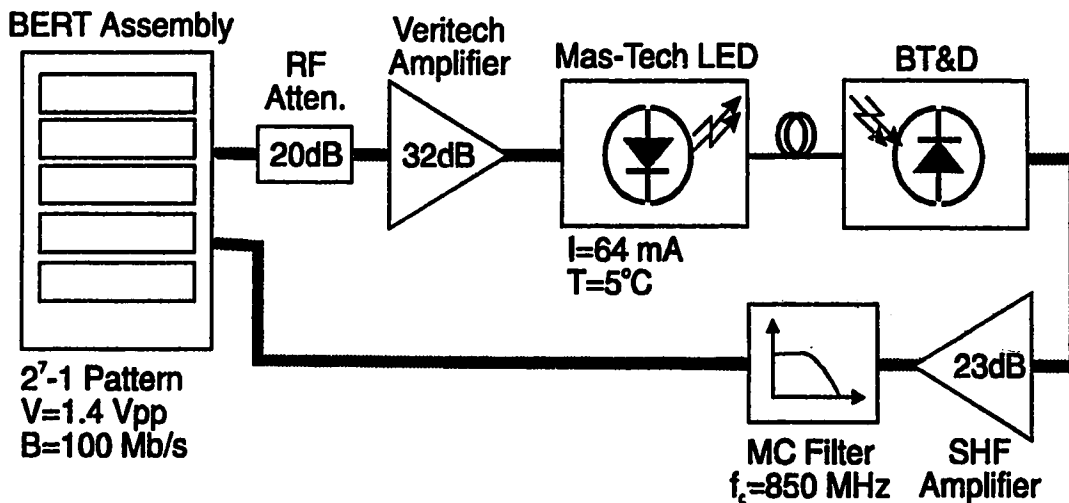


Figure 5.9: Setup for the rise and fall time measurements

For the measurements, the BERT pattern generator was used to drive the LED and the digitizing oscilloscope, to monitor the waveforms. The pattern generator settings were as follows:

- Pattern: 2^7-1 pseudo-random sequence
- Peak to peak voltage amplitude: 1.4 V
- Bit rate: 622 Mb/s .

Figure 5.10 shows the pattern generator output in (a), the Veritech amplifier output in (b) and the LED optical output as detected by the BT&D photodetector in (c). As we can see, the driving waveforms (electrical) are almost perfectly square. The slightly rounded edges observed for the waveform at the output of the Veritech amplifier (Figure 5.10 (b)) is not caused by the amplifier but by the coaxial cable and its connectors. Also, the LED optical output waveform (Figure 5.10 (c)) appears distorted. This can be partly caused by the

LED itself but also by the electrical response of both the BT&D photodetector and the 850 MHz electrical filter. The 850 MHz filter is used to remove the noise from the signal.

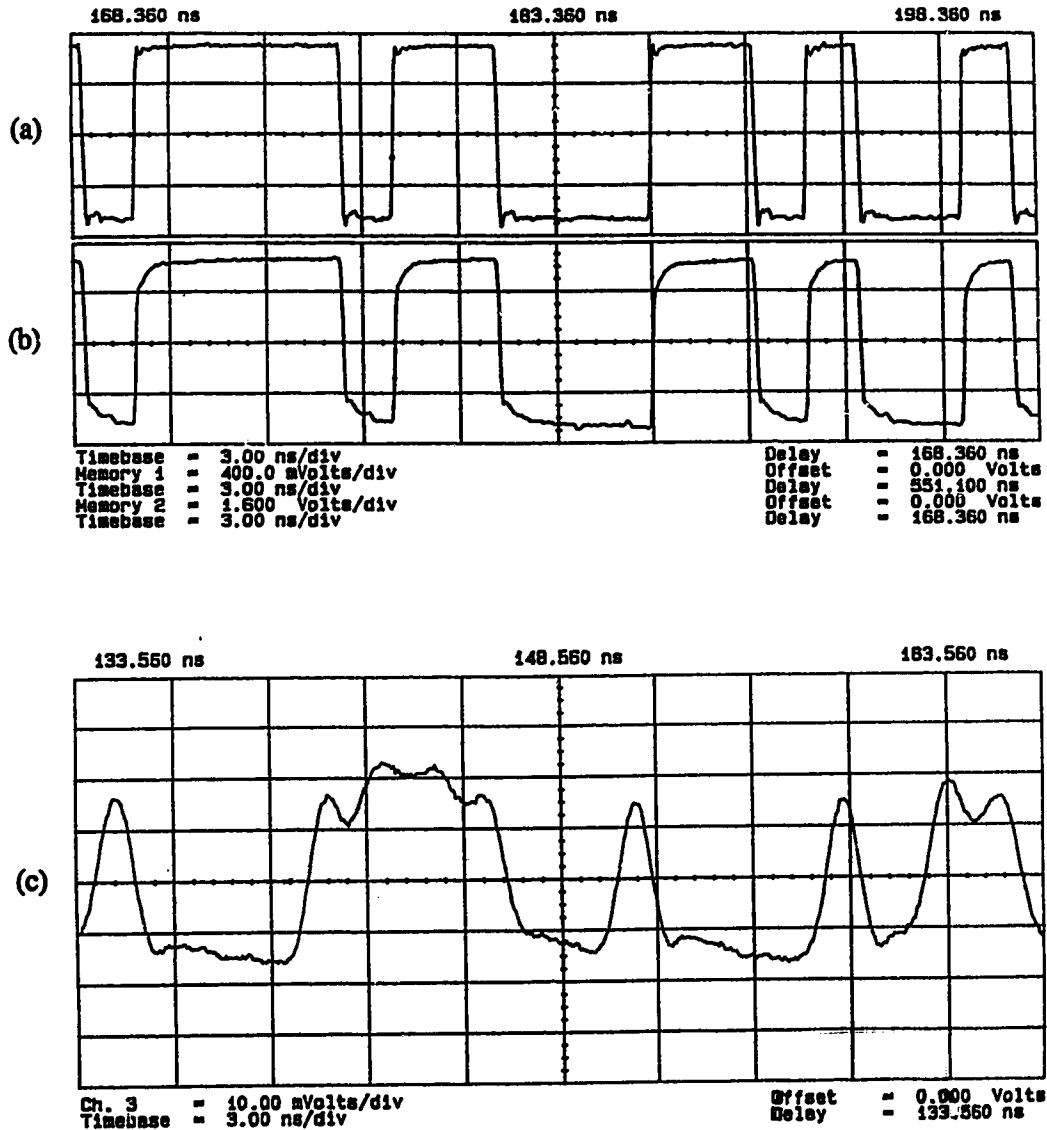


Figure 5.10: Waveforms (a) Pattern generator, (b) Veritech amplifier and (c) LED through the BT&D photodetector.

To measure the rise and fall times adequately, we need to find a pulse surrounded by a long sequence of zeros to ensure that the pulse reaches its steady state value. Instead of using a 622 Mb/s signal which has a pulse width of 1.6 ns, we used a 100 Mb/s signal

that has a width 10 ns. The rise time of the pattern generator output is not affected by the bit rate settings, only the pulse width is changed. Performing the measurement at 100 Mb/s allows us to have longer pulses surrounded by zeros. The results of the rise and fall time measurements appear in Figure 5.11. We obtained a rise time of 952 ps and a fall time of 914 ps. This give a minimum pulse width of about 1.87 ns. This is slightly longer than the pulse width of 622 Mb/s modulation and can account for some of the distortion observed in the waveform.

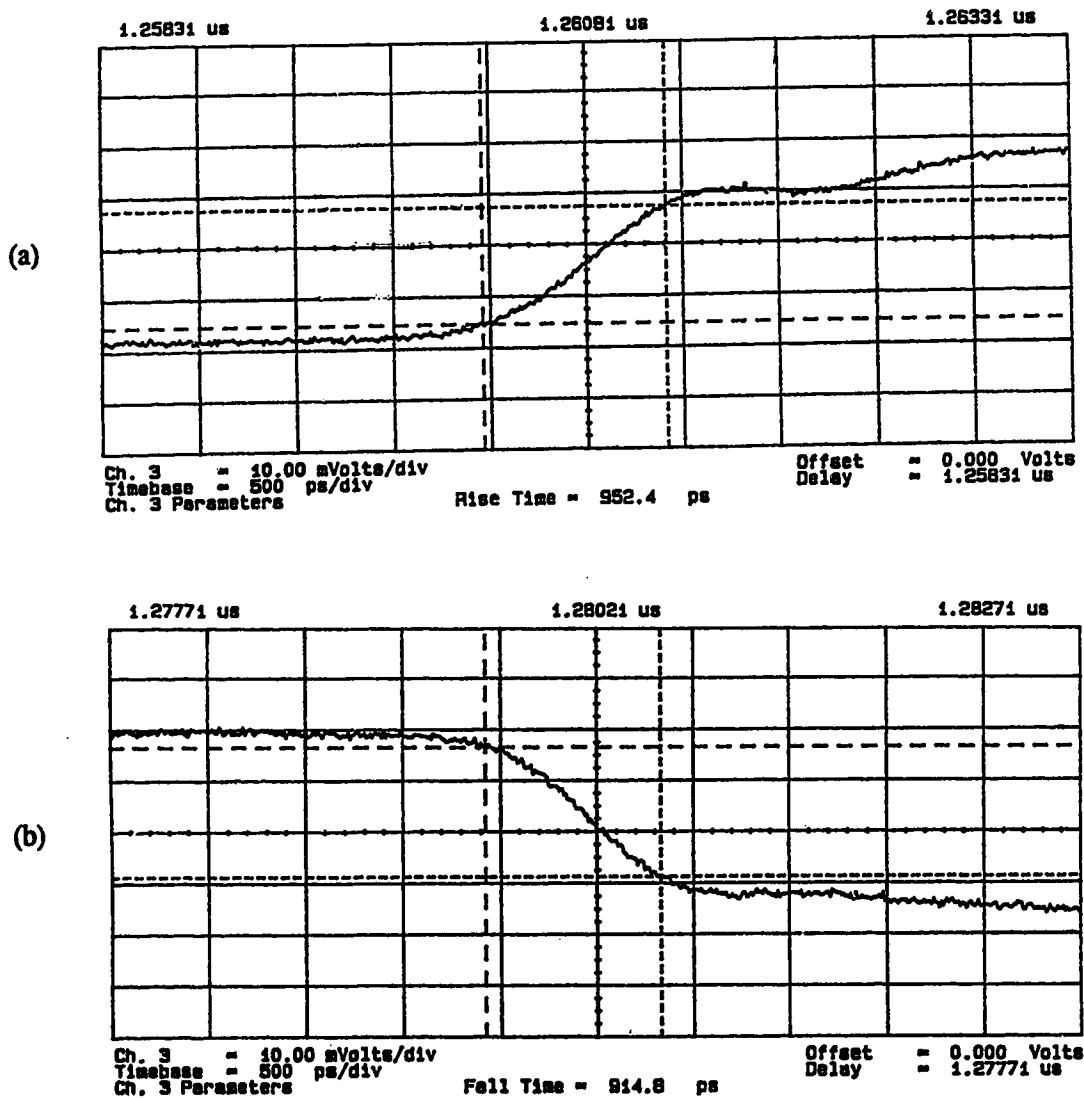


Figure 5.11: Mas-Tech LED rise (a) and fall (b) times

Here also, we observed a shift in the LED optical power when we turned the modulation on. This time, the shift was about $6 \mu\text{W}$. This causes the DC bias current point to effectively move upward by 8 mA. Taking that into account, a new value for the

extinction ratio can be calculated. The value obtained is 16 to 1, or 12 dB. Finally, the distortion observed in the optical waveform is suspected to affect the effective extinction ratio, however, this effect is not quantified.

5.3 Optical Link

The optical link is the main part of the spectral slicing setup. It is where the EDFA amplification and the optical filtering occur. The optical link is composed of five components: an input filter, a first variable optical attenuator (VOA), an EDFA, an output filter and a second VOA with a 10% power monitor branch. The optical link components are shown in a block diagram form in Figure 5.12. In the following, we will discuss the characteristics of the optical filters and of the EDFAs only. The characteristics of the attenuators are not discussed here since they are accessory to the setup. Their only use is to vary the input power level to the EDFA and to the optical receiver. Their main characteristics are however listed in Appendix 5E.

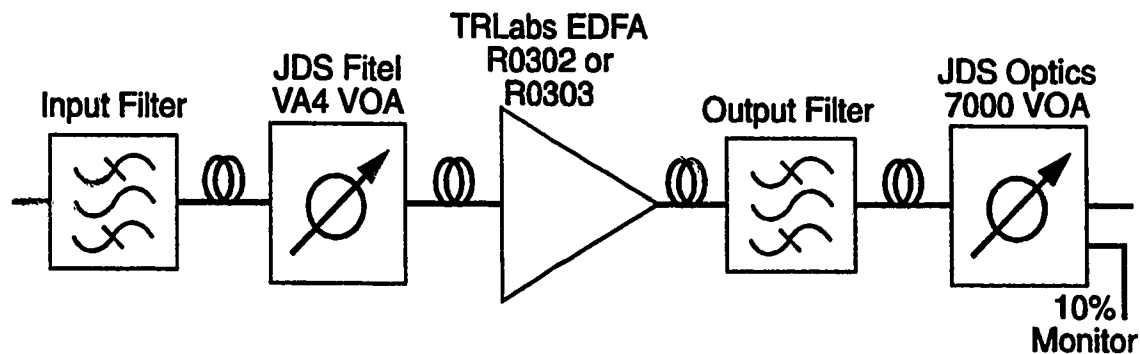


Figure 5.12: Block diagram of the optical link

5.3.1 Input Filter

The input filter applies the first slicing on the LED transmitter spectrum and reduces the input power to the EDFA in order to avoid its saturation. The JDS TB1570 tunable bandpass filter was used for this purpose. A justification of this is given at the end of the section. The JDS Fitel TB1570 is a multilayer dielectric type tunable optical bandpass filter. The wavelength tunability is achieved by a knob which controls the tilting angle of the multilayer dielectric plate. The TB1570 filter is fiber pigtailed with Corning 9/125 SMF28 type fiber and connectorized with FC/APC (Angular Physical Contact) type connectors. The TB1570 has a range of tunability that goes from 1520 to 1567 nm and its

bandwidth (FWHM), from 3.5 to 2.5 nm. It has an insertion loss that varies from 3.5 to 2.5 dB and a return loss which is less than -40 dB. We measured the transmittance of the TB1570 filter using the Mas-Tech LED and the Digikrom 240 monochromator using the setup shown in Figure 5.13. The resolution used for the scan was about 0.4 nm. Once again, we made use of *LabVIEW* to control the instruments.

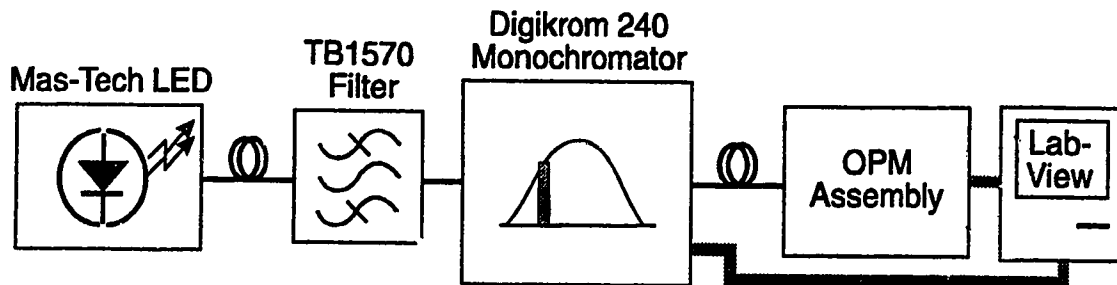


Figure 5.13: Setup for the measurement of the TB1570 transmittance

Figure 5.14 shows the measured transmittance of the TB1570 when centered at 1537 nm. Its FWHM bandwidth is about 3.7 nm. The insertion loss of the TB1570 was also measured. It is 1.4 dB.

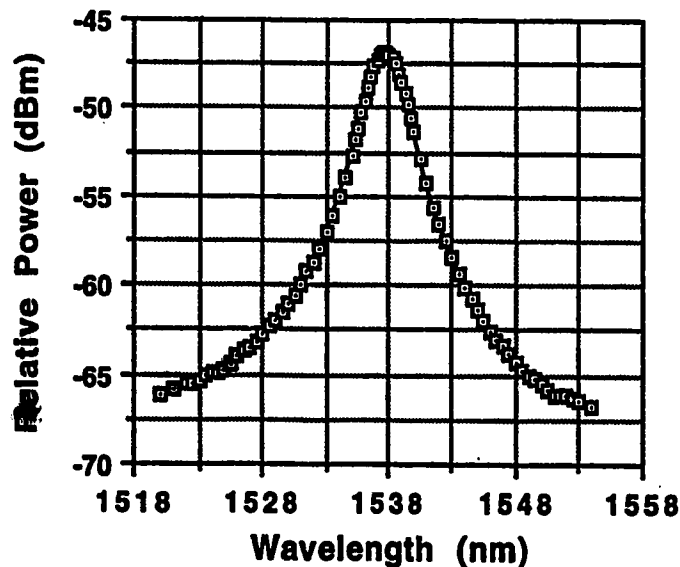


Figure 5.14: Transmittance of the TB1570 filter at 1537 nm

5.3.2 Output Filter

The output filter has two purposes: optical amplifier noise removal and additional LED spectrum slicing. To achieve this, we used the JDS TB1500B filters. This filter is, as the TB1570, a multilayer dielectric type tunable optical bandpass filter. It is also fiber pigtailed with Corning 9/125 SMF28 type fiber and connectorized with FC/APC connectors. The tuning range of the TB1500B goes from 1510 to 1562 nm and its FWHM bandwidth goes from 1.4 to 1.3 nm. Its insertion loss varies from 3.2 to 1.7 dB and its return loss is also less than -40 dB. The measurement setup used is the same as Figure 5.13. Figure 5.15 shows the measured transmittance of the TB1500B when centered at 1537 nm. Its FWHM bandwidth is about 1.3 nm and its measured insertion loss, 2.6 dB.

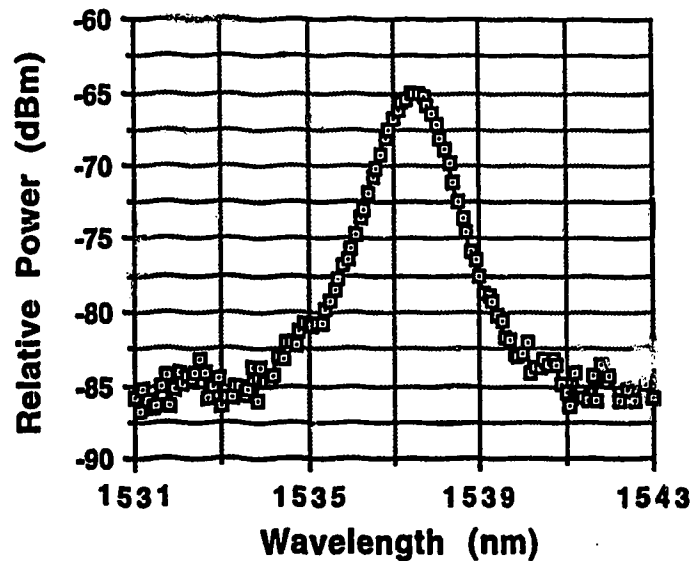


Figure 5.15: Transmittance of the TB1500B filter at 1537 nm

The input filter reduces the input power to the EDFA and ensures that it operates in the linear regime, i.e., not in saturation. In Chapter 3, we assumed that the same filtering was applied to both the LED and the EDFA which resulted in the same number of modes for both the negative binomial PDF describing the LED emission and the BDI medium which models the EDFA amplification. However, the input filter introduced in the experimental setup makes that, strictly speaking, the LED and the EDFA do not have the same optical filtering anymore. The LED is effectively filtered twice whereas the EDFA,

only once. This creates a difference in the number of modes of the negative binomial PDF and of the BDI medium. In the case where this input filter is wide enough compared to the output filter, it does not introduce much of a difference in the number of modes. The JDS TB1570 filter provides sufficient filtering to reduce the input power to the EDFA and at the same time is wide enough to prevent the introduction of a large difference in the number of modes. The percentage of difference in the number of modes can be calculated by evaluating bandwidth of the TB1570 and the TB1500B filter cascaded and comparing it with the bandwidth of the TB1500B filter alone.

5.3 EDFAs

The EDFA is used to amplify the LED output power to compensate for the spectral slicing losses. Two EDFAs packaged at TRILabs were used in the optical link: EDFA #R0302 and EDFA #R0303. Both have similar characteristics which are described in the next subsections. Two important characteristics are looked at: the gain and the noise. More information on the packaging of these EDFAs can be found in Appendix 5E.

EDFA Gain and Inband ASE

The EDFA gain is determined by four factors: the erbium doping concentration, the fiber length, the pump power and the input signal power. The first two factors are set by the design requirements and are considered fixed (i.e. we cannot change them). However, the other two can be varied. The pump power can be adjusted by varying the drive current of the pump laser and the input signal depends on the particular application. The gain is generally proportional to the pump power but inversely proportional to the input signal power. For small values of input power gain is constant and is called the small signal gain. As the input power is increased, the EDFA enters in the saturation regime and the gain starts to decrease. In addition to amplifying the input optical signal, the EDFA also produces a small amount of optical noise. This noise is caused by the amplified spontaneous emission or ASE. The amount of ASE produced by an EDFA is determined essentially by the same four factors that determine the gain. The ASE behaves essentially like the gain. It is constant for small input powers and decreases when the EDFA is in saturation, i.e., when the input signal power gets large.

The gain of both TRILabs EDFAs was measured using two methods. We will call the first one the maximum ASE method and the second one, the polarization method [49]. The measurement setups are shown in Figure 5.16 and 5.17, respectively. The setups are similar except for a polarization rotator and a polarization splitter in the polarization method setup. A 1537 nm Northern Telecom distributed feedback (DFB) type laser is

used as the input signal to the EDFAs. This laser has an output power of about 1 mW. It is followed by the JDS 7000 optical attenuator which is used to control the EDFA input power. The input signal power to the EDFA can be monitored with an OPM assembly at the 10 % output of the attenuator. The EDFA is followed by a JDS TB1500B optical filter for optical noise removal purposes. As the input signal power to the EDFAs is varied, the output power after the filter is recorded with a second OPM assembly. The output power contains the amplified signal but also some ASE. The actual EDFA gain is determined by the ratio of the output to the input power to the EDFA once the ASE has been taken into account.

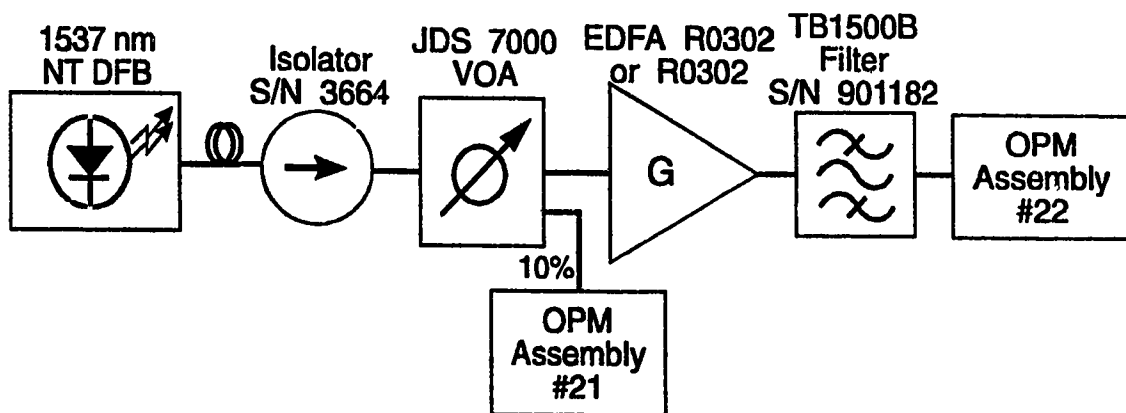


Figure 5.16: Measurement setup for EDFA gain using the maximum ASE method.

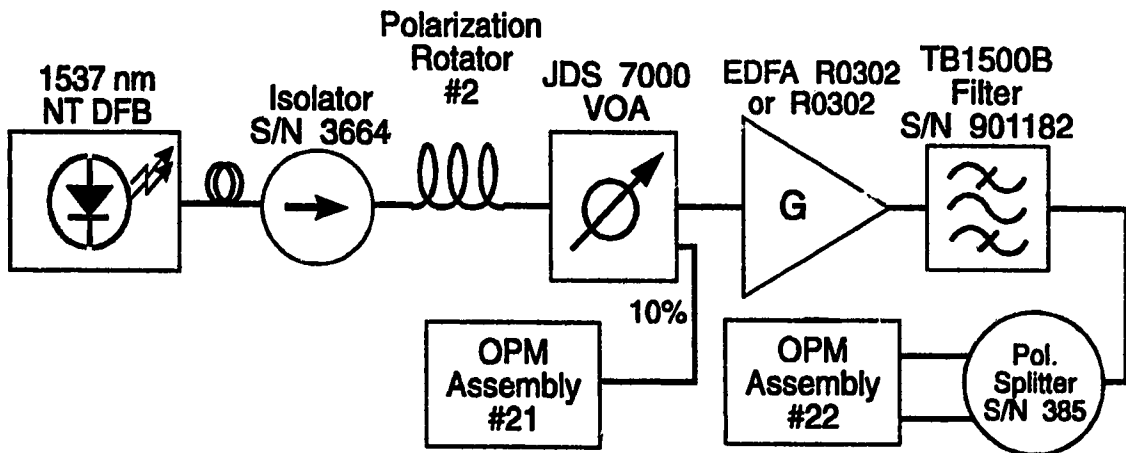


Figure 5.17: Measurement setup for the EDFA gain using the polarization method.

The maximum ASE method uses the fact that the ASE is maximum and approximately constant at low input signal power to the EDFA. Since the power at the output of the EDFA P_{out} contains the amplified input signal power GP_{sig} and some ASE P_{ASE} and since the ASE power is a also function of the input signal power ($P_{ASE} = P_{ASE}(P_{sig})$), we have:

$$P_{out} = GP_{sig} + P_{ASE}(P_{sig}). \quad (5.1)$$

The EDFA gain can be estimated by subtracting the maximum ASE power P_{ASEmax} from the output power and dividing by the input signal power as follows:

$$G = \frac{P_{out} - P_{ASEmax}}{P_{sig}} = G - \left(\frac{P_{ASEmax} - P_{ASE}(P_{sig})}{P_{sig}} \right). \quad (5.2)$$

As we can see, for large input signal power, the gain obtained with this method is close to the real EDFA gain. However, as the input signal power gets small, it becomes difficult to determined the gain accurately because it is determined by the ratio of two small quantities. Consequently, the maximum ASE method provides a way to measure the gain of the EDFA but the method is less accurate as the input signal power gets smaller.

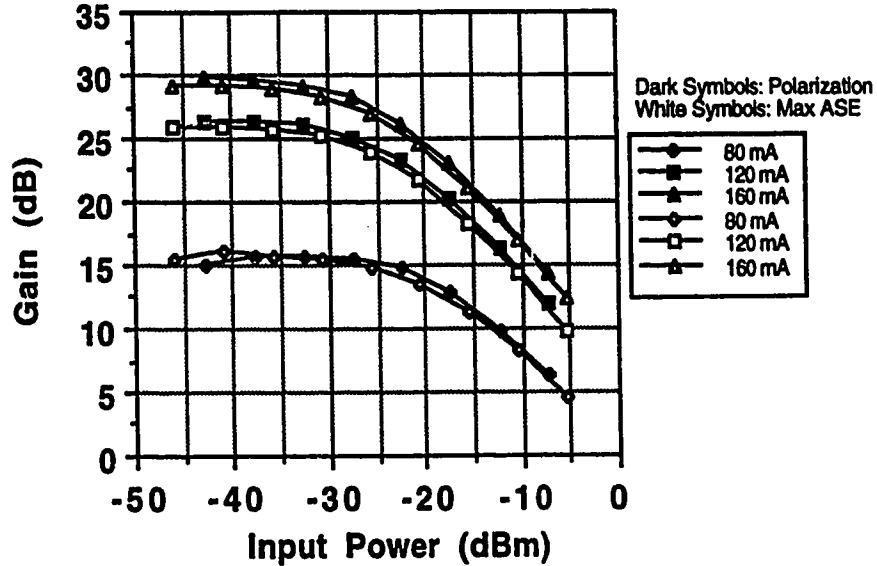
The second method, the polarization method, allows us to measure both the gain and the ASE power of the EDFA. It uses the polarization of the light to isolate the amplified signal from the ASE. It is in principle more accurate but also more complex and less stable due to polarization maintaining problems. The output of a DFB laser is generally highly linearly polarized while the ASE is entirely unpolarized. By using a polarization rotator in conjunction with a polarization splitter, it is possible to isolate the input signal from the ASE. In fact, if the degree of polarization of the DFB laser is high enough and if the polarization splitter provides a good isolation between the two polarizations, there will be half the ASE power P_{ASE} in each of the polarization splitter branches and the amplified input signal power GP_{sig} in only one as indicated in Figure 5.18.



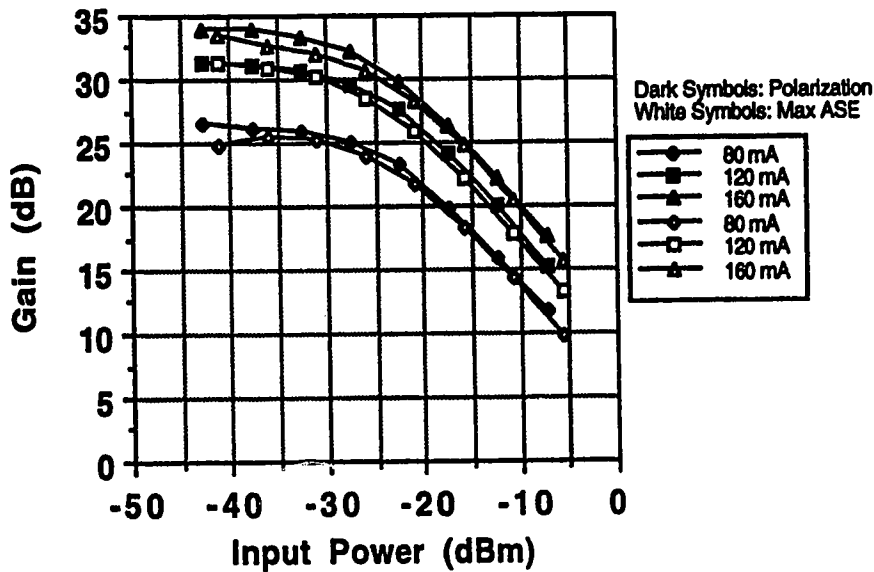
Figure 5.18: Visualization of the polarization method.

Both the gain and the ASE of the EDFA can be obtained using this method. Note that a factor of two must be added to the measured ASE to obtain the total ASE power. The insertion loss of the optical filter must also be taken into account.

The gain versus input signal power to the EDFA is plotted for different pump drive currents for EDFA #R0302 in (a) and #R0303 in (b) in Figure 5.19. The white symbols designate the gain measured according to the maximum ASE method and the black ones, the polarization method. Both methods give the same values of the gain within approximately 1 dB.



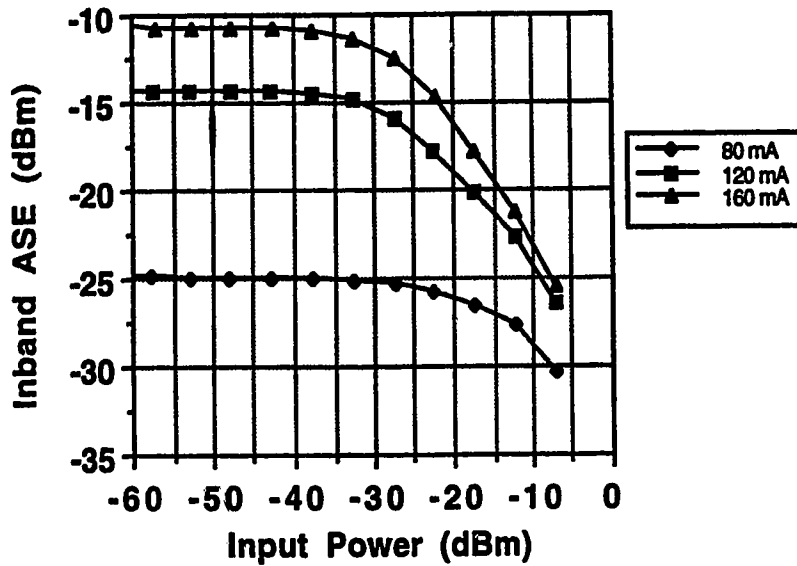
(a)



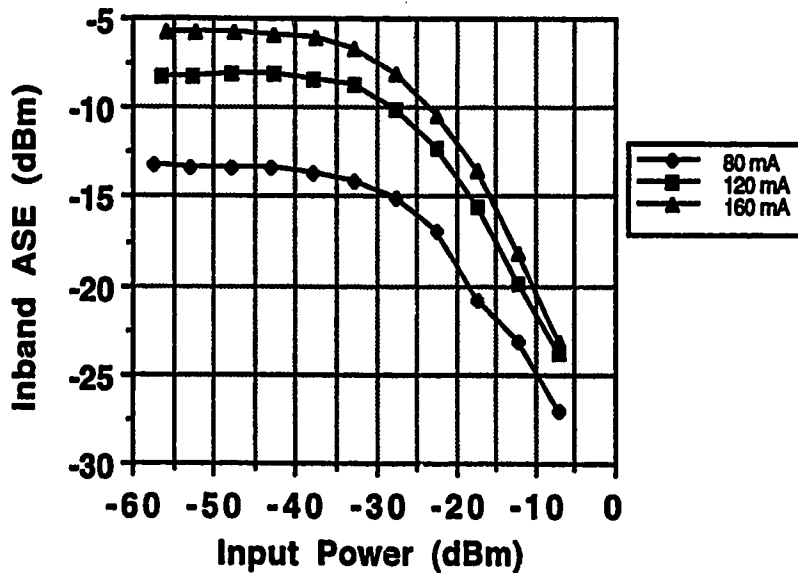
(b)

Figure 5.19: Gain measurement (a) EDFA #R0302, (b): EDFA #R0303

In the same way, the inband ASE is plotted as a function of the input signal power to the EDFA and for different pump drive currents in Figure 5.20 for EDFA #R0302 in (a) and #R0303 (b).



(a)



(b)

Figure 5.20: Results for the ASE measurements. (a) EDFA #R0302
(b) EDFA #R0303

From Figure 5.19 and 5.20 (a), we see that EDFA #R0302 has a small signal gain of about 28, 25 and 15 dB and an inband ASE power of about -9, -12 and -23 dBm at 160, 120 and 80 mA pump drive current, respectively. Because of saturation, the gain

starts to decrease around -30 dBm and is down by 1 dB at about -27 dBm. In the same way, we can see, from Figure 5.19 and 5.20 (b), that EDFA #R0303 has a small signal gain of about 33, 30, 25 dB and an inband ASE power of about -4, -7 and -12 dBm at 50, 120 and 80 mA pump drive current, respectively. As for EDFA #R0302, the gain of EDFA #R0303 has decreased by 1 dB around -27 dBm.

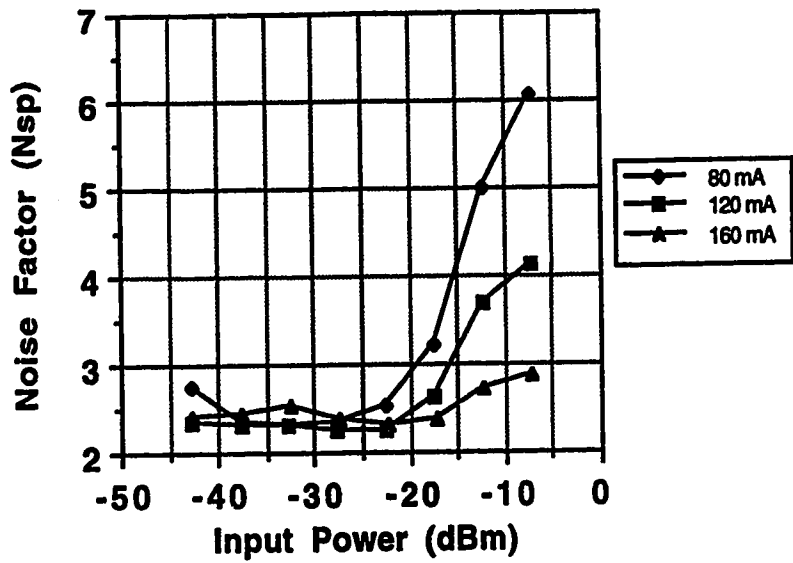
From these measured gain and ASE values, we can determine the EDFA noise factor N_{sp} as a function of the pump drive current and the EDFA input signal power. N_{sp} is used to characterize the performance of optical amplifiers. An ideal amplifier would have an N_{sp} of 1. To calculate the noise factor, we use the following formula:

$$P_{ASE} = 2N_{sp}(G-1)h\nu B_o \quad (5.3)$$

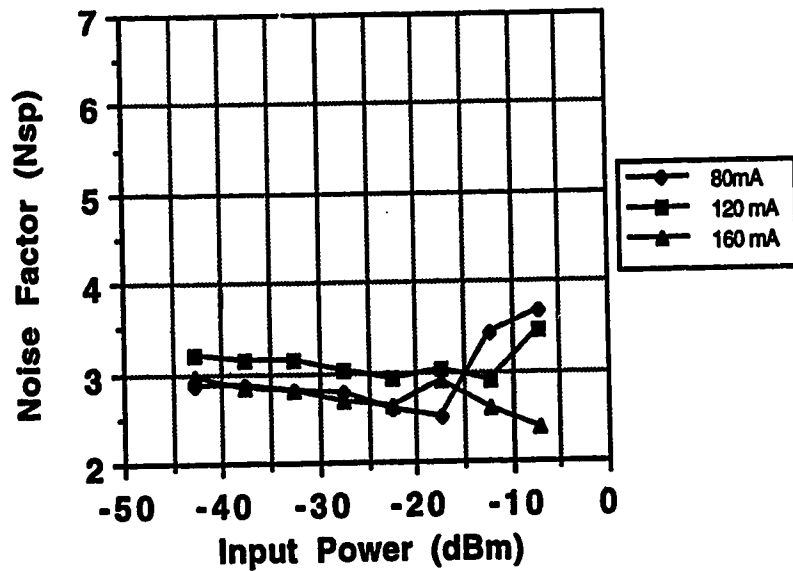
Solving for the noise factor N_{sp} , we find:

$$N_{sp} = \frac{P_{ASE}}{2(G-1)h\nu B_o} \quad (5.4)$$

The result of this calculation is shown in Figure 5.21 for both EDFAs. The first observation is that EDFA #R0302 shows better performance than #R0303 with an average N_{sp} value slightly under 2.5 compared to 3. The higher N_{sp} values found at higher input signal power can be attributed to isolation problems and should not be taken into account.



(a)



(b)

Figure 5.21: Noise factor N_{sp} for (a) EDFA #R0302 and (b) #R0303.

5.4 Optical Receiver

The optical receiver used in our system is a BNR OC12 receiver. Its main characteristics are described in the following subsections.

5.4.1 BNR OC12 Receiver

The BNR OC12 receiver is a digital receiver optimized for OC12 operation (622 Mb/s). It is composed of an ANADIGICS model ATA06210 AGC (automatic gain control) transimpedance amplifier with a PIN detector of 0.7 A/W responsivity. This unit is followed by two ADVANTEK 1.5 GHz variable gain amplifiers and a noise filter. The overall nominal sensitivity of the receiver is -33 dBm at OC12. The schematic of the BNR OC12 receiver is given in Appendix 5F along with additional information.

5.4.2 Electrical Response

A typical frequency response of the BNR OC12 receiver was provided by Bruce Beggs from BNR Ottawa and is reproduced in Appendix 5F. The 3 dB single-sided bandwidth is around 360 MHz and the roll off follows the response of a fourth order Butterworth filter. This gives a single-sided equivalent rectangular bandwidth of approximately 370 MHz.

5.4.3 Sensitivity

The sensitivity of an optical receiver is defined as the power required for a BER of 10^{-9} . The sensitivity of the BNR OC12 receiver was measured using setup is shown in Figure 5.22. The Mas-Tech LED was digitally modulated at OC12 with a 2^7-1 long pseudo-random sequence of peak to peak amplitude of 108 mA as previously for the rise and fall time measurements. Gradually, the optical power going into the BNR OC12 receiver was increased from a very small value to the point where the BERT records a BER of 10^{-9} .

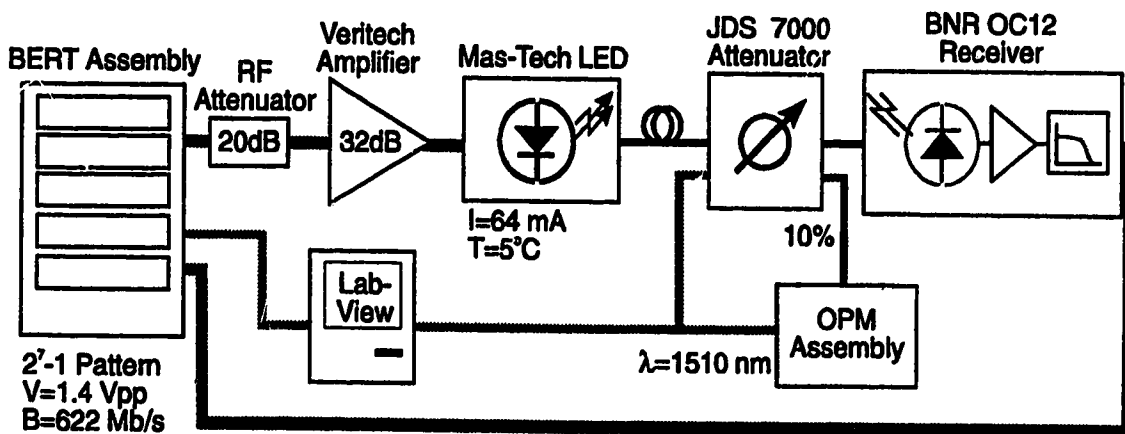


Figure 5.22: BNR OC12 receiver sensitivity measurement setup.

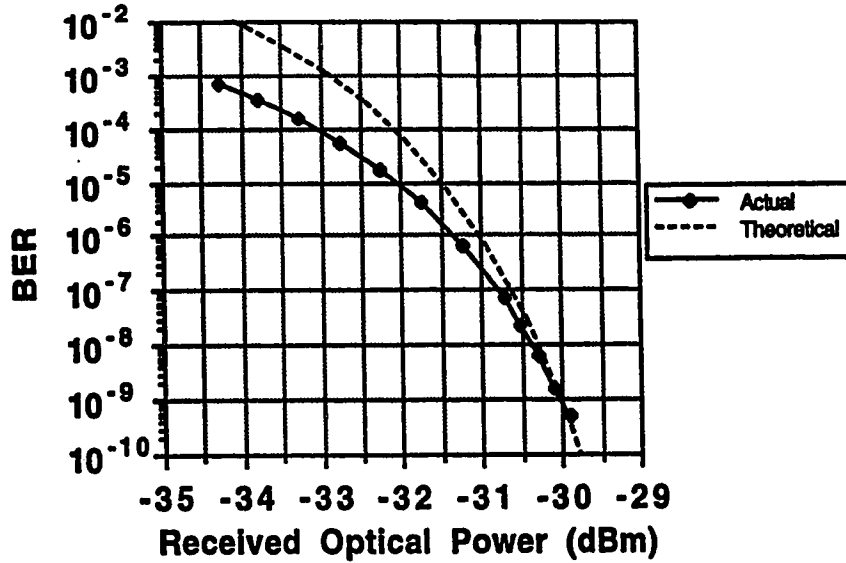


Figure 5.24: BNR OC12 receiver sensitivity curve. (solid line: actual, dashed line: theoretical)

The performance of an optical receiver is always limited by thermal noise of its electrical components. As mentioned earlier, the thermal noise is Gaussian in nature and the expression for its equivalent mean square photocurrent was given in the previous chapter (see Equation (4.40)). As also mentioned in this chapter, in the case of Gaussian noise, a Q of 6 is required to obtain a BER of 10^{-9} . Assuming that the SNR is approximately equal to Q^2 , we obtain:

$$Q^2 = 36 \approx SNR = \frac{I_s^2}{I_{th}^2} \quad (5.5)$$

The signal photocurrent is given by photodetector responsivity times the optical power, $I_{sig} = \mathfrak{R}P_{opt}$. Taking $\mathfrak{R}=0.7$ A/W and $P_{opt} = -30\text{dBm} = 1\mu\text{W}$, we obtain for the thermal noise photocurrent squared: 1.36×10^{-14} A². This gives an R_L of 452 Ω . In order to account for the LED extinction ratio (12 dB) this value increases to 580 Ω . The theoretical OC12 receiver sensitivity curve is compared to the actual one in Figure 5.24. We notice that the actual OC12 receiver sensitivity curve is slightly shallower than the theoretical one. This is caused by the fact that some additional sources of noise are present in the optical receiver. These were not taken into account here.

5.5 Conclusion

In this chapter, we described an experimental spectral slicing setup and characterized each of its components. This setup will be used in the next chapter for a study of the performance of spectral slicing.

6. Experimental Results

In the previous chapter, we described an experimental spectral slicing system and characterized each of its components. In this chapter, we present the results of a series of BER measurements that was performed on this system. These results are compared to the theory developed in the earlier chapters.

The chapter is divided into four parts. In the first part, we present an example of power budget. In the second parts, we perform a noise analysis to see which of the noise terms is dominant for our system. In the third part, the system parameters are varied and a series of BER results is presented and compared with the theory where possible. Finally, the chapter ends with a discussion on spectral slicing in a WDM application and a conclusion.

6.1 Power Budget

The power budget of an optical communication link is the determination of the power levels at different important points in the link. This measurement allows us to track down which components in the link introduce the most loss and how they affect the overall system performance. Here we present an example of power budget measurements for the case where the EDFA R0302 is in the spectral slicing link. The setup is shown in Figure 6.1. The EDFA R0302 is operated for a pump laser drive current of 160 mA which give a gain and a noise factor of about 28 dB and 2.5, respectively. The polarization splitter used just before the OC12 receiver is to provide linearly polarized light; its insertion loss is about 0.6 dB. The power is measured at the six different points identified on Figure 6.1. with the OPM assembly #22. The results are summarized in Table 6.1.

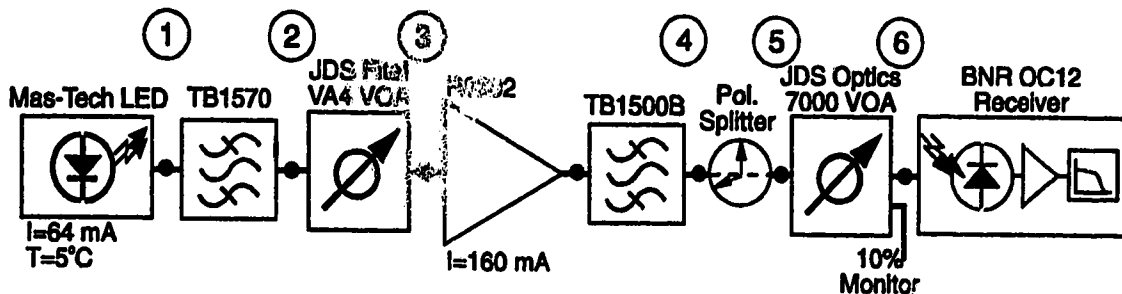


Figure 6.1: Setup for the power budget measurement.

Point #	Power (dBm)	Difference (dB)
1	-14.9	-
2	-31.2	-16.3
3	-33.8	-2.6
4	-9.6	+24.2
5	-13.2	-3.6
6	-16.6	-3.4

Table 6.1: Power budget results

This simple measurement shows that in the case where the two variable optical attenuators (VOAs) are set for minimum attenuation, the power at the OC12 receiver is -16.6 dBm which is well above its sensitivity (i.e., -30 dBm). The measurement also indicates that most of the loss in the system is due to the filtering.

6.2 Noise Analysis

A noise analysis allows us to compare the various noise terms discussed earlier and verify that when the optical power at the receiver is large, the dominant noise is the photon noise. The expressions for the equivalent mean squared photocurrent of the signal and the various noise terms were defined in Chapter 4 (see Equations (4.14) to (4.20)). As mentioned in the previous chapter, because of the TB1570 filter in front of the EDFA, a correction factor that we called double filtering factor was introduced in these equations. This factor was determined by taking the ratio of the bandwidth of the TB1570 and TB1500B filters cascaded to the that of the TB1500B filter alone. It is evaluated to approximately 0.85. This gives a number of modes of about 280. A comparison between the noise terms is presented for the setup of Figure 6.1 in the case of a constant input power to the EDFA (measured at point #3 on Figure 6.1) of -36 dBm. The results are shown in Figure 6.2. The listing of the program used for the calculations can be found in appendix 6A.

As we can see from this figure the thermal noise of the receiver dominates the noise up to an optical power at the receiver of about -25.5 dBm where N_{s-sp} and N_{th} are approximately equal. N_{sp-sp} and N_{ex} come next with slightly smaller values. As the received power increases N_{s-sp} , N_{sp-sp} and N_{ex} all overcome N_{th} . Around -20 dBm, they

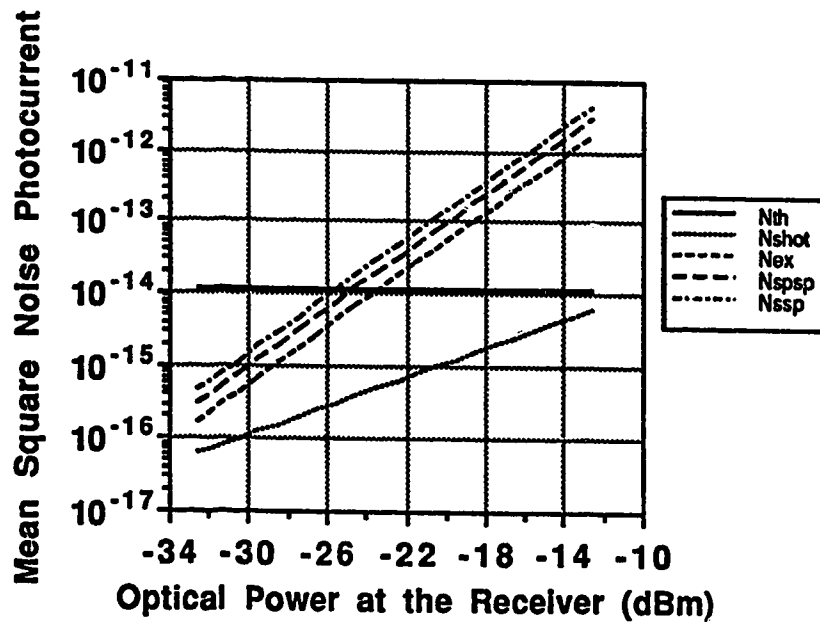


Figure 6.2: Equivalent mean square noise photocurrents plotted as a function of the optical power at the receiver.

are about one order of magnitude larger than the thermal noise. At this point, the noise is definitely dominated by the photon noise. The terms N_{s-sp} and N_{sp-sp} dominate over N_{ex} because of the relatively large noise factor of EDFA R0302 and number of modes. Eventhough this plot was obtained for only one set of system parameters, it will be useful to explain the BER results presented in the next section.

6.3 BER Measurements

In this section, the results of a series of experimental BER measurements are presented. First, we looked at the effect of the input power to the EDFA, then the EDFA gain and noise factor and finally the optical filter bandwidth (number of modes). In each case, the measured BER floors are compared to the those predicted theoretically using both the negative binomial PDF and the Gaussian approximation methods to calculate the BER. (see Equations (4.34) with (4.34) and (4.35) with (4.36)) The setup for the BER measurements is shown in Figure 6.3. It is very similar to the OC12 receiver sensitivity measurement seen in the previous chapter except for the addition of the spectral slicing optical link between the LED transmitter and the OC12 receiver. Here again, the polarization splitter placed just before the OC12 receiver is used to provide linearly polarized light. The settings on both the BERT assembly and the LED are the same as for

the OC12 receiver sensitivity measurement and here also, *LabVIEW* was used to control the instruments and facilitate the data acquisition.

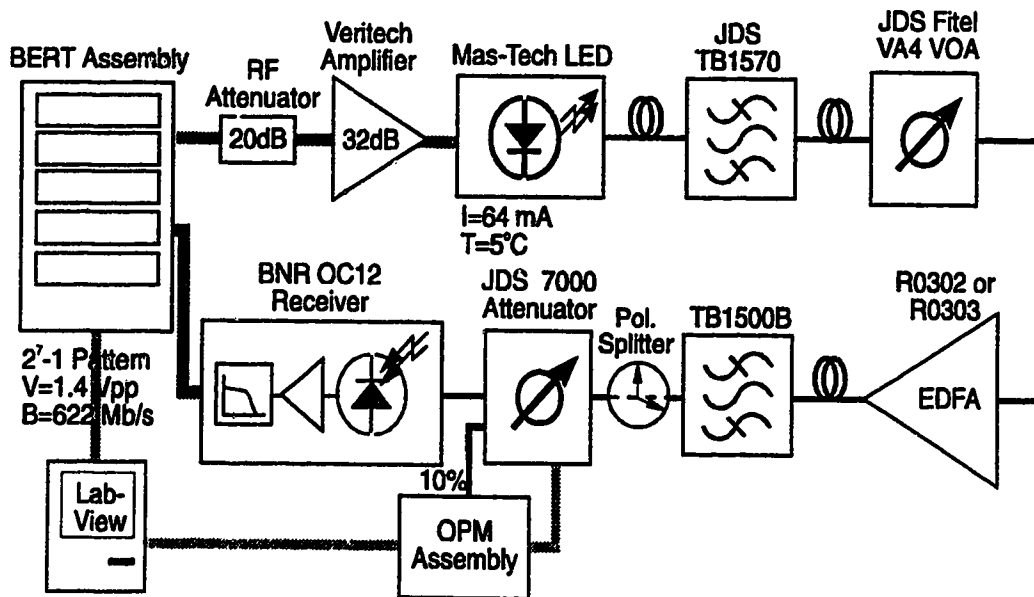


Figure 6.3: BER measurement setup

Using this setup, the BER was measured as a function of the optical power at the OC12 receiver. To obtain significant BER values, we waited until 35 errors were recorded on the BERT. This is a commonly assumed value to evaluate BER down to 10^{-9} . The required measurement time can be evaluated by the following simple formula:

$$T_m = \frac{35}{(B \times BER)} \quad (6.1)$$

where B is the bit rate. At OC12 ($B=622$ Mb/s), the time required to obtain a BER of 10^{-9} is approximately one minute.

6.3.1 EDFA Input Power

In Chapter 4, we looked at the effect of the LED power on the BER performance of a theoretical spectral slicing system. We found that the sensitivity improved and that the BER floor shifted down with increasing value of the LED power. In this section, we also look at the effect of the LED power however, the LED power was measured after the TB1570 filter in the setup of Figure 6.3 and consequently, the name input power to the EDFA is more appropriate. Figure 6.4 shows the measured BER plotted as a function of the optical power at the OC12 receiver for different values of the input power to the

EDFA. The values of input power to the EDFA range from -31.2 to -37.7 dBm. This figure is obtained for the case where the EDFA R0303 operated with a pump drive current of 160 mA is used in the system of Figure 6.3. This gives a small signal gain of about 33 dB with a noise factor of 2.8. The OC12 receiver nominal sensitivity curve is also shown on Figure 6.4 for comparison.

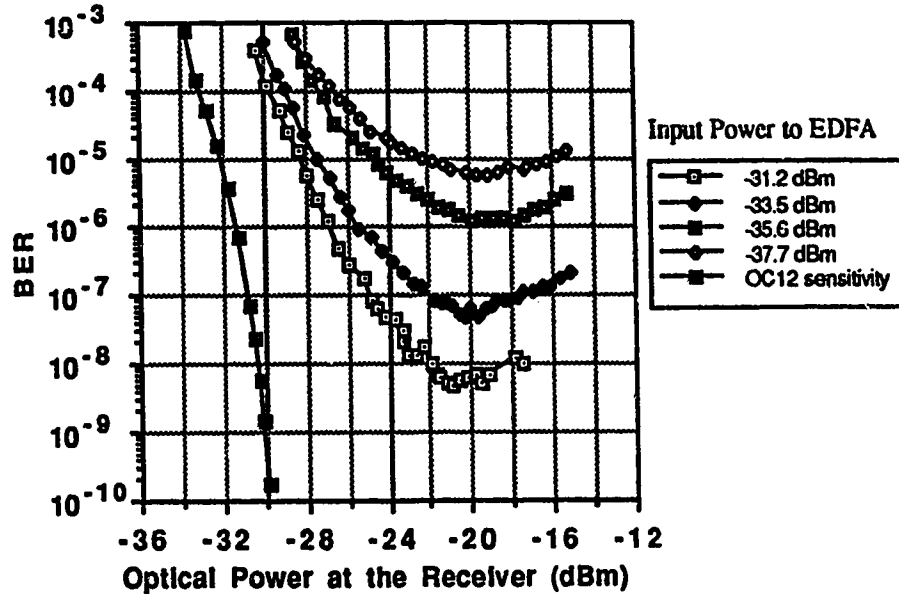


Figure 6.4: BER curves as a function of the optical power at the OC12 receiver with the input power to the EDFA as a parameter. (EDFA R0303 @ 160 mA, gain $G=33$ dB, noise factor $N_{sp}=2.8$, polarization splitter used, number of modes $N=280$)

The BER curves follow a general waterfall-like behavior as for the receiver sensitivity curve at least for low optical power at the OC12 receiver. As the power at the receiver increases, BER floors are observed and their value is shifted down for larger values of input power to the EDFA. Note that the 10^{-9} point is never reached. As discussed in Chapter 4, these BER floors are caused by the excess noise of the LED. The plot comparing the noise terms of the system (Figure 6.2) demonstrates how the excess noise of the LED and the EDFA beat noises dominate over the other noise terms as the optical power at the OC12 receiver becomes large. The smallest value for the BER is about 5×10^{-9} and is obtained for the largest input power to the EDFA (-31.2 dBm). The BER floors can be compared to those calculated theoretically using the negative binomial PDF and the Gaussian approximation methods. The calculated BER floor values are obtained with the *Mathematica* programs used in Chapter 4. The listings of the programs

can be found in appendix 6A. A comparison between the calculated and measured BER floors is shown in Figure 6.5. In this figure (see upper part), the solid line designates the BER floor predicted with the negative binomial PDF and the dashed lines that predicted with the Gaussian approximation, respectively. The small dark squares represent the measured values for the BER floor. As we can see, the calculated BER floors for both methods seem to overestimate the measured BER floor at low input power to the EDFA and seem underestimate it when this power is large. This results in only a moderate agreement and the reasons for this will be given later in the discussion section.

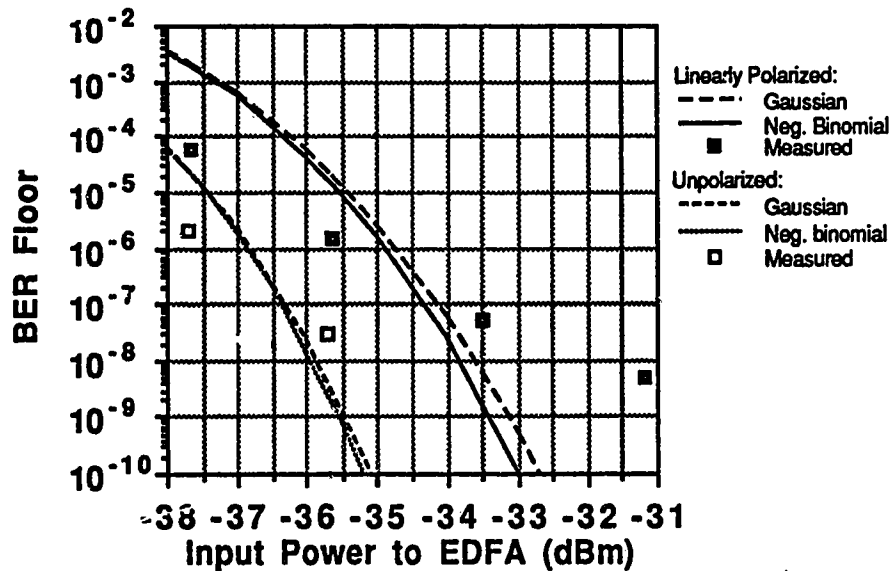


Figure 6.5: Calculated and measured BER Floors as a function of input power to the EDFA for linearly polarized and unpolarized light. (EDFA gain $G=33$ dB, noise factor $N_{sp}=2.8$)

As mentioned in Chapter 2, the number of modes of unpolarized light is twice larger than that of linearly polarized light for the same filtering and as discussed in Chapter 4, the BER performance improves with an increase in the number of modes. This can be verified by removing the polarization splitter before the OC12 receiver. Removing the polarization splitter in the setup of Figure 6.3 not only increases the number of modes by a factor of two, but also increases the power at the OC12 receiver. The results of the BER measurement as a function of the power at the OC12 receiver are shown in Figure 6.6 for the same values of input power to the EDFA as for the case treated just above. As predicted, the removal of the polarization splitter produces an improvement of the

performance. Now, the 10^{-9} point is reached for two values of the input power to the EDFA. Compared to the OC12 receiver nominal sensitivity, there is a sensitivity penalty of approximately 5 dB for an EDFA input power of -31.2 dBm, and 8 dB when the input power to the EDFA is reduced to -33.5 dBm. For an input power of -35.7 dBm and below, the BER never reaches the 10^{-9} point. The BER floors are compared to the calculated ones in Figure 6.5. In this figure (see lower part), the dotted line designates the BER floor predicted using the negative binomial PDF method and the small-dashed line designates that predicted with the Gaussian approximation method. The measured values for the BER floor in this case are indicated by the two white squares in the figure. As for linearly polarized light, the calculated BER floors for unpolarized light overestimate the measured BER floor for low input power to the EDFA and underestimate it when this power gets large. The figure allows a quick comparison between the BER floors for the case of linearly polarized and unpolarized light at the receiver.

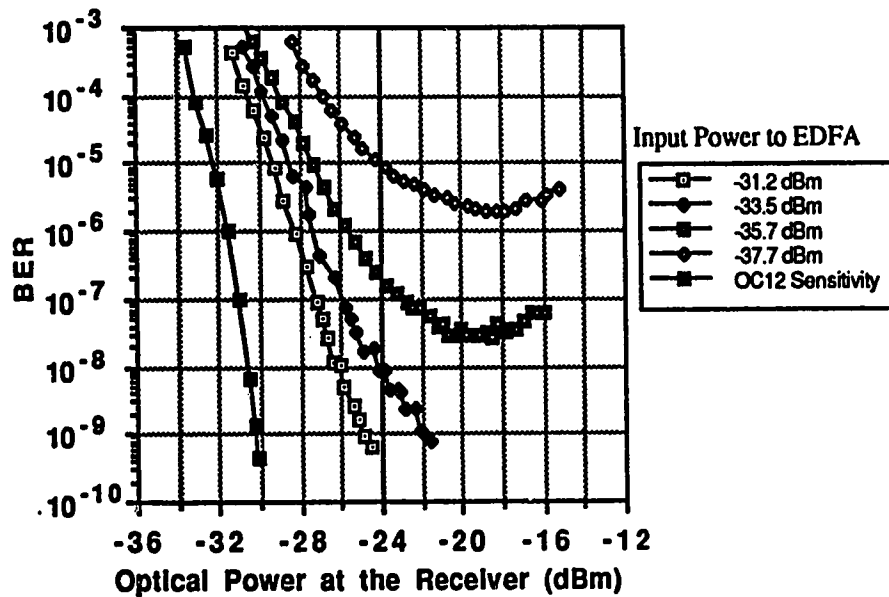


Figure 6.6: BER curves as a function of the optical power at the OC12 receiver with the input power to the EDFA as a parameter. (EDFA R0303 @ 160 mA, gain $G=33$ dB, noise factor $N_{sp}=2.8$, polarization splitter removed, number of modes $N=560$)

In this section, the effect of the input power to the EDFA on the BER performance has been confirmed. Increasing values of input power to the EDFA produces an improvement of the BER sensitivity as well as a downward shift of the BER floor. In

addition, the effect of the polarization is also confirmed. However, a comparison between the measured and calculated BER floors showed only a moderate agreement.

6.3.2 EDFA Characteristics

As discussed in Chapter 4, the characteristics of the EDFA used in the spectrally slicing system affect also the BER performance. For instance, we found that the noise factor had a relatively large effect on the BER floor compared to the gain. In fact, for the system studied in Chapter 4, a variation of a few tenths in the value of the noise factor shifts the BER floor by several orders of magnitude whereas the change of two orders of magnitude in the gain only shifts the BER floor by a factor 2 or 3. In the previous chapter, we characterized the two TRILabs EDFAs and determined their gain and noise factor as a function of the input signal power for three pump drive currents. In this section, we compare the measured BER performance of the system of Figure 6.3 when the EDFA R0303 is replaced by the EDFA R0302.

Noise Factor

For a pump drive current of 160 mA, the EDFA R0302 has a gain and a noise factor of 28 dB and 2.5, respectively. This noise factor is smaller than that of EDFA R0303. Consequently, if we replace the EDFA R0303 by R0302 in the system of Figure 6.3, we should observe improved sensitivities and lower BER floors for the same input power to the EDFA. The BER measurements were repeated for the case where the polarization splitter is not present before the OC12 receiver (unpolarized light). The measured BER curves plotted as a function of the optical power at the receiver for different input power to the EDFA are shown in Figure 6.7. As expected, the use of EDFA R0302 improves the BER performance. For the same values of input power to the EDFA, the sensitivity penalty compared to the OC12 receiver nominal sensitivity is 3.5 and 4.5 dB for an input power of -31.6 and -34 dBm, respectively, as opposed to 5 and 8 dB previously. For an input of -36 dBm and below, the 10^{-9} point is never reached and BER floors are observed. The measured BER floors obtained here are compared to the calculated ones and to those obtained with the EDFA R0303 in Figure 6.8. In this figure, the case of N_{sp} equal to 2.8 corresponds to the EDFA R0303 and the case of N_{sp} equal to 2.5 corresponds to the EDFA R0302.

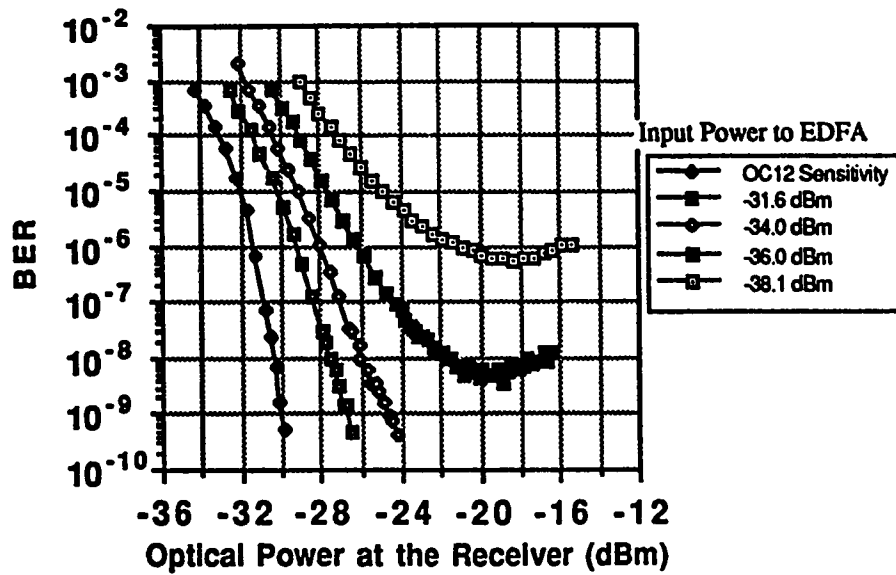


Figure 6.7: BER curves as a function of the optical power at the OC12 receiver with the input power to the EDFA as a parameter. (EDFA R0302 @ 160 mA, gain $G=28$ dB, noise factor $N_{sp}=2.5$, polarization splitter removed, number of modes $N=560$)

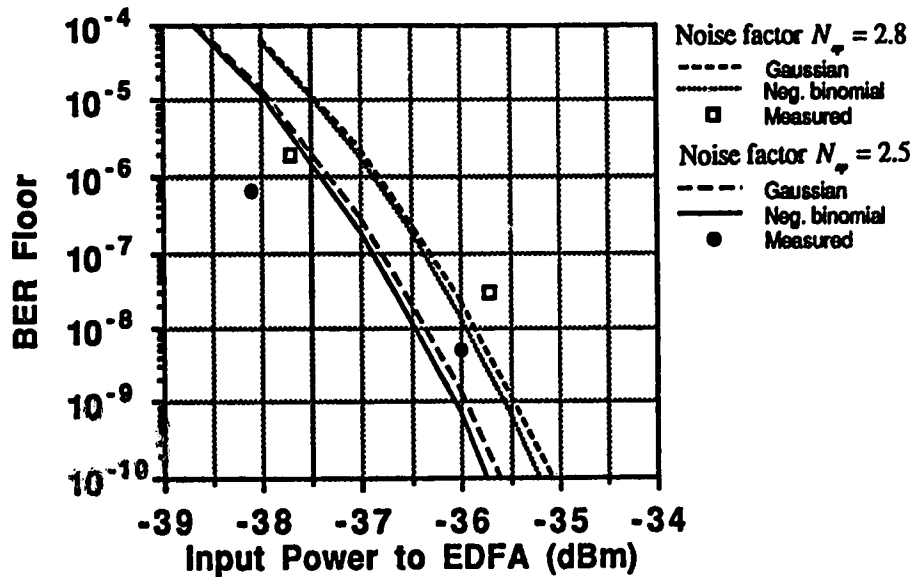


Figure 6.8: Comparison of the BER floors as a function of the input power to the EDFA obtained with EDFA R0302 @ 160 mA ($N_{sp}=2.5$) and R0303 @ 160 mA ($N_{sp}=2.8$) (polarization splitter removed, $N=560$).

Gain

The effect of the gain on the BER performance was also discussed in Chapter 4. It is relatively small compared to that of the input power to the EDFA and of the noise factor. This can be verified experimentally by reducing the gain of the EDFA R0302 and repeating the BER measurements. To reduce the gain, we simply decrease the pump laser drive current of the EDFA. However, in doing so, the noise factor also changes slightly. The EDFA R0302 appears to exhibit the smallest changes in the noise factor as function of the pump drive current and has therefore been used for the measurement. The small signal gain of EDFA R0302 is about 28 dB when the pump current is set at 160 mA and this value drops by 3 dB to 25 dB when this current is set at 120 mA. The BER measurements were repeated again and the results are shown in Figure 6.9. As we can see, the performance is practically not affected by the 3 dB reduction of the gain. The penalty on the nominal sensitivity seems to have slightly reduced by approximately less than 0.5 dB and the change on the BER floors is not noticeable as expected. In the same way as before, the BER floors are compared in Figure 6.10. Note in this figure that the calculated BER floors for both values of gain sit almost exactly on top of each other. The measured BER floor values are also pretty close for both gains.

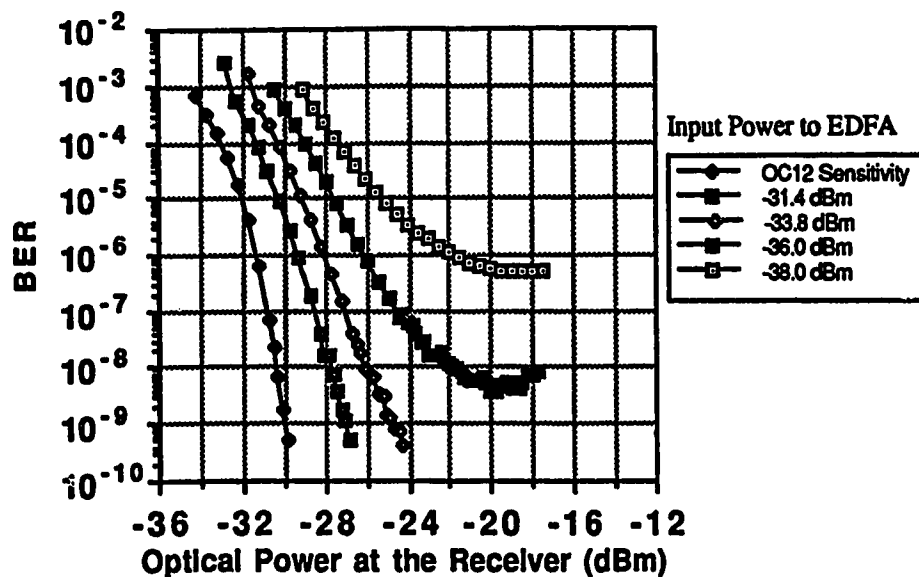


Figure 6.9: BER curves as a function of the optical power at the OC12 receiver with the input power to the EDFA as a parameter. (EDFA R0302 @ 120 mA, $G=25$ dB, $N_{sp}=2.4$, polarization splitter removed, $N=560$)

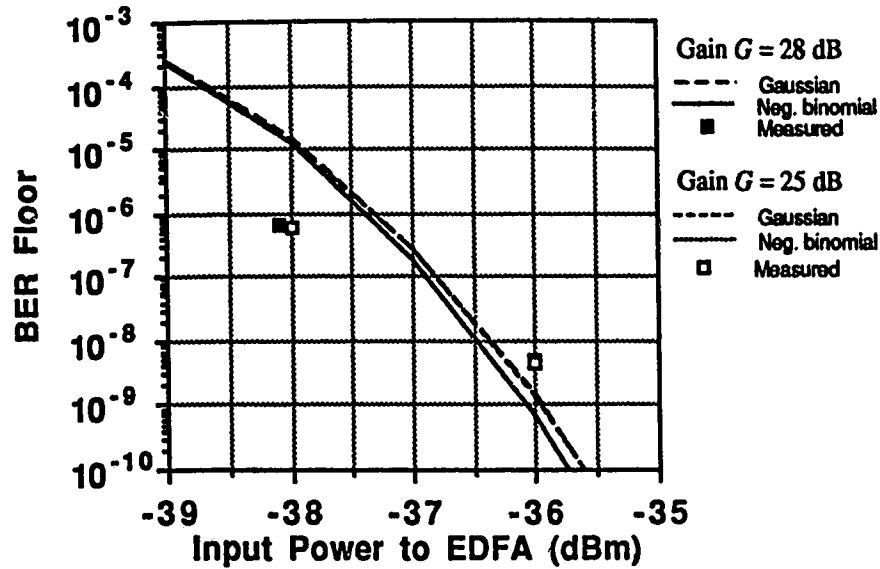


Figure 6.10: Comparison of the BER floors as a function of the input power to the EDFA obtained with EDFA R0302 operated with a pump current of 160 mA ($G=28$ dB) and 120 mA ($G=25$ dB).

The gain is a function of input power to the EDFA. At low input power, the gain is approximately constant and is called the small signal gain or linear gain. As the input power is increased beyond a certain value, the gain starts to decrease because the EDFA starts operating in the saturation regime. As seen in Chapter 5, for the EDFA R0302 operated at a pump current of 160 mA, the 1 dB gain compression is obtained for an input power of about -27 dBm.

The use of an input filter before the EDFA reduces the input power to prevent saturation operation. If this filter is removed however, the input power becomes too large and the EDFA is in saturation. Since the gain of an EDFA in saturation is lower, the performance is expected to be degraded. Here, we present a comparison between the case where the TB1570 filter is used in front of the EDFA and the case with no input filter. For this study, we keep the effective input power spectral density the same for both cases. For the comparison, the gain of EDFA R0302 must be decreased in the first case to match the saturation gain obtained when no input filter is present in front of the EDFA. Using the Figure 5.23, the saturation gain of EDFA R0302 was determined for an input of -19.6, -21.6 and -23.6 dBm when operated at 160 mA. The corresponding gain values are approximately 23, 24 and 25 dB, respectively. To obtain about the same small signal gain the pump drive current of EDFA R0302 must be set to 110, 115 and 120 mA. We

repeated the BER measurements and obtained the results shown in Figure 6.11. The agreement is very good for all values of input power to the EDFA.

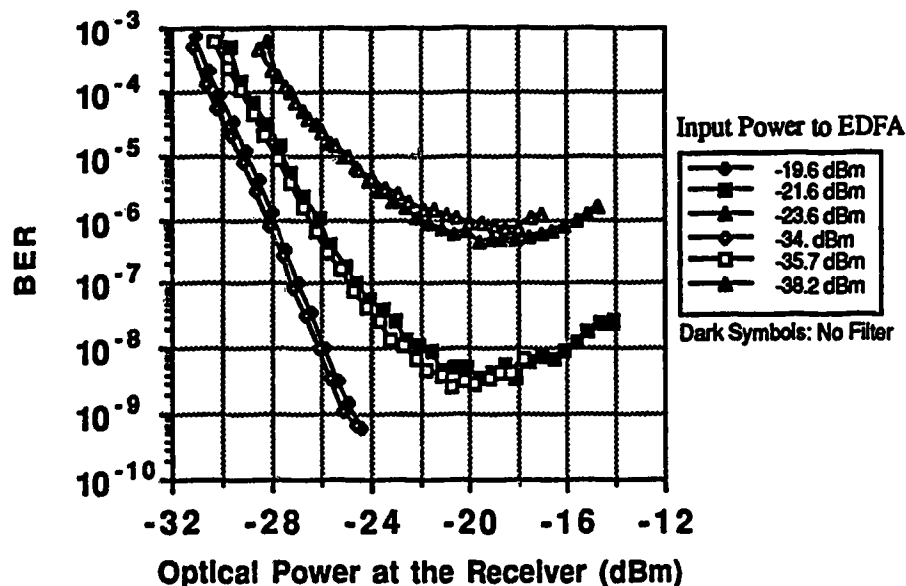


Figure 6.11: Comparison between the BER curves measured as a function of the optical power at the receiver obtained when the EDFA R0302 is operated in the linear and the saturated regimes. (power splitter removed $N=560$)

In this section, the effect of the EDFA characteristics on the BER were studied. First, we found that the EDFA R0302 gives a better BER performance than the EDFA R0303 due mainly to its smaller noise factor. Second, we found that a reduction of the EDFA gain from 28 to 25 dB does not affect much the BER. Finally, we observed that the effect of the saturation of the EDFA only corresponds to a reduction of the effective EDFA gain. All these findings and observations confirm the theoretical predictions.

6.3.3 Optical Bandwidth

Two important parameters are affected by the optical filtering in the spectral slicing system. The first one is the total optical power incident on the photodetector and the second one is the number of modes of the photon number distribution. As seen in Chapter 4, the BER performance is largely affected by the number of modes. Both the sensitivity and the BER floor values get smaller with an increasing number of modes. To measure the effect of the optical filtering on the BER performance, we replaced the output TB1500B filter by a Queensgate QMF filter. This is a piezo-tuned Fabry-Perot type that has a

FWHM bandwidth of about 0.8 nm and an insertion loss of 7.2 dB. This optical bandwidth corresponds to about 330 modes. Because of insufficient power at the OC12 receiver due to the high insertion loss of this filter, we could not obtain well defined BER floors; only the beginning of the floors was observed. This can be seen in Figure 6.12 where the measured BER curves obtained for the case of where the EDFA R0302 operated at a pump current of 120 mA and the Queensgate filter are used in the setup of Figure 6.3.

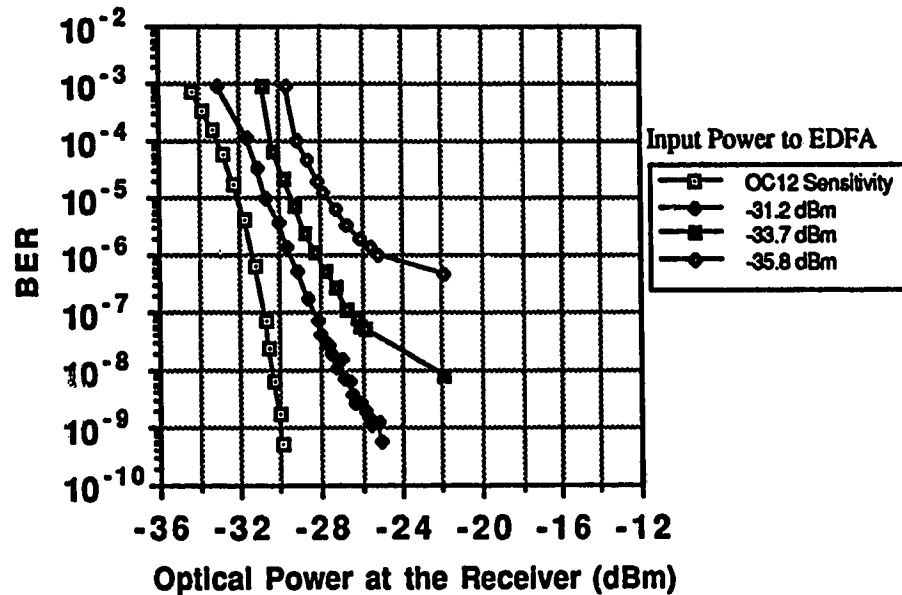


Figure 6.12: BER curves as a function of the optical power at the OC12 receiver with the input power to the EDFA as a parameter using the EDFA R0302 @ 120 mA and the output Queensgate QMF filter. (gain $G=25$ dB, noise factor $N_{sp}=2.4$, polarization splitter removed, number of modes $N=330$)

In Figure 6.13, we present a comparison between the calculated and measured BER floors for an input power to the EDFA of about -36 dBm. In this figure, the solid line designates the negative binomial PDF method and the dashed line, the Gaussian approximation method. The two little squares represent the measured BER floors for the case where the TB1500B filter and the Queensgate filter are used, respectively as output filters. The agreement between the calculated and measured BER floors is relatively good. Note however that strictly speaking, the point obtained for the Queensgate filter is not the true BER floor value since the final BER floor could not be obtained in that case because of a lack of power at the receiver.

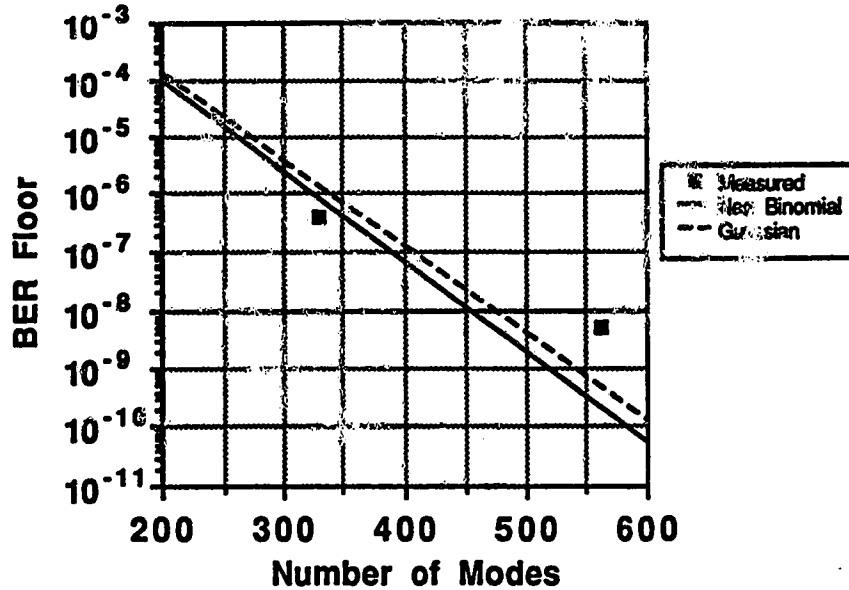


Figure 6.13: Comparison of the BER floor as a function of the number of modes for an input power to the EDFA of about -36 dBm using the EDFA R0302 @ 120 mA (gain $G=25$ dB, noise factor $N_{sp}=2.4$, polarization splitter removed)

In this section, the effect of a reduction in the optical filter bandwidth was studied. As we expected, a reduction of the optical bandwidth reduces the number of modes and in a degradation of the BER performance.

6.4 Discussion

The quality of the agreement between the calculated and measured BER can be attributed to two main reasons. First, it can be due to some assumptions we made in our model for the description of the statistical behavior of the optically filtered amplified LED emission. Second, it can be caused by the fact that our degree of control on the experimental system parameters may not be sufficient.

The first reason can be examined by reviewing our assumptions. We assumed first that that optically filtered LED could be described by a filtered thermal source. This assumption is reasonable since the LED emission consists of spontaneous emission of photons which has a thermal behavior [17]. Then we assumed that the number of modes is given by the ratio of the optical to the electrical bandwidth in the case of large value of this ratio (>10). This is also justified in our case since the number of modes is never less than a few hundred. The assumption that the EDFA was pumped uniformly and that it was

operated in the linear regime may not be the cause of problems although this is questionable for the cases where the input to the EDFA is larger than about -27 dBm which occurs only for unfiltered LED input. The most problematic assumption was certainly to assume the same number of modes for both the negative binomial PDF that characterizes the LED emission and for the BDI medium which describes the EDFA amplification. In our case, the optical filtering on the LED is different from that of the EDFA and consequently, strictly speaking this assumption is not truly valid. Even if the difference in the number of modes resulting from that is relatively small, it could affect the photon number PDF at the output of the system and consequently the BER. The second main reason to explain the quality of the agreement between the calculated and measured BER can be examined by looking at the relative importance of each of the experimental system parameters and the method we used to obtain them. As we saw in Chapter 4 and also in this chapter, the LED power and extinction ratio, the EDFA noise factor and the number of modes can all shift the BER floors of the system by several decades for relatively small variations in their value. Although we believe that the LED power and the number of modes can be determined quite accurately, it is not the same for the LED extinction ratio and the EDFA noise factor. As mentioned in Chapter 5, a shift in the optical power was observed when the LED was modulated. Even if the LED extinction ratio was modified to take this shift into account, this problem is not fully understood. Also, the method used to measure the EDFA noise factor was not very stable because it involved polarization control which is not simple to do. We believe that the noise factor is probably the less accurate parameter in our system. Finally, other factors such as the distortions of the waveform by the LED, the RF amplifiers and the clipping effect of the automatic gain control of the OC12 receiver could also cause some additional problems.

6.4.1 WDM Application

As we did at the end of Chapter 4, we can calculate the maximum number of channels that our experimental spectral slicing system would give if it was used in a WDM application. The TB1500B has a FWHM bandwidth of 1.3 nm. If we assume a total available optical bandwidth is limited by the EDFA bandwidth, i.e., 30 nm, the maximum number of channel is (using Equation (4.41)):

$$\text{Max \# of Channels} = \frac{30 \text{ nm}}{1.3 \text{ nm}} \approx 23 \quad (6.2)$$

This of course assumes that perfect spectral slicing can be achieved. If we take a 1 nm margin on the bandwidth for each channel, the total number of channels is reduced to

about 13. Each of these channels is modulated at OC12 (622 Mb/s) which means a total throughput of 8.1 Gb/s for the WDM system. Assuming a WDM system such as the one of Figure 4.1 (a) in which one EDFA only is placed after the spectral slicing WDM, we can evaluate the distance over which our 13 channels can be transmitted. To do that, we perform a link power budget calculation which is summarized in Table 6.2. The best sensitivity obtained for our experimental spectral slicing system (-27 dBm) was accomplished when we used the EDFA R0302 operated at 120 mA ($G=25$ dB and $N_{sp}=2.4$) and when the input power to it was -31.4 dBm or 720 nW (see Figure 6.9). This input power to the EDFA is obtained for an LED power of -15 dBm or 32 μ W. This gives a system gain of 37.0 dB. Assuming a FWHM bandwidth of 90 nm for the LED, the spectral slicing loss can be obtained by taking the ratio of the FWHM bandwidth of the TB1500B filter to that of the LED. This gives a loss of 18.5 dB. We assume also an additional loss of 2 dB for the optical carrier that is centered at the wavelength the furthest from that of the LED emission peak and 4.5 dB and 2 dB for the spectral slicing WDM and the tunable filter insertion losses, respectively. Keeping a margin of 3 dB, that leaves 7 dB for the transmission loss. Assuming finally a fiber loss=0.25 dB/km, we obtain a transmission distance of 28 km.

LED power (dBm)	-15.0
EDFA Gain (dB)	25.0
Sensitivity (dBm)	<u>-27.0</u>
Available System Gain (dB)=	37.0
Losses(dB)	
Spectral Slicing	18.5
Wavelength offset from peak of LED	2.0
WDM Insertion Loss	4.5
Tunable filter Insertion Loss	2.0
System Margin (dB)	3.0
Total Loss=	30.0
Transmission Loss (dB)	7.0
Distance @ 0.25 dB/km (km)	28

Table 6.2: WDM system link power budget

6.5 Conclusion

In this chapter, the BER performance of an actual spectral slicing system was evaluated and compared with the theory developed in the previous chapters. In the first part, we presented an example of power budget and then, we performed a noise analysis in which a comparison was made between the noise terms of the system. This was followed by a series of BER results presented as a function of various system parameters. Finally, we enumerated possible reasons to explain the quality of the agreement obtained between the theory and the experiment and discussed the performance of our experimental spectral slicing system in a WDM application.

The following chapter will summarize the work accomplished in this project.

7. Conclusion

This work has presented a study of the performance of spectral slicing of LEDs for fiber optic transmission systems. This study has provided us with a better understanding of both the spectral slicing method and the EDFA amplification process as well as with some indication on the limitation of the spectral slicing method to generate optical carriers in an optical FDM or WDM application. The motivation behind this work was to explore an alternative to the need for several semiconductor laser sources with very tight specifications on the operating frequency generally required in FDM transmission systems.

7.1 Overview of the Results

In Chapter 2, we modeled the LED emission based on its internal statistics (spontaneous emission) and found that the output photon emission of a filtered LED can be described by a negative binomial PDF. Also in this chapter, we introduced the notion of modes. We found that the number of modes of a negative binomial PDF is related to the ratio of the detection time to the coherence time of the LED or equivalently to the ratio of the optical filter bandwidth to the electrical detector bandwidth. Finally, we identified a term in the variance of the negative binomial PDF that is dependent on the number of modes. This term is often called the excess noise term and is due to the incoherency of the LED.

In Chapter 3, we introduced the BDI medium to model the output photon emission of an EDFA operating in the linear regime. The birth, death and immigration rates were associated with the stimulated emission, the stimulated absorption and spontaneous emission, respectively, occurring inside an EDFA. A key theoretical result was that the resulting PDF of a filtered optically amplified LED is a convolution between two negative binomial PDFs. Specifically, in the case where both the negative binomial characterizing the filtered LED emission and the BDI medium describing the EDFA amplification have the same number of modes, that is when the same filtering is applied to both the LED and the EDFA, the resulting PDF reduces to a single negative binomial. Finally, in the last section of this chapter, we associated the BDI parameters to the physical quantities characterizing an EDFA such as the gain, the noise factor and the optical bandwidth and identified in the variance of the BDI output the various beat noise terms encountered in the detection of optically amplified signals.

In Chapter 4, we used the theory of Chapters 2 and 3 to model a spectral slicing system composed of an LED, an EDFA, an optical filter and a noiseless optical receiver. Using this model, we were able to obtain the BER as a function of various system parameters such as the LED power and extinction ratio, the EDFA gain and noise factor and the optical filter bandwidth. We found that the BER is ultimately limited by the excess noise of the LED which causes floors in the BER curves as a function of the power at the optical receiver. We studied the sensitivity of these floors as a function of the system parameters. We found that all the system parameters except the EDFA gain have an important effect on them. Also in this chapter, we compared our model for calculating the BER to an approximate model often used in digital communication which assumes Gaussian noise at the optical receiver. We showed that the BER floors predicted with the two models are relatively close for low LED powers but differ quite significantly as this power becomes large. In fact, the Gaussian approximation model predicts a minimum BER floor for a large LED power. Finally, in the end of Chapter 4, we presented a calculation of the maximum number of channels achievable for our theoretical spectral slicing system in a WDM application.

Finally, in Chapter 5, we described a experimental setup designed to verify the theory of the earlier chapters. We characterized each of the components and in Chapter 6, we presented a series of BER results as a function of the LED power, the EDFA gain, noise factor and the optical filter bandwidth. In addition, we observed the effect of the polarization of the light and the effect of saturation of the EDFA on the BER performance. The results of the BER measurements confirmed the existance of BER floors predicted in Chapter 4. These floors were studied as a function of the system parameters and compared with our model and with the Gaussian approximation. The trends predicted in Chapter 4 were similarly observed and the comparison between the measured and calculated BER floor values showed a reasonably good agreement. Finally, we presented an example of a power budget in the case where our experimental spectral slicing system was used in a WDM application. The result of this calculation demonstrated that 13 channels modulated at OC12 (622 Mb/s) could be transmitted over 28 km.

7.2 System Improvements

As we saw in Chapters 4 and 5, both the BER sensitivity and the BER floors improve with increasing LED power; consequently, a more powerful LED in the spectral slicing system would improve the BER performance. Powerful LEDs are difficult to get in reality

especially in the 1.5 μm range. The LED used in our experimental spectral slicing system has an output power of about -15 dBm (32 μW) and is considered a high power LED in the 1.5 μm range. There exist more powerful LEDs in the 1.3 μm range that could be used; however, in that wavelength range EDFAs could not be used. Even if the LED provides more power, we can not achieve a better sensitivity than that of the optical receiver. Consequently, using an optical receiver having a better sensitivity could further improve the performance. Also, a faster LED with a driver circuit optimized for digital modulation could reduce the distortion of the optical waveform and also improve the LED extinction ratio and the performance. Finally, since the extinction ratio is always degraded by the added noise of the EDFA an additional improvement of the system performance could be obtained by the use of an EDFA that has a small noise factor.

7.3 Future Work

This project, unlike others taking place at TRILabs, has not been built on top of a previous one. Consequently, a lot of digging had to be done at the beginning before being able to actually get some results. However, now that most of this part has been done, it should make things easier for a follow up project.

There is some additional work to be done on both the theoretical and the experimental sides. First, on the theoretical side, some work could be done to include the case of nonuniform pumping and the saturation of the EDFA into the BDI model and the effect of a different optical filtering on the LED and the EDFA. On the experimental side, it could be useful to verify the PDF of LED emission alone and that of the output of the EDFA. Finally, a more in depth system approach would be required in order to perform a capacity study for an eventual implementation of a WDM system using spectral slicing.

References

- [1] M. H. Reeve et al., "LED Spectral Slicing For Single-Mode Local Loop Applications.", *Electronics Letters.*, vol. 24, no.7, p. 389-390, 1988.

- [2] H. Toba, "100-Channel Optical FDM Transmission/Distribution at 622 Mbit/s over 50 km Utilising a Waveguide Frequency Selection Switch.", *Electronics Letters*, Vol.26, p.376-377, 1990.

- [3] S. S. Wagner and T. E. Chapuran, "Broadband High Density WDM Transmission using Superluminescent Diodes.", *Electronics Letters*, Vol.26, p.696-697, 1990.

- [4] P. D. D. Kilkelly et al., "Experimental Demonstration of a Three-Channel WDM System over 110 km Using Superluminescent Diodes.", *Electronics Letters*, Vol.26, p.1671-1673, 1990.

- [5] K. Liu, "Noise Limits of Spectral Slicing in Wavelength-Division Multiplexing Applications.", *OFC'92*, WN7, 1992.

- [6] J. M. Senior, **Optical Fiber Communications: Principles and Practice.**, Prentice-all International, 558pp. 1985.

- [7] C. A. Brackett, "Dense Wavelength Division Multiplexing Networks: Principles and Appications.", *IEEE Journal of Selected Areas in Communications*, Vol.8, No.6, p.948-964, 1990.

- [8] F. G. Stremier, **Communication Systems.**, Addison-Wesley, Third Edition, 757pp., 1990.

- [9] C. Lin et al., "Wavelength-Tunable 16 Optical Channel Transmission Experiment at 2 Gbit/s and 600 Mbit/s for Broadband Subscriber Distribution. *Electronics Letters*, Vol.24, p.1215-1217, 1988.

- [10] R. Welter et al., "Sixteen-Channel Coherent Broadcast Network at 155 Mbit/s.", *Journal of Lightwave Technology*, Vol.7, No.10, p.1438-1444, 1989.
- [11] M. W. Maeda et al., "Multigigabit/s Operation of 16 Wavelength Vertical-Cavity Surface-Emitting Laser Array.", *IEEE Photonics Technology Letters*, Vol.3, No.10, p.863-865, 1991.
- [12] T. E. Chapuran et al., "Broadband Multichannel WDM Transmission with Superluminescent Diodes and LEDs.", Bell Communications Research Technical Memo, 1991.
- [13] B. E. A. Saleh and M. C. Teich, Fundamentals of Photonics., Wiley-Interscience, 966pp., 1991.
- [14] P. Urquhart, "Review of Rare Earth Doped Fibre Lasers and Amplifiers.", *IEE Proceedings*, Vol.135, Pt. J., No.6, p.385-407, 1988.
- [15] E. Desurvire, "Erbium-doped fiber amplifiers for new generations of optical communication systems.", *Optics & Photonics News*, p. 6-11, January 1991
- [16] B. J. Ainslie, "A Review of the Fabrication and Properties of Erbium-Doped Fibers for Optical Amplifiers.", *Journal of Lightwave Technology*, Vol.9, No.2, p.220-227, 1991
- [17] K. Petermann, Laser Diode Modulation and Noise, Kluwer Academic Publisher, 315pp., 1988.
- [18] R. C. Giles and E. Desurvire, "Modeling Erbium Doped Fiber Amplifiers.", *Journal of Lightwave Technology*, Vol.9, No.2, 1991
- [19] N. A. Olsson, "Lightwave Systems with Optical Amplifiers.", *Journal of Lightwave Technology*, Vol.7, No.7, p.1071-1082, 1989.
- [20] P. W. France, Editor, Optical Fibre Lasers and Amplifiers, Blackie, 259pp. 1990.

- [21] W. S. Gornall, "The World of Fabry-Perots.", *Lasers & Applications*, p. 47-52, July 1986.
- [22] C. M. Miller, "Characteristics and Applications of High Performance, Tunable, Fiber Fabry-Perot Filters.", *Electronics Components & Technology Conference*, Atlanta, Georgia, May 1991.
- [23] G. F. Williams, Topics in Lightwave Transmission Systems, chapter on Lightwave receivers, 1989.
- [24] H. Kressel, Semiconductor Devices, Springer-Verlag, 441pp., 1978.
- [25] B. Saleh, Photoelectron Statistics, Springer-Verlag, 441pp., 1978.
- [26] C. L. Metha, "Theory of Photoelectron Counting", *Progress in Optics*, Edited by E. Wolf, Vol. VIII, p. 372-440, 1970.
- [27] R. M. Gagliardi and S. Karp, Optical Communications, Wiley and Sons, 432pp., 1976.
- [28] J. W. Goodman, Statistical Optics, Wiley Interscience, 550pp., 1985.
- [29] M. Le Berre, "Photodetection and Photostatistics", *Photons and Quantum Fluctuations*, Edited by E. R. Pike and H. Walter, p. 31-50, 1988.
- [30] L. Mandel, "Fluctuations of Photon Beams and their Correlations.", *Proceedings of the Physical Society (London)*, Vol. 72, p. 1032-1048, 1958.
- [31] G. Lachs, *Physical Review B*, Vol. 138, p. 1012, 1965.
- [32] S. O. Rice, *Bell System Technical Journal*, Vol. 24, p.46, 1945.
- [33] L. Mandel, *Proceedings of the Physical Society (London)*, Vol. 74, p. 233, 1959.
- [34] H. Hodara, "Statistics of Thermal and Laser Radiation", *Proceedings of the IEEE*, Vol. 53, p.696-704, 1965.

- [35] W. B. Jones jr., **Introduction to Optical Communication Systems.**, Holt, Rinehart and Winston, 347pp., 1988.
- [36] K. Shimoda et al., "Fluctuations in Amplification of Quanta with Application to Maser Amplifiers.", *Journal of the Physical Society of Japan*, vol. 12, no. 6, p. 686-700, 1957.
- [37] P. Diament and M. C. Teich, "Evolution of the Statistical Properties of Photons Passed Through a Traveling-Wave Laser Amplifier.", *IEEE Journal of Quantum Electronics*, vol. 28, no. 5, p. 1325-1334, 1992.
- [38] T. Li and M. Teich, "Bit-Error Rate For a Lightwave Communication System Incorporating an Erbium-Doped Fiber Amplifier.", *Electronics Letters*, vol. 27, no. 7, p.598-600, 1991
- [39] E. L. Goldstein and M. C. Teich, "Noise in Resonant Optical Amplifiers of General Resonator Configuration.", *IEEE Journal of Quantum Electronics*, vol. 25, no. 11, p. 2289-2296, 1989.
- [40] E. Parzen, **Stochastic Processes.**, Chap. 7, 1962.
- [41] A. Papoulis, **Probability, Random Variables and Stochastic Processes.**, Second Edition, McGraw-Hill, Chap. 12, 1984.7
- [42] N. B. Abraham, "Quantum theory of a saturable optical amplifier.", *Physical Review A*, Vol. 21, p. 1595-1601, 1980.
- [43] G. Oliver and C. Bendjaballah, "Statistical properties of radiation in a nonlinear optical amplifier.", *Physical Review A*, Vol. 22, p. 631-634, 1980.
- [44] C. Bendjaballah and G. Oliver, "Comparison of statistical properties of two models for saturated laser-light amplifier", *Physical Review A*, Vol. 22, p. 2726-2731, 1980.
- [45] P. R. Morkel et al., "Noise Characteristics of High-Power Doped-Fibre Superluminescent sources.", *Electronics Letters*, Vol. 26, p.96-98, 1990.

- [46] B. Sklar, Digital Communications, Prentice-Hall, XXXpp., 1988.
- [47] S. Wolfram, Mathematica A System for Doing Mathematics by Computer. 2nd Edition, Addison-Wesley, 961pp., 1991.
- [48] National Instruments, LabVIEW 2, User Manual, 1992.
- [49] J, Aspell et al., "Accurate noise figure measurements of erbium-doped fiber amplifiers in saturation conditions.", *OFC'92*, ThA4, 1992.
- [50] H. Kressel, Semiconductor Devices for Optical Communications., Springer-Verlag. 1983.
- [51] G. K Chang et al., "Novel High-Speed LED Transmitter for Single-Mode Fibre and Wideband Loop Transmission System.", *Electronics Letters*, Vol. 23, p.1338-1340, 1987.
- [52] L. A. Johnson, "Controlling Temperature Of Diode Lasers And Detectors Thermoelectrically.", [Unknown], TR Labs Technical Notes.

Appendix 2A: Bandwidth Definitions

Optical Spectrum Shape $S(\nu)$	τ_c	$\Delta\nu_{FWHM}$	$\Delta\nu_{ER}$	$\Delta\nu_c$
Rectangular: $\begin{cases} \frac{N_o}{B}, & \nu < B/2 \\ 0, & \text{otherwise} \end{cases}$	$1/B$	B	B	B
Lorentzian: $\left(\frac{A_o}{\gamma^2 + \nu^2} \right)$	$1/(2\pi\gamma)$	2γ	$\pi\gamma$	$2\pi\gamma$
Gaussian: $S_o \exp\left(-\frac{\nu^2}{2\sigma^2}\right)$	$1/(2\pi\sigma)$	$2\sqrt{2 \ln 2}\sigma$	$\sqrt{2\pi}\sigma$	$2\pi\sigma$

Table 2A.1: Bandwidth definitions

Appendix 2B: Expressions for the Number of Modes

Optical Spectrum Shapes $S(\nu)$	Autocorrelation Function $ g(\tau) $	Number of Modes N
Rectangular: $\begin{cases} \frac{N_o}{B}, & \nu < B/2 \\ 0, & \text{otherwise} \end{cases}$	$\frac{\sin(2\pi B\tau)}{(2\pi B\tau)}$	$\frac{(2\pi B T)^2}{[-1 + \cos(4\pi B T) + (4\pi B T) \int_0^{4\pi B T} \left(\frac{\sin u}{u}\right) du + \int_0^{4\pi B T} \left(\frac{\cos u - 1}{u}\right) du]}$
Lorentzian: $\left(\frac{A_o}{\gamma^2 + \nu^2}\right)$	$\exp(-2\pi\gamma\tau)$	$\frac{2(2\pi\gamma T)^2}{[4\pi\gamma T + \exp(-4\pi\gamma T) - 1]}$
Gaussian: $S_o \exp\left(-\frac{\nu^2}{2\sigma^2}\right)$	$S_o \exp(-2\pi^2\sigma^2\tau^2)$	$\frac{(2\pi\sigma T)^2}{[\sqrt{\pi}(2\pi\sigma T) \operatorname{erf}(2\pi\sigma T) + \exp(-(2\pi\sigma T)^2) - 1]}$

Table 2B.1: Expressions for the number of modes

Appendix 4A: Decision Threshold Derivation for the Negative Binomial PDF

According to the maximum likelihood criterion, the receiver decision rule is based on the a posteriori probabilities $P(s|z)$ as follows:

$$P(s_o|z) \underset{H_1}{\overset{H_o}{\geq}} P(s_1|z). \quad (4A1)$$

This means that hypothesis H_o will be chosen if $P(s_o|z)$ is greater than $P(s_1|z)$ and H_1 if the contrary happens. We can express the a posteriori probability in term of the conditional probability distribution of z , $p(z|s_i)$, using the Baye's theorem:

$$P(s_i|z) = \frac{p(z|s_i)P(s_i)}{p(z)}. \quad (4A2)$$

Substituting (A2) in (A1), we obtain:

$$\frac{p(z|s_1)}{p(z|s_o)} \underset{H_o}{\overset{H_1}{\geq}} \frac{P(s_o)}{P(s_1)}. \quad (4A3)$$

In the case of equally likely symbols s_i , which is the usual case, equation (A3) becomes:

$$\frac{p(z|s_1)}{p(z|s_o)} \underset{H_o}{\overset{H_1}{\geq}} 1. \quad (4A4)$$

Now, assuming that the probability distribution $p(z|s_i)$ is a Negative Binomial as defined by equation (1), we have:

$$p(z|s_i) = p(n|\eta_i) = \frac{\Gamma(n+N)}{n! \Gamma(N)} \frac{1}{(1+\eta_i/N)^N} \frac{1}{(1+N/\eta_i)^n}. \quad (4A5)$$

If \bar{n}_{off} and \bar{n}_{on} represent the mean number of photons in the case of IM modulation for the off and on states, equation (A4) becomes:

$$\frac{p(n|\bar{n}_{on})}{p(n|\bar{n}_{off})} = \frac{\Gamma(n+N) \frac{1}{n! \Gamma(N)} \frac{1}{(1+\bar{n}_{on}/N)^N (1+N/\bar{n}_{on})^n}}{\Gamma(n+N) \frac{1}{n! \Gamma(N)} \frac{1}{(1+\bar{n}_{off}/N)^N (1+N/\bar{n}_{off})^n}}$$

$$\Rightarrow \frac{p(n|\bar{n}_{on})}{p(n|\bar{n}_{off})} = \left(\frac{1+(\bar{n}_{off}/N)}{1+(\bar{n}_{on}/N)} \right)^N \left(\frac{1+(N/\bar{n}_{off})}{1+(N/\bar{n}_{on})} \right)^n \stackrel{H_1}{\underset{H_0}{>}} 1. \quad (4A6)$$

Taking the logarithm on each side, we finally get the expression for the decision threshold:

$$n \stackrel{H_1}{\underset{H_0}{>}} N \frac{\ln\left(\frac{1+\bar{n}_{on}/N}{1+\bar{n}_{off}/N}\right)}{\ln\left(\frac{1+N/\bar{n}_{off}}{1+N/\bar{n}_{on}}\right)} = \gamma_o. \quad (4A7)$$

Appendix 4B: Program Listings

initmath

```
(***** Mathematica Initialization *****)
(**** Load Mathematical Packages ****)
<<Statistics`DiscreteDistributions` ;
<<Graphics`Graphics` ;
(**** Set Plots Defaults ****)
$DefaultFont={"Helvetica-Bold",14}; SetOptions[Plot, PlotRange->All, Axes->None,
Frame->True,AspectRatio->1]; SetOptions[ListPlot,PlotRange->All, Axes->None,
Frame->True, AspectRatio->1];

(***** End of Mathematica Initialization *****)
```

constants

```
(*****Constants *****)
pi=3.141592653589793238462643383279502884197169399375105820974
944592307816406286208998628034825342117068;
hp=6.626176 10^-34; (*Planck's Constant*)
v=2.99792458 10^8; (*Speed of Light*)
q=1.6021892 10^-19; (*Electron Charge*)
kB=1.380662 10^-23; (*Boltzmann Constant*)
T=298.; (*Room Temperature in Kelvin*)
(*****End of Constants*****)
```

thparam.prx

```
(*****      Input  Parameters      *****)
mt=1;                                     (*Polarization of Light at photodetector*)
Nsp=1;                                    (*Spontaneous Noise Factor*)
GdB=30;                                   (*EDFA Gain dB*)
G=10^(0.1 GdB);
lambda=1540 10^-9;                       (*Signal Wavelength*)
nu=v/lambda;
Blout=0.5 10^-9;                          (*Output Filter Equivalent rectangular BW*)
Bout=v (Blout/(lambda^2));
muin=0.8;                                 (*EDFA Input Coupling Efficiency*)
muOut=0.8;                                (*EDFA Output Coupling Efficiency*)
B=1000 10^6;                              (*Modulation Bit Rate*)
Be=0.6 B;                                 (*Electrical Bandwidth (Raised Cosine Assumed)*)
Eff=0.8;
Fn=1;
r=100; (*20 dB*)                          (*LED Extinction Ratio*)
P0dBm=-13;                                (*LED Source Power: -13 dBm=50 uW*)
P0=10^(0.1 P0dBm - 3)/N;
Bl0= 100. 10^-9;                          (*LED rectangular bandwidth*)
B0=v (Bl0/(lambda^2));
outputfilename="thber1a-13" ;             (*Output data Filename*)
(*****      End of Input Parameters      *****)
```


thbernb.prx

```
( ..... )
( * * )
(* This program has been created by Eric Cauchon (August 1993) * )
( * * )
(* This program gives the BER versus power at received of a spectral slicing system * )
(*composed of an LED that is DIRECTLY modulated, an EDFA, an optical filter and an * )
(*optical receiver. * )
(* The LED photon distribution is modeled by a Negative BOomial distribution and * )
(*the EDFA amplification is modeled by a BDI (birth-death-immigration) model * )
(*Introduced by Shimoda et al.(1980) and extended by Teich et al.(1989-1992) * )
( * * )
( ..... )
(*<<initmath;*) (*Read initialization file for Mathematica*)
<<constants; (*Read program constant file*)
<<thparam.prx; (*Read parameter file for Ber calculations*)
    (..... Input Distribution Parameters (LED) .....*)
    PO= PO (mt/2);
    n0ON=(PO 2 r)/((r+1) hp nu 2 Be); (*Average Input # of Photons for ON*)
    n0OFF=(PO 2)/((r+1) hp nu 2 Be); (*Average Input # of Photons for OFF*)
    NM= mt (Bout)/(2 Be); (*Number of Modes of the Source*)
    (** Built-in Negative BOomial pdf **)
    NBDist[alpha_,N_]=NegativeBOomialDistribution[alpha,alpha/(N+alpha)];
    varNBD[x_]=(muin muOut L x)+((muin muOut L x)^2)/NM; (*Negative BOomial
    variance*)
    nav[OFF_,ON_]=(OFF+ON)/2;
    (..... BDI Parameters (EDFA) .....*)
    M=mt (Bout)/(2 Be); (*Number of Modes of the BDI Medium*)
    t=Log[G]/Bout; (*Time of Traversal*)
    a=(Nsp Bout); (*Birth Rate*)
    b=a-Bout; (*Death Rate*)
```

```

c=M a; (*Immigration Rate*)
h=Exp[(b-a) t];
k=(a/(b-a)) (h-1);
(****Variance of BDI Medium ****)
outvar[x_,L_]=(((muin muOut L x)+ muOut L (c/a) k)/h+(((muin muOut L x)+
muOut L (c/a) k)/h)^2)/NM) ((2 Eff q Be)^2);
(***** Display Parameters *****)
Print["-----
-----"];
Print["INPUT DISTRIBUTION: Negative BOomial"];
Print["Number of Modes=",NM];
Print["Average LED Power= ",PO," = ",POdBm];
Print["Extinction Ratio=",r];
Print["-----
-----"];
Print["BDI MEDIUM:"];
Print["Birth Rate a=",ScientificForm[a,6]];
Print["Death Rate b=",ScientificForm[b,6]];
Print["Immigration Rate c=",ScientificForm[c,6]];
Print["Time of Traversal t=",t];
Print["Spont. Emission Factor Nsp=(a/(a-b))=",ScientificForm[Nsp,6]];
Print["Number of Modes (c/a)=",ScientificForm[M,6]];
Print["h=",ScientificForm[h,6]," k=",ScientificForm[k,6]];
Print["Gain (1/h)=",ScientificForm[1/h,6]];
Print["BDI Transfer function (c/a)k/h=",ScientificForm[(c/a)k/h,6]];
Print["-----
-----"];
(***** OISSON'S Noise Terms *****)
(**** Spontaneous emission ****)
Psp=(c/a) (k/h) hp nu (2 Be); (*=mt (k/h) hp nu Bout*)
Isp=Psp (Eff q)/(hp nu);
(**** Signal ****)

```

```

Is[x_]=x (2 q Eff Be) ( Bout/BO);
S[x_,L_]=(muin muOut L (Is[x]/h))^2;
Nperbit[x_,L_]=(Eff muOut L (muin (((Is[x]/(2 q Eff Be))/h)+(c/a)(k/h))));
(***** Excess noise term introduced by the LED source *****)
Nex[x_,L_]=(((muin muOut L (Is[x]/h))^2)/NM));
(***** Noise terms *****)
Nshot[x_,L_]=(2 q Be muOut L)((muin (Is[x]/h))+Isp);
Nsigsp[x_,L_]=(2 (Is[x]/h) muin (muOut^2) Isp (L^2))/NM (*(2 Be)/Bout);*
Nspsp[L_]=((muOut L Isp)^2)/NM; (*(2 Be)/Bout);*
Nth=0;
(***** Summation of the Noise components *****)
Ntot[x_,L_]=Nex[x,L]+Nshot[x,L]+Nsigsp[x,L]+Nspsp[L];
(***** Received optical power in Watt and dBm *****)
Prx[L_]=((nav[Is[n0ON],Is[n0OFF]]/h ((hp nu)/(Eff q)) muin + Psp) muOut L);
PrxdBm[L_]=10 Log[10,1000 Prx[L]]//N;
(***** BER Calculations *****)
BERNB={}; (*Initialization of vector containing PrxdBm and BER*)
L=.; (*Initialization of the attenuation variable*)
jinc=2;
(***** BER Calculation Loop *****)
For[j=0,j<61,j=j+jinc,
Print["-----
-----"];
Print["BER CALCULATIONS"];
LdB=ILC-60+j; (*Attenuation calculation in dB*)
L=10^(0.1 LdB)//N;
(***** Attenuation and Power Display *****)
Print["LdB=",LdB," L=",L];
Print["PrxdBm=",PrxdBm[L]]//N;
(***** Noise Term Display *****)
Print["-----"];
Print["NOISE COMPONENTS"];

```

```

Print["ASE Power Psp=",Psp "=",10 Log[10,1000 Psp]//N];
Print["*****Olsson-BDI Model*****"];
Print[" ON OFF"];
Print["-----"];
Print["S= ",S[n0ON,L]//N," ",S[n0OFF,L]//N];
Print["Nex= ",Nex[n0ON,L]//N," ",Nex[n0OFF,L]//N];
Print["Nshot= ",Nshot[n0ON,L]//N," ",Nshot[n0OFF,L]//N];
Print["Nsigsp=",Nsigsp[n0ON,L]//N," ",Nsigsp[n0OFF,L]//N];
Print["Nspssp= ",Nspssp[L]//N];
Print["Nth= ",Nth//N];
Print["Ntot= ",Ntot[n0ON,L]//N," ",Ntot[n0OFF,L]//N];
Print["outvar=",outvar[(n0ON ( Bout/BO)),L]//N," ",outvar[(n0OFF (
Bout/BO)),L]//N];
(*****Negative BOomial BER Calculations *****)
NM=Round[NM];
DTNB=Round[If[Nperbit[n0OFF,L]>0,NM
Log[(1+Nperbit[n0ON,L]/NM)/(1+Nperbit[n0OFF,L]/NM)]/Log[(1+NM/Nperbit[n0
OFF,L]/(1+NM/Nperbit[n0ON,L])),0]]//N; Print["DTNB=",DTNB];
BERnbbdi=.;
BERnbbdi=SetPrecision[0.5 ((1-
CDF[NBDist[NM,Round[Nperbit[n0OFF,L]],DTNB])+CDF[NBDist[NM,Round[Nperbit[n
0ON,L]],DTNB]),30]//N;
(***** Negative BOomial BER Display
*****)
Print["-----"];
Print["BERnbbdi=",ScientificForm[BERnbbdi,6]];
(** Creation of BER vector **)
BERNB=Append[BERNB,{PrxdBm[L],BERnbbdi}];
L=.;
];
PO=.;
(***** BER Curve Plotting *****)

```

```

Print["Plotting..."];
bernb=LogListPlot[BERNB,PlotJoined->True,FrameLabel->{"Received Optical Power
(dBm)","BER","Negative BOomial Approx., POdBm=ToString[POdBm],""}];
(***** Writing Data to a File *****)
(**The format used is space seperated numbers**)
stmp=OpenWrite[outputfilename, FormatType->OutputForm];
Print["Writing data into ", outputfilename," ..."];
WriteString[stmp,"PO=",ToString[POdBm]," dBm\n"];
WriteString[stmp,"PrxdBm ", " ", "BER\n"];
For[{{j=1,jj<Round[(61/jinc)+1],jj++},
      Write[stmp, BERNB[{{j}}][[1]], " ", FortranForm[BERNB[{{j}}][[2]] ]];
];
Close[stmp];
(***** End of Program *****)

```

thbergg.prx

```
( ***** )
( * * )
(* This program has been created by Eric Cauchon (August 1993) * )
( * * )
(* This program gives the BER versus power at received of a spectral slicing system * )
(*composed of an LED that is DIRECTLY modulated, an EDFA, an optical filter and an * )
(*optical receiver. * )
(* The LED photon distribution is modeled by a gaussian distribution with a mean and * )
(*variance of a negative BOomial passed through and the a BDI model introduced by * )
(*Shimoda et al.(1980) and extended by Teich et al.(1989-1992) * )
( * * )
( ***** )
(*<<initmath;*) (*Read initialization file for Mathematica*)
<<constants; (*Read program constant file*)
<<thparam.prx; (*Read parameter file for Ber calculations*)
    (*****Input Distribution Parameters (LED) *****)
PO= PO (mt/2);
n0ON=(PO 2 r)/((r+1) hp nu 2 Be); (*Average Input # of Photons for ON*)
n0OFF=(PO 2)/((r+1) hp nu 2 Be); (*Average Input # of Photons for OFF*)
    NM=mt (Bout)/(2 Be); (*Number of Modes of the Source*)
(*** Built-in Negative BOomial pdf ***)
NBDist[alpha_,N_]=NegativeBOomialDistribution[alpha,alpha/(N+alpha)];
varNBD[x_]=(muin muOut L x)+((muin muOut L x)^2)/NM; (*Negative BOomial
variance*)
nav[OFF_,ON_]=(OFF+ON)/2;
    (***** BDI Parameters (EDFA) *****)
M=mt (Bout)/(2 Be); (*Number of Modes of the BDI Medium*)
t=Log[G]/Bout; (*Time of Traversal*)
a=(Nsp Bout); (*Birth Rate*)
b=a-Bout; (*Death Rate*)
```

```

c=M a;                                     (*Immigration Rate*)
h=Exp[(b-a) t];
k=(a/(b-a)) (h-1);
(***** Variance of BDI Medium *****)
outvar[x_,L_]=(((muin muOut L x)+ muOut L (c/a) k)/h+(((muin muOut L x)+
muOut L (c/a) k)/h)^2)/NM) ((2 Eff q Be)^2);
(***** Display Parameters *****)
Print["-----
-----"];
Print["INPUT DISTRIBUTION: Negative BOomial"];
Print["Number of Modes=",NM];
Print["Average LED power= ",PO," = ",POdBm];
Print["Extinction Ratio=",r];
Print["-----
-----"];
Print["BDI MEDIUM:"];
Print["Birth Rate a=",ScientificForm[a,6]];
Print["Death Rate b=",ScientificForm[b,6]];
Print["Immigration Rate c=",ScientificForm[c,6]];
Print["Time of Traversal t=",t];
Print["Spont. Emission Factor Nsp=(a/(a-b))=",ScientificForm[Nsp,6]];
Print["Number of Modes (c/a)=",ScientificForm[M,6]];
Print["h=",ScientificForm[h,6]," k=",ScientificForm[k,6]];
Print["Gain (1/h)=",ScientificForm[1/h,6]];
Print["BDI Transfer function (c/a)k/h=",ScientificForm[(c/a)k/h,6]];
Print["-----
-----"];
(***** OISSON'S Noise Terms *****)
(***** Spontaneous emission *****)
Psp=(c/a) (k/h) hp nu (2 Be); (*=mt (k/h) hp nu Bout*)
Isp=Psp (Eff q)/(hp nu);
(***** Signal *****)

```

```

Is[x_]=x (2 q Eff Be) ( Bout/BO);
S[x_,L_]=(muin muOut L (Is[x]/h))^2;
Nperbit[x_,L_]=(Eff muOut L (muin (((Is[x])/(2 q Eff Be))/h)+(c/a)(k/h)));
(***** Excess noise term introduced by the LED source *****)
Nex[x_,L_]=(((muin muOut L (Is[x]/h))^2)/NM);
(***** Noise terms *****)
Nshot[x_,L_]=(2 q Be muOut L)((muin (Is[x]/h))+Isp);
Nsigsp[x_,L_]=(2 (Is[x]/h) muin (muOut^2) Isp (L^2))/NM; (*(2 Be)/Bout);*)
Nspsp[L_]=((muOut L Isp)^2)/NM; (*(2 Be)/Bout);*)
Nth=0;
(***** Summation of the Noise components *****)
Ntot[x_,L_]=Nex[x,L]+Nshot[x,L]+Nsigsp[x,L]+Nspsp[L];
(***** Gaussian BER Formulas *****)
Q[x0_,x1_,L_]=(Sqrt[S[x1,L]]-
Sqrt[S[x0,L]])/(Sqrt[Ntot[x1,L]]+Sqrt[Ntot[x0,L]]); BER[x0_,x1_,L_]=0.5
Erfc[Q[x0,x1,L]/Sqrt[2]];
(***** Received optical power in Watt and dBm *****)
Prx[L_]=((nav[Is[n0ON],Is[n0OFF]]/h ((hp nu)/(Eff q)) muin + Psp) muOut L);
PrxdBm[L_]=10 Log[10,1000 Prx[L]]/N;
(***** BER Calculations *****)
BERG={}; (*Initialization of vector containing PrxdBm and BER*)
L=.; (*Initialization of the attenuation variable*)
jinc=2;
(***** BER Calculation Loop *****)
For[j=0,j<61,j=j+jinc,
Print["-----
-----"];
Print["BER CALCULATIONS"];
LdB=ILC-60+j; (*Attenuation calculation in dB*)
L=10^(0.1 LdB)/N;
*****Attenuation and Power Display *****)
Print["LdB=",LdB," L=",L];

```



```

Print["PrxdBm=",PrxdBm[L]/N];
(***** Noise Term Display *****)
Print["-----"];
Print["NOISE COMPONENTS"];
Print["ASE Power Psp=",Psp*1000 Log[10,1000 Psp]/N];
Print["*****Olsson-BDI Margin*****"];
Print[" ON OFF"];
Print["-----"];
Print["S= ",S[n0ON,L]/N," ",S[n0OFF,L]/N];
Print["Nex= ",Nex[n0ON,L]/N," ",Nex[n0OFF,L]/N];
Print["Nshot= ",Nshot[n0ON,L]/N," ",Nshot[n0OFF,L]/N];
Print["Nsigsp=",Nsigsp[n0ON,L]/N," ",Nsigsp[n0OFF,L]/N];
Print["Nspsp= ",Nspsp[L]/N];
Print["Nth= ",Nth/N];
Print["Ntot= ",Ntot[n0ON,L]/N," ",Ntot[n0OFF,L]/N];
Print["outvar=",outvar[(n0ON ( Bou/BO)),L]/N," ",outvar[(n0OFF (
Bout/BO)),L]/N];
(***** Gaussian BER Display *****)
Print["-----"];
Print["BER=",ScientificForm[BER[n0OFF,n0ON,L],6]];
(** Creation of BER vector **)
BERG=Append[BERG,{PrxdBm[L],BER[n0OFF,n0ON,L]};
L=.;
];
PO=.;
(***** BER Curve Plotting *****)
Print["Plotting..."];
bergg=LogListPlot[BERG,PlotJoined->True,FrameLabel->{"Received Optical Power
(dBm)","BER","Gaussian Approx., POdBm="ToString[POdBm],""}];
(*****Writing Data to a File *****)
(**The format used is space seperated numbers**)
stmp=OpenWrite[outputfilename, FormatType->OutputForm];

```

```

Print["Writing data into ", outputfilename, "..."];
WriteString[stmp,"PO=",ToString[POdBm], " dBm\n"];
WriteString[stmp,"PrxdBm ", " ", "BER\n"];
For[jj=1, jj<Round[(61/jinc)+1], jj++,
    Write[stmp, BERG[[j]][[1]], " ", FortranForm[BERG[[j]][[2]]] ];
];
Close[stmp];

(*****End of Program *****)

```

Appendix 5A: Veritech Amplifier Information

Model: VMA3k10C-232

Bandwidth: 3 kHz to 10 GHz

Small Signal Gain: 32 dB (typ.)

Power Output: +17 dBm (min.)

Gain Ripple: ± 1 dB (max.)

Group Delay: 1400 ps (typ.)

Rise Time: 55 ps (typ.)

Noise Figure: 8 dB

DC Current at +15 V: 600 mA (max)

DC Current at -15 V: 50 mA (max)

Frequency Response:

(as measured by us)

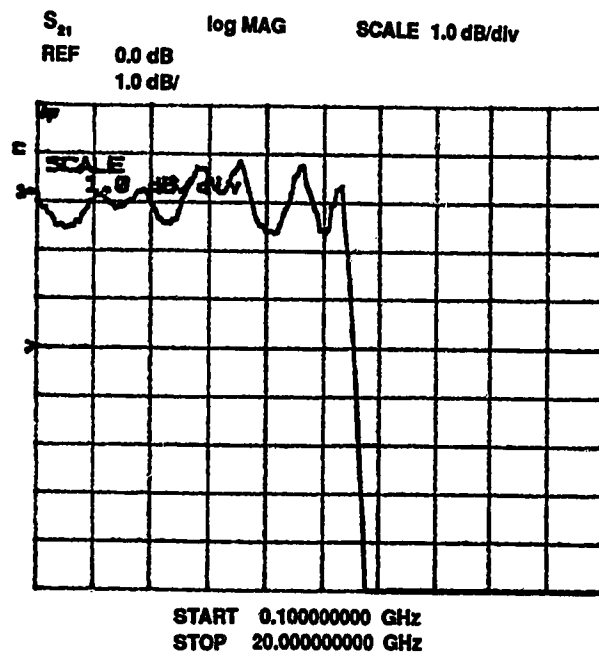


Figure 5A.1: Veritech VMA3k10C-232 amplifier frequency response

Appendix 5B: Mas-Tech LED Information

LED Specifications:

Model: E15D1-002 (Edge-Emitting)

Absolute Ratings:

Forward Bias Current: 150 mA

Reverse Voltage: 1V

Cooler Current: 1.2 A

Operating Temperature: -20 to +65 °C

Optical and Electrical Characteristics:

(Bias Current: 100mA, Temperature: 25°C)

Output Optical Power: 24 uW

Forward Voltage: 1.45 V

Centerwavelength: 1531 nm

Optical Bandwidth (FWHM): 108 nm

Rise and Fall Times: 2 and 3 ns, respectively (typ.)

Cooler Capacity: 40°C (min.)

Thermistor Resistance: 10 kΩ (typ.)

Figure 5B.1 shows the optical spectrum of the Mas-Tech LED as provided by the manufacturer.

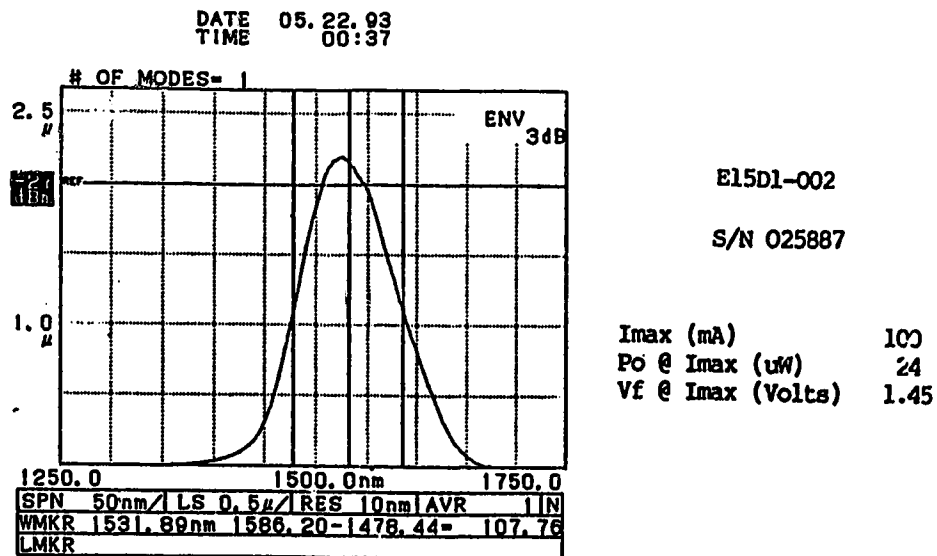


Figure 5B.1: Mas-Tech LED E15D1-002 power spectrum

LED Hardware

A number of electronic circuits were required to ensure that the LED be properly and safely operated. All these circuits were designed by TRILabs Laboratory Manager, Mr. Dave Clegg, with the exception of one which was designed by a former master's student at TRILabs, Ken Benterud. In addition, the LED and its circuitry were put in a aluminum box to protect them from the external environment. The design, the building and the packaging were done at TRILabs. Here is the list of the LED circuits:

1. Laser Bias Insertion Unit-02
2. Thermoelectric Cooler-02 (K Benterud, modified version)
3. Pump Laser Drive Unit-01 (modified version)
4. Positive and Negative Regulator-02
5. Digital Voltmeter and LED Display-02

Drive Circuit

The simplified version of the Mas-Tech LED drive circuit is shown in figure 5B.1. It is essentially a variable current source which provides the DC bias on the LED plus an AC modulation input branch. A ferrite bead and an inductor $L=100$ nH in the vertical branch provide AC isolation and a capacitor $C=100$ nF in the modulation branch provides DC isolation. Since the LED dynamic resistance is around 4 ohms a resistor R of 47 ohms (47 is the closest nominal value to 46 ohms) has been added to the modulation branch to match the 50 ohms coaxial transmission line that carries the modulation to the LED. The DC bias current can be adjusted by a knob on the LED box front panel. The actual LED drive circuit is a lot more complicated than the one presented here because it contains a series of safety features and additional circuitry to insure stable operation. More complex LED drivers optimized for digital modulation [50, 51] could have been used but this one was chosen for simplicity.

TEC Control

The Mas-Tech LED package comes with a TEC system and a thermistor. The TEC is based on Peltier effect [52] which states that by passing an electric current through a junction of different metals, heat can be created or absorbed at the junction. This device is used to cool the LED down to increase its output power. The thermistor is a device that has an electrical resistance that varies generally non linearly with temperature. The LED thermistor has a negative temperature coefficient, that is its resistance drops with increasing temperature. The TEC control circuit consists essentially in a feedback loop in which the TEC is driven by an unbalance signal coming from a resistor bridge containing the thermistor and a variable resistor. The desired temperature can be set by a knob on the

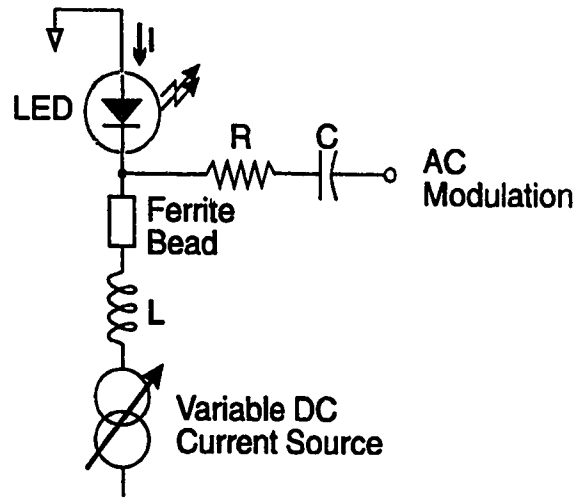


Figure 5B.1: Simplified version of the Mas-Tech LED driver

LED box front panel which controls the bridge variable resistor. The resistor bridge circuit is shown in figure 5B.2 (a).

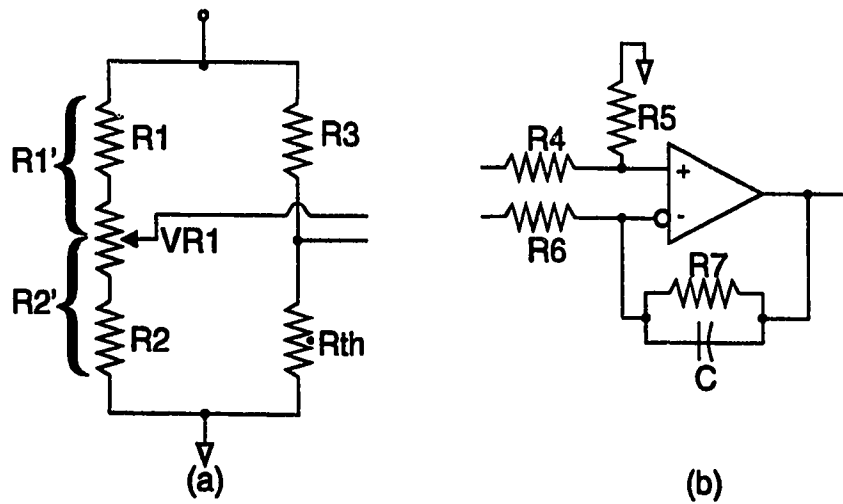


Figure 5B.2(a): Thermistor bridge . **(b)** TEC comparator

From the circuit, R_{th} is easily determined by the simple equation:

$$R_{th} = \frac{R2' R3}{R1'} \tag{5.1}$$

With $R1=5k$, $R2=R3=10k$ and $VR1=0-10k\Omega$, the range values for R_{th} goes from $6.67k$ to $40k\Omega$ which corresponds to a temperature range going from 35 to $-5^\circ C$.

The unbalance signal is sent to a comparator shown in figure 5B.2 (b). This is basically an integrator that drives the TEC according to the unbalance signal from the bridge. The component values are: $R_4=R_6=3\text{k}\Omega$, $R_5=R_7=100\text{k}\Omega$ and $C=15\text{nF}$. This gives a loop gain of 33.3 with a RC time constant of 15 ms.

Appendix 5C: BT&D, SHF and Mini-Circuit Filter Information

BT&D Photodetector

Model: PDC4310

Absolute Ratings:

Reverse Voltage: 10 V (max.)

Forward Current: 500 μ A (max.)

Forward Voltage: 0.5 V (max)

Operating Temperature: 5 to 50 $^{\circ}$ C

Optical and Electrical Characteristics:

(Temperature: 25 $^{\circ}$ C and Reverse Bias: 5 V)

Responsivity at 1550 nm: 0.75 (typ.)

Return Loss: 30 dB (typ.)

3 dB Bandwidth: 25 GHz (typ.)

Flatness: \pm 1.5 dB (typ.)

Loss in Responsivity at 1 GHz: 1 dB (typ.)

Chip Capacitance: 0.12 pF (typ.)

Dark Current: <1 nA (typ.)

Electrical Frequency Response:

(as measured by us)

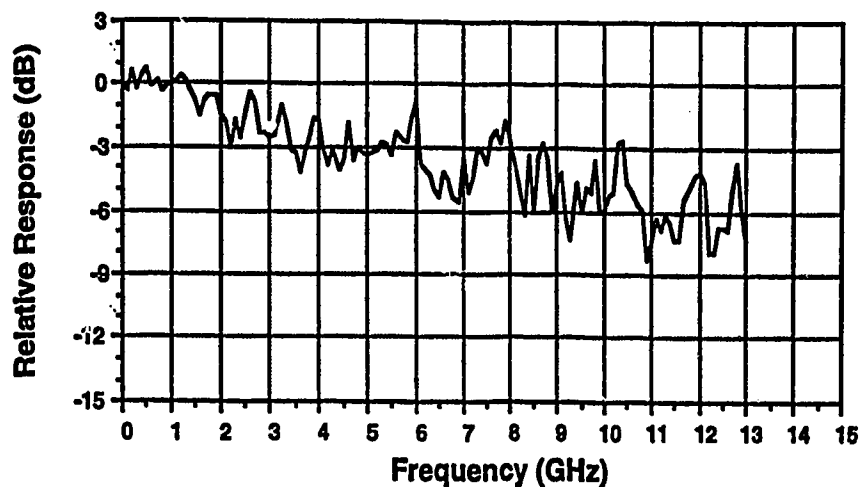


Figure 5C.1: BT&D photodetector electrical frequency response

SHF Amplifier

Model: 90 P

Bandwidth: 10 kHz to 15 GHz

Small Signal Gain: 23 \pm 1 dB

Gain Ripple: \pm 1.5 dB

Output Power at 1 dB Compression: +10 dBm

Maximum Input: 0 dBm (630 mVpp)

Rise Time: <30 ps

Overshoot: <8 %

Noise Figure: 7 dB (typ.)

Voltage Supply: +12 V, 110 mA

Frequency Response:

(as measured by us)

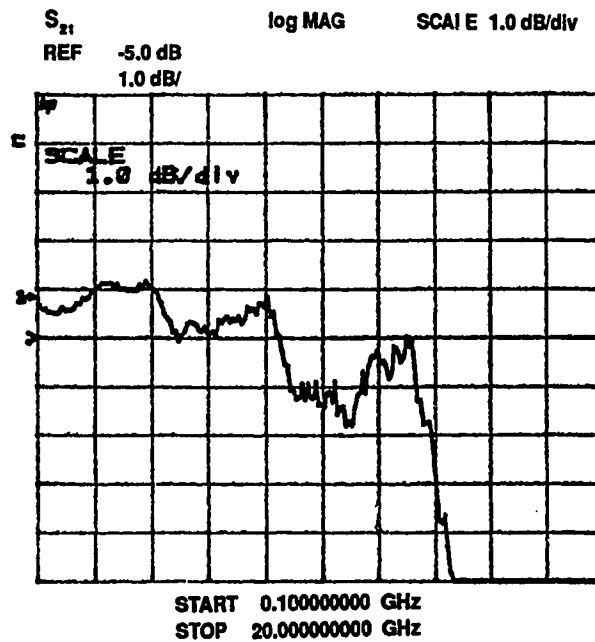


Figure 5C.2: SHF 90 P amplifier frequency response

Mini-Circuit Filter

Model: SLP-850

Passband (Loss<1 dB): DC to 780 MHz (min.)

3 dB Bandwidth: 850 MHz (nom.)

Frequency Response:

(as measured by us)

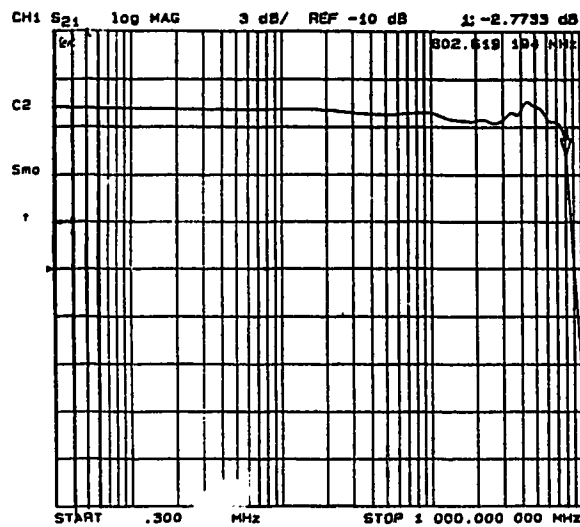


Figure 5C.3: Mini-Circuit SLP-850 filter frequency response

Appendix 5D: Characteristics of Attenuators

Two attenuators are used in the optical link. The first one is to reduce the input power to the EDFA and the second is to reduce the power hitting the photodetector. The attenuation is provided by an attenuating medium of variable thickness that is carefully moved in and out of the optical path. The following describes the main characteristics of the two attenuators used in the optical link.

JDS Fitel VA4 Attenuator

The JDS Fitel VA4 is a portable variable optical attenuator calibrated at 1300 and 1500 nm to provide continuous variable attenuation up to 40 dB with an accuracy of ± 0.5 dB. At 1500 nm, it has an IL of 2.5 dB and it can handle power level as high as 200 mW. It also has -35 dB backreflection.

JDS Optics 7000 Attenuator

The JDS Optics 7000 is a programmable and GPIB controllable variable optical attenuator that provides continuously variable attenuation up to a total light block (∞ attenuation) with 0.1 dB increments. It is calibrated at 0.83, 1.3 and 1.55 μm . It can handle a maximum power of 200 mW and has an insertion loss of about 3.3 dB at 1550 nm. Its backreflection is -50 dB.

Appendix 5E: TR Labs EDFAs Information

The two TR Labs EDFA packages are essentially identical. They consist of a Lasertron pump laser with its driver, two WDMs and a length of erbium doped fiber (EDF). A WDM (wavelength division multiplexor) is basically a frequency sensitive coupler. One WDM is used to combine the 980 nm pump with the 1550 nm signal to be sent through the length of EDF. A second WDM is used after the EDF to separate the pump from the useful signal. The schematic is shown in figure 5E.1.

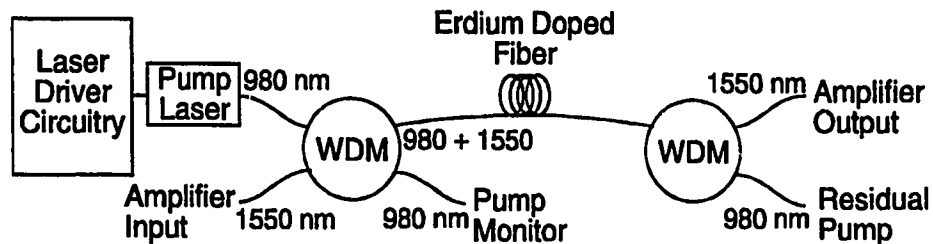


Figure 5E.1: Schematic of TR Labs EDFA packages.

Components:

Pump: Lasertron QLM9S450001

Output Power: 50 mW (typ.)

Input WDM: Gould

Erbium doped fiber: National Optics Institute #4

Output WDM: SIFAM

Appendix 5F: BNR OC12 Receiver Information

The schematic of the BNR OC12 receiver is shown in figure 5F.1.

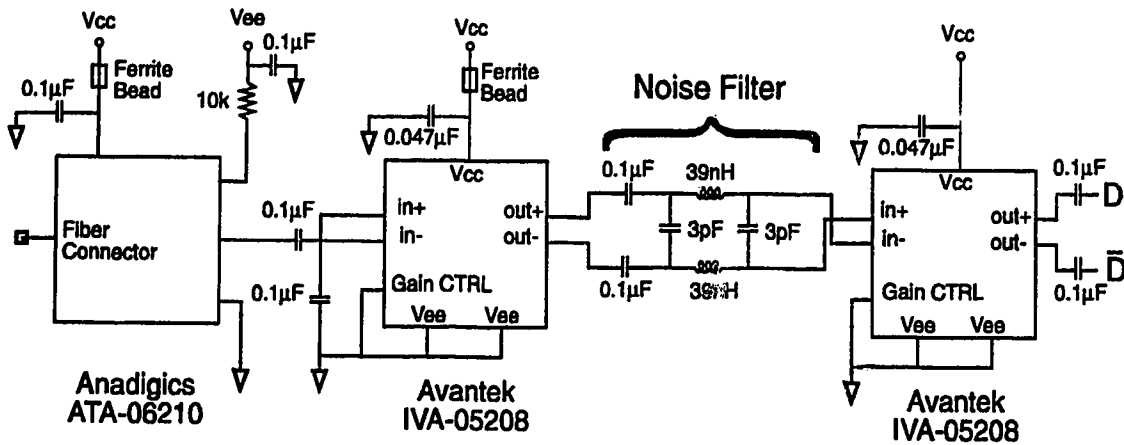


Figure 5F.1: Schematic of the BNR OC12 receiver.

Anadigics AGC Transimpedance Amplifier:

(typical values at 25°C)

DC Characteristics:

- Responsivity: 0.7 A/W
- Transresistance: 10 k Ω
- Input Impedance: 280 Ω
- Input FET Leakage Current: 50 nA
- Supply Current: 35 mA, 5V

AC Characteristics:

- Transresistance: 4 k Ω
- Input Capacitance: 0.4 pF
- 3 dB bandwidth: 450 MHz
- Input Noise Spectral Density: 3.75 pA/ $\sqrt{\text{Hz}}$
- Input Current Noise: 54 nA rms
- Optical Overload: -3 dBm
- Optical Sensitivity: -33 dBm

AGC Time Constant: 10 ms

Avantek Amplifiers:

(typical values at 25°C)

Power Gain: 30 dB

Gain Flatness: ± 0.8 dB

3 dB bandwidth: 1.8 GHz

Gain Control Range: 30 dB

Noise Figure: 9 dB

Output at 1 dB Compression: -3 dBm

Group Delay: 400 ps

Supply Current: 35 mA, 5 V.

Frequency Response:

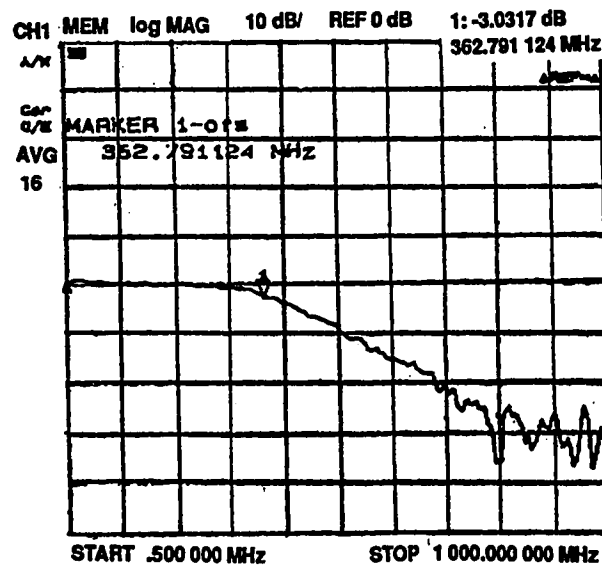


Figure 5F.2: BNR OC12 receiver frequency response. (Bruce Beggs, BNR Ottawa)

Appendix 6A: Program Listings

berparameters2a

```
(*****      Input  Parameters      *****)
ml=2;                                     (*Polarization of Light at photodetector*)
Nsp=2.8;                                  (*EDFA #R0303 @ 160 mA pump Spontaneous Noise Factor*)
GdB=33;                                   (*EDFA #R0303 Gain @ 160 mA pump in dB*)
G=10^(0.1 GdB);
lambda=1537 10^-9;                        (*Signal Wavelength*)
nu=v/lambda;
Blin=5.2 10^-9;                            (*Input Filter JDS TB1570 Equivalent Noise BW*)
Bin=v (Blin/(lambda^2));
Blout=1.94 10^-9;                          (*Output Filter JDS TB1500B Equivalent Noise BW*)
Bout=v (Blout/(lambda^2));
DFfactor=0.85;                             (*Correction introduced because of Filter Cascade*)
muin=0.8;                                  (*EDFA Input Coupling Efficiency*)
muOut=0.8;                                 (*EDFA Output Coupling Efficiency*)
B=622 10^6;                                (*Modulation Bit Rate*)
Be=373 10^6;                               (*OC12 Receiver Electrical Bandwidth *)
Eff=0.57;                                  (*OC12 Receiver Quantum Efficiency*)
Rl=580;                                    (*OC12 FE Receiver Noise Resistor (Sensitivity=-30 dBm)*)
Fn=1;                                      (*OC12 Receiver Noise Figure*)
r=15; (*12 dB*)                            (*LED Extinction Ratio*)
PindBm=-38;                                (*Input Signal Power to EDFA*)
Pin=10^(0.1 PindBm - 3)//N;
outputfilename="ber2a38" ;                 (*Output data Filename*)
(*****End of Input Parameters *****)
```


exbern.b.prx

```
( ..... )
( * * )
(* This program has been created by Eric Cauchon (August 1993) *)
(* Modified version of the program thbern.b.prx *)
( * * )
(* This program gives the BER versus power at received of a spectral slicing system *)
(* composed of an LED that is DIRECTLY modulated, an EDFA, an optical filter and an *)
(* optical receiver. *)
(* The LED photon distribution is modeled by a Negative Binomial distribution and *)
(* the EDFA amplification is modeled by a BDI (birth-death-immigration) model *)
(* introduced by Shimoda et al.(1980) and extended by Teich et al.(1989-1992) *)
( * * )
( ..... )
(*<<initmath;*) (*Read initialization file for Mathematica*)
<<constants; (*Read program constant file*)
<<berparameters2a; (*Read parameter file for Ber calculations*)
(***** Input Distribution Parameters (LED) *****)
Pin= Pin (mt/2);
n0ON=(Pin 2 r)/((r+1) hp nu 2 Be); (*Average Input # of Photons for ON*)
n0OFF=(Pin 2)/((r+1) hp nu 2 Be); (*Average Input # of Photons for OFF*)
NM=DFactor mt (Bout)/(2 Be); (*Number of Modes of the Source*)
(*** Built-in Negative Binomial pdf ***)
NBDist[alpha_,N_]=NegativeBinomialDistribution[alpha,alpha/(N+alpha)];
varNBD[x_]=(muin muOut L x)+((muin muOut L x)^2)/NM; (*Negative Binomial
variance*)
nav[OFF_,ON_]=(OFF+ON)/2;
(***** BDI Parameters (EDFA) *****)
M=mt (Bout)/(2 Be); (*Number of Modes of the BDI Medium*)
t=Log[G]/Bout; (*Time of Traversal*)
a=(Nsp Bout); (*Birth Rate*)
```

```

b=a-Bout;                                     (*Death Rate*)
c=M a;                                         (*Immigration Rate*)
h=Exp[(b-a) t];
k=(a/(b-a)) (h-1);
(***** Variance of BDI Medium *****)
outvar[x_,L]=(((muin muOut L x)+ muOut L (c/a) k)/h+(((muin muOut L x)+
muOut L (c/a) k)/h)^2)/NM ((2 Eff q Be)^2);
(***** Display Parameters *****)
Print["-----
-----"];
Print["INPUT DISTRIBUTION: Negative Binomial"];
Print["Number of Modes=",NM];
Print["Average Input Power= ",Pin," = ",PindBm];
Print["Extinction Ratio=",r];
Print["-----
-----"];
Print["BDI MEDIUM:"];
Print["Birth Rate a=",ScientificForm[a,6]];
Print["Death Rate b=",ScientificForm[b,6]];
Print["Immigration Rate c=",ScientificForm[c,6]];
Print["Time of Traversal t=",t];
Print["Spont. Emission Factor Nsp=(a/(a-b))=",ScientificForm[Nsp,6]];
Print["Number of Modes (c/a)=",ScientificForm[M,6]];
Print["h=",ScientificForm[h,6]," k=",ScientificForm[k,6]];
Print["Gain (1/h)=",ScientificForm[1/h,6]];
Print["BDI Transfer function (c/a)k/h=",ScientificForm[(c/a)k/h,6]];
Print["-----
-----"];
(*****OISSON'S Noise Terms *****)
(***** Spontaneous emission *****)
Psp=(c/a) (k/h) hp nu (2 Be); (*=mt (k/h) hp nu Bout*)
Isp=Psp (Eff q)/(hp nu);

```

```

(**** Signal ****)
Is[x,L]=(2 q Eff Be) (DFfactor Bout/Bin);
S[x,L]=muin muOut L (Is[x]/h)^2;
Nperbit[x,L]=(Eff muOut L (muin (((Is[x]/(2 q Eff Be))/h)+(c/a)(k/h)))));
(**** Access noise term introduced by the LED source ****)
Nex[x,L]=(((muin muOut L (Is[x]/h))^2)/NM));
(**** Noise terms ****)
Nshot[x,L]=(2 q Be muOut L)((muin (Is[x]/h))+Isp);
Nsigsp[x,L]=(2 (Is[x]/h) muin (muOut^2) Isp (L^2))/NM (*((2 Be)/Bout);*)
Nspsp[L]=((muOut L Isp)^2)/NM; (*((2 Be)/Bout);*)
Nth=((4 kB T) Fn Be)/RI;
(**** Summation of the Noise components ****)
Ntot[x,L]=Nex[x,L]+Nshot[x,L]+Nsigsp[x,L]+Nspsp[L];
(**** Received optical power in Watt and dBm ****)
Prx[L]=((nav[Is[n0ON],Is[n0OFF]]/h ((hp nu)/(Eff q)) muin + Psp) muOut L);
Prxdbm[L]=10 Log[10,1000 Prx[L]]/N;
(**** BER Calculations ****)
BER=BER; (*Initialization of vector containing Prxdbm and BER*)
L=.; (*Initialization of the attenuation variable*)
jinc=2;
(**** BER Calculation Loop ****)
For[j=0,j<61,j=j+jinc,
Print{'-----
-----'}];
Print['BER CALCULATIONS'];
LdB=LdB+2; (*Attenuation calculation in dB*)
L=10^(0.1 LdB)/N;
(**** Attenuation and Power Display ****)
Print['LdB=',LdB,' L=',L];
Print['Prxdbm=',Prxdbm[L]/N];
(**** Noise Term Display ****)
Print{'-----'}];

```

```

Print["NOISE COMPONENTS"];
Print["ASE Power Psp=",Psp=",10 Log[10,1000 Psp//N];
Print["*****Olsson-BDI Model*****"];
Print["      ON                      OFF"]; Print["-----
-----"];
Print["S=      ",S[n0ON,L]//N,"      ",S[n0OFF,L]//N];
Print["Nex=     ",Nex[n0ON,L]//N,"      ",Nex[n0OFF,L]//N];
Print["Nshot=   ",Nshot[n0ON,L]//N,"      ",Nshot[n0OFF,L]//N];
Print["Nsigsp=  ",Nsigsp[n0ON,L]//N,"      ",Nsigsp[n0OFF,L]//N];
Print["Nspssp=  ",Nspssp[L]//N];
Print["Nth=     ",Nth//N];
Print["Ntot=    ",Ntot[n0ON,L]//N,"      ",Ntot[n0OFF,L]//N];
Print["outvar=  ",outvar[(n0ON (DFfactor Bout/Bin)),L]//N,"      ",outvar[(n0OFF
(DFfactor Bout/Bin)),L]//N];
(***** Negative Binomial BER Calculations *****)
NM=Round[Nperbit[n0OFF,L]];
DTNB=Round[If[Nperbit[n0OFF,L]>0,NM
Log[(1+Nperbit[n0ON,L]/NM)/(1+Nperbit[n0OFF,L]/NM)]/Log[(1+NM/Nperbit[n0
OFF,L])/(1+NM/Nperbit[n0ON,L]),0]]//N; Print["DTNB=",DTNB];
BERnbbdi=.;
BERnbbdi=SetPrecision[0.5 ((1-
CDF[NBDist[NM,Round[Nperbit[n0OFF,L]]],DTNB])+CDF[NBDist[NM,Round[Nperbit[n
0ON,L]]],DTNB]),30]//N;
(***** Negative Binomial BER Display *****)
Print["-----"];
Print["BERnbbdi=",ScientificForm[BERnbbdi,6]];
(** Creation of BER vector **)
BERNB=Append[BERNB,{PrxdBm[L],BERnbbdi}];
L=.;
];
Pin=.;
(***** BER Curve Plotting *****)

```

```

Print["Plotting..."];
bernb=LogListPlot[BERNB,PlotJoined->True,FrameLabel->{"Received Optical Power
(dBm)","BER","Negative Binomial Approx.", PindBm="ToString[PindBm],""}];
(***** Writing Data to a File *****)
(**The format used is space seperated numbers**)
stmp=OpenWrite[outputfilename, FormatType->OutputForm];
Print["Writing data into ", outputfilename," ..."];
WriteString[stmp,"Pin=",ToString[PindBm]," dBm\n"];
WriteString[stmp,"PrxdBm ", " ", "BER\n"];
For[jj=1, jj<Round[(61/jinc)+1], jj++,
    Write[stmp, BERNB[[jj]][[1]], " ", FortranForm[BERNB[[jj]][[2]] ]];
];
Close[stmp];
(***** End of Program *****)

```

exbergg.prx

```
( ***** )
( * * )
(* This program has been created by Eric Cauchon (August 1993) * )
(* Modified version of the program thbergg.prx * )
( * * )
(* This program gives the BER versus power at received of a spectral slicing system * )
(*composed of anLED that is DIRECTLY modulated, an EDFA, an optical filter and an * )
(*optical receiver. * )
(* The LED photon distribution is modeled by a gaussian distribution with a mean and * )
(*variance of a negative binomial passed through and the a BDI model introduced by * )
(*Shimoda et al.(1980) and extended by Teich et al.(1989-1992) * )
( * * )
( ***** )
(*<<initmath;*) (*Read initialization file for Mathematica*)
<<constants; (*Read program constant file*)
<<berparameters2a; (*Read parameter file for Ber calculations*)
    (*****Input Distribution Parameters (LED) ***** )
Pin= Pin (mt/2);
n0ON=(Pin 2 r)/((r+1) hp nu 2 Be); (*Average Input # of Photons for ON*)
n0OFF=(Pin 2)/((r+1) hp nu 2 Be); (*Average Input # of Photons for OFF*)
NM=DFfactor m (Bout)/(2 Be); (*Number of Modes of the Source*)
(** Built-in Negative Binomial pdf **)
NBDist[alpha_,N_]=NegativeBinomialDistribution[alpha,alpha/(N+alpha)];
varNBD[x_]=(muin muOut L x)+((muin muOut L x)^2)/NM; (*Negative Binomial
variance*)
nav[OFF_,ON_]=(OFF+ON)/2;
(***** BDI Parameters (EDFA) ***** )
M=mt (Bout)/(2 Be); (*Number of Modes of the BDI Medium*)
t=Log[G]/Bout; (*Time of Traversal*)
a=(Nsp Bout); (*Birth Rate*)
```

```

b=a-Bout; (*Death Rate*)
c=M a; (*Immigration Rate*)
h=Exp[(b-a) t];
k=(a/(b-a)) (h-1);
(***** Variance of BDI Medium *****)
outvar[x_,L_]=(((muin muOut L x)+ muOut L (c/a) k)/h+(((muin muOut L x)+
muOut L (c/a) k)/h)^2)/NM ((2 Eff q Be)^2);
(***** Display Parameters *****)
Print["-----
-----"];
Print["INPUT DISTRIBUTION: Negative Binomial"];
Print["Number of Modes=",NM];
Print["Average Input Power= ",Pin," = ",PindBm];
Print["Extinction Ratio=",r];
Print["-----
-----"];
Print["BDI MEDIUM:"];
Print["Birth Rate a=",ScientificForm[a,6]];
Print["Death Rate b=",ScientificForm[b,6]];
Print["Immigration Rate c=",ScientificForm[c,6]];
Print["Time of Traversal t=",t];
Print["Spont. Emission Factor Nsp=(a/(a-b))=",ScientificForm[Nsp,6]];
Print["Number of Modes (c/a)=",ScientificForm[M,6]];
Print["h=",ScientificForm[h,6]," k=",ScientificForm[k,6]];
Print["Gain (1/h)=",ScientificForm[1/h,6]];
Print["BDI Transfer function (c/a)k/h=",ScientificForm[(c/a)k/h,6]];
Print["-----
-----"];
(***** OISSON'S Noise Terms *****)
(***** Spontaneous emission *****)
Psp=(c/a) (k/h) hp nu (2 Be); (*=mt (k/h) hp nu Bout*)
Isp=Psp (Eff q)/(hp nu);

```

```

(***** Signal *****)
Is[x_]=x (2 q Eff Be) (DFfactor Bout/Bin);
S[x_,L_]=(muin muOut L (Is[x]/h))^2;
Nperbit[x_,L_]=(Eff muOut L (muin (((Is[x]/(2 q Eff Be))/h)+(c/a)(k/h))));
(***** Excess noise term introduced by the LED source *****)
Nex[x_,L_]=(((muin muOut L (Is[x]/h))^2)/NM);
(***** Noise terms *****)
Nshot[x_,L_]=(2 q Be muOut L)((muin (Is[x]/h))+Isp);
Nsigsp[x_,L_]=(2 (Is[x]/h) muin (muOut^2) Isp (L^2))/NM; (*(2 Be)/Bout);*)
Nspsp[L_]=((muOut L Isp)^2)/NM; (*(2 Be)/Bout);*)
Nth=((4 kB T) Fn Be)/Rl;
(***** Summation of the Noise components *****)
Ntot[x_,L_]=Nex[x,L]+Nshot[x,L]+Nsigsp[x,L]+Nspsp[L];
(***** Gaussian BER Formulas *****)
Q[x0_,x1_,L_]=(Sqrt[S[x1,L]]-
Sqrt[S[x0,L]])/(Sqrt[Ntot[x1,L]]+Sqrt[Ntot[x0,L]]); BER[x0_,x1_,L_]=0.5
Erfc[Q[x0,x1,L]/Sqrt[2]];
(***** Received optical power in Watt and dBm *****)
Prx[L_]=((nav[Is[n0ON],Is[n0OFF]]/h ((hp nu)/(Eff q)) muin + Psp) muOut L);
PrxdBm[L_]=10 Log[10,1000 Prx[L]]//N;
(***** BER Calculations *****)
BERG={}; (*Initialization of vector containing PrxdBm and BER*)
L=.; (*Initialization of the attenuation variable*)
jinc=2;
(***** BER Calculation Loop *****)
For[j=0,j<61,j=j+jinc,
Print["-----
-----"];
Print["BER CALCULATIONS"];
LdB=ILC-60+j; (*Attenuation calculation in dB*)
L=10^(0.1 LdB)//N;
*****Attenuation and Power Display *****)

```



```

Print["LdB=",LdB," L=",L,];
Print["PrxdBm=",PrxdBm[L]/N];
(***** Noise Term Display *****)
Print["-----"];
Print["NOISE COMPONENTS"];
Print["ASE Power Psp=",Psp=",10 Log[10,1000 Psp]/N];
Print["*****Olsson-BDI Model*****"];
Print[" ON OFF"];
Print["-----"];
Print["S= ",S[n0ON,L]/N," ",S[n0OFF,L]/N];
Print["Nex= ",Nex[n0ON,L]/N," ",Nex[n0OFF,L]/N];
Print["Nshot= ",Nshot[n0ON,L]/N," ",Nshot[n0OFF,L]/N];
Print["Nsigsp=",Nsigsp[n0ON,L]/N," ",Nsigsp[n0OFF,L]/N];
Print["Nspssp= ",Nspssp[L]/N];
Print["Nth= ",Nth/N];
Print["Ntot= ",Ntot[n0ON,L]/N," ",Ntot[n0OFF,L]/N];
Print["outvar=",outvar[(n0ON (DFfactor Bout/Bin)),L]/N," ",outvar[(n0OFF
(DFfactor Bout/Bin)),L]/N];
(***** Gaussian BER Display *****)
Print["-----"];
Print["BER=",ScientificForm[BER[n0OFF,n0ON,L],6]];
(** Creation of BER vector **)
BERG=Append[BERG,{PrxdBm[L],BER[n0OFF,n0ON,L]};
L=. ;
];
Pin=.;
(***** BER Curve Plotting *****)
Print["Plotting..."];
bergg=LogListPlot[BERG,PlotJoined->True,FrameLabel->{"Received Optical Power
(dBm)","BER","Gaussian Approx., PindBm="ToString[PindBm],""}];
(*****Writing Data to a File *****)
(**The format used is space seperated numbers**)

```

```

stmp=OpenWrite[outputfilename, FormatType->OutputForm];
Print["Writing data into ", outputfilename, " ..."];
WriteString[stmp,"Pin=",ToString[PindBm], " dBm\n"];
WriteString[stmp,"PrxdBm ", " ", "BER\n"];
For[ $jj=1, jj < Round[(61/jinc)+1], jj++$ ,
      Write[stmp, BERG[[ $jj$ ]][[1]], " ", FortranForm[BERG[[ $jj$ ]][[2]] ]];
];
Close[stmp];

(*****End of Program *****)

```